DEVELOPMENT OF THE SUBSEA ROBOT ANNE
(AUTONOMOUS PNEUMATIC NAUTICAL EXPLORER)

REENI CATHERINE WOOLGAR

National Library
of Canada

Acquisitions and
Bibliographic Services

395 Wellington Street
Ottawa ON K1A 0N4
Canada

Bibliothèque nationale
du Canada

Acquisitions et
services bibliographiques

395, rue Wellington
Ottawa ON K1A 0N4
Canada

Your file Votre référence

Our file Notre référence

0-612-42463-4

Canada

DEVELOPMENT OF THE SUBSEA ROBOT ANNE (AUTONOMOUS PNEUMATIC NAUTICAL EXPLORER)

BY

© REENI CATHERINE WOOLGAR, B.ENG.

A thesis submitted to the
School of Graduate Studies
in partial fulfillment of the
requirements for the degree of
Master of Engineering

Faculty of Engineering and Applied Science
Memorial University of Newfoundland
April 1999

St. John's Newfoundland Canada

Dedicated to the loving memory of my father,
David Walter Woolgar

Worry is the rehearsal for failure.

Author Unknown

Abstract

In 1997, a small drifter subsea robot known as NO MAD was developed at Memorial University of Newfoundland (MUN). This robot uses a simple air-water ballast tank for depth control. Although NO MAD is modular in construction, it does not provide easy assembly as all of the structural components are either bolted or screwed and the majority of the electrical components are hard-wired. It uses five float switches equally spaced vertically in the ballast tank to control the level of water in the ballast tank. Unfortunately, this control strategy does not provide adequate depth control.

This thesis describes the development of a more robust version of NO MAD known as the Autonomous Pneumatic Nautical Explorer (ANNE). ANNE is extremely modular in design and complete assembly requires thirty minutes. Components are locked together using a simple twist mechanism and suction is used to close the instrumentation boxes. To improve the control strategy, ANNE uses an accelerometer to determine whether it is over or under buoyant which controls the amount of flow into and out of the ballast tank. With these modifications, tests in a deep tank at the Faculty of Engineering and Applied Science, MUN, illustrated that ANNE achieved adequate depth control.

Although ANNE was developed for educational purposes, it has potential for industrial benefits as ANNE could be placed in the ocean upstream of a region of interest. It would be carried by the local current and used for either measurements at preset depths or seabed exploration.

Acknowledgements

Financial support is greatly acknowledged from the Natural Sciences and Engineering Research Council (NSERC) Scholarship; the Faculty of Engineering and Applied Science, Memorial University of Newfoundland (Supplemental Support); and the author's supervisor, Dr. Michael James Hinchey.

The author is forever indebted to Dr. Hinchey for his excellent supervision throughout the duration of the research. Dr. Hinchey provided assistance with the project, spending numerous hours with the author during the experimentation aspect. His kindness, support, respect and understanding must at this time be acknowledged.

Personal thanks are extended to the author's fiancé, John Hiscock, for his hands-on assistance with the construction and experimentation work of the robot. Thanks to the Technical Services staff at Memorial University of Newfoundland, namely Humphrey Dye and Leo Spurrell of the machine shop, as well as Jim Andrews and Mac Butler of the welding shop. Special thanks to special friends Peter Saturley and Prasanna Raghavan for their support and assistance throughout the project.

Contents

List of Figures

List of Tables

List of Symbols

γ	negative constant
Δh	change in elevation
ΔP	change in pressure
Δt	sampling or loop rate
λ	bandwidth
ρ	density of air in the ballast tank
σ	density of the flowing fluid (water)
a	constant used in squashing function
A	cross-sectional area of the ballast tank
A_f	frontal area exposed to flow
B	buoyancy force on small subsea robot
C	term which accounts for wake drag
$\mathbf{C}$	best estimate for term that accounts for wake drag
C_D	drag coefficient
C_o	head loss coefficient
D	disturbance force from the surroundings
$\mathbf{D}$	best estimate of disturbance force from the surroundings
E	difference between desired and actual small subsea robot position (depth error)
f	squashing function
F	force generated by the propulsion system
$\mathbf{F}$	best estimate of force generated by the propulsion system

g	acceleration due to gravity
h_L	head loss
H	flow area
I	command position of small subsea robot
I_N	neural network input
$I_N J_N$	neural network with two inputs
J_N	neural network input
k	specific heat ratio
K_a	measure of air compressibility
K	relay strength
K_D	derivative gain
K_I	integral gain
K_P	proportional gain
K_R	relay gain
L	constant involving C, D and M
$\boldsymbol{L}$	best estimate of constant involving $\boldsymbol{C}$, $\boldsymbol{D}$ and $\boldsymbol{M}$
M	inherent and added water mass of small subsea robot
$\boldsymbol{M}$	best estimate of inherent and added water mass of small subsea robot
M_A	mass of high-pressure compressed air from divers bottle to the ballast tank
M_{max}	maximum mass of water that the ballast tank can withstand
N	negative fuzzy logic input
NN	negative-negative fuzzy logic control signal output

NP	negative-positive fuzzy logic control signal output
NZ	negative-zero fuzzy logic control signal output
O	actual vertical position of small subsea robot
O_N	neural network output
P	positive fuzzy logic input
PN	positive-negative fuzzy logic control signal output
PP	positive-positive fuzzy logic control signal output
PZ	positive-zero fuzzy logic control signal output
P	driving pressure
Q_W	volumetric flow rate of water flowing into the ballast tank (positive)
Q_W	volumetric flow rate of water through the orifice during purging (negative)
Q_{in}	flow rate of air into ballast tank from the divers bottles
Q_{out}	flow rate of air out of the ballast tank through the top hole
R	vertical submergence depth of small subsea robot
sg	specific gravity
S	control signal
t	time
t_p	purge period
T	half height of the ballast tank
V	pseudo-energy
V_a	volume of air in the ballast tank
V_f	volume of fluid

V_t	maximum terminal speed of small subsea robot
W	weight force
W_{BO}	output weight for bias neuron
W_{BX}	input weight for input bias neuron
W_{XI}	input weight
W_{XJ}	input weight
W_{XO}	output weight
Y	water level measured positive downward from the center of the ballast tank
Z	zero fuzzy logic input
ZN	zero-negative fuzzy logic control signal output
ZP	zero-positive fuzzy logic control signal output
ZZ	zero-zero fuzzy logic control signal output

List of Abbreviations

ABE	Autonomous Benthic Explorer
ALACE	Autonomous Lagrangian Circulation Explorer
AM	ABE altitude sensor
ANNE	Autonomous Pneumatic Nautical Explorer
AUV	Autonomous Underwater Vehicle
CON	ABE controller of seven thrusters
Controller	Z-WORLD Rugged Giant C-Programmable Miniature Controller
DP	ABE depth sensor
MUN	Memorial University of Newfoundland
NAV	ABE navigator
NC-NO	normally closed – normally open relay
PD	Proportional Derivative Control
PID	Proportional Integral Derivative Control
ROV	Remotely Operated Vehicle
XPD	ABE safety communications
3D	Three-dimensional

Chapter 1

Introduction

Often the most plentiful and worthwhile resources provided by nature are located in environments inhospitable to humans. The ocean is a storage space for mineral resources as well as oil and gas reserves. The living resources held within promise a supply of protein for many future generations [1]. Success in recovering these resources depends on technology and innovation. Besides economic potential, the military also recognizes the strategic importance of the ocean. These factors make ocean exploration and the removal of humans from working in these environments increasingly important.

Throughout the development of modern underwater robotic vehicles, there has been a growth from manned submersibles to remotely operated vehicles (ROVs), which can be either tethered or untethered, and finally to autonomous underwater vehicles (AUVs), which are entirely untethered. The trend is to eliminate the presence of humans for underwater tasks through the development of subsea robots. This requires that the units be preprogrammed and autonomous.

As the underwater environment is without structure and uniformity, it contains numerous simulation and modeling uncertainties. These must be considered when designing a control system for underwater vehicles. The technology that has developed for land-based systems cannot be transferred to underwater robotics due to differences in dynamic characteristics. The area of underwater vehicles has grown enormously in the last decade and has become paramount to such areas as the offshore oil industry.

In 1997, a small drifter subsea robot known as NO MAD was developed at Memorial University of Newfoundland (MUN) as part of a Doctoral degree for ZhongQun Lu [2]. The main objective of this thesis is to describe the development of a more robust version of the original NO MAD, known as the Autonomous Pneumatic Nautical Explorer (ANNE). Assembly and disassembly of ANNE will be somewhat easier than that of NOMAD, requiring less time for the start-up and ending of missions. The robust features of ANNE will include the use of an accelerometer for depth control and a more effective use of high-pressure air consumption as required by the control strategy, which will ultimately provide longer mission durations than NOMAD.

The thesis starts with background on underwater robotic vehicles, Chapter 2, with information on some of the most advanced subsea robots presently in existence. In Chapter 3, the main control strategies being used by developers of underwater vehicles are described. The robust version of NO MAD, referred to as ANNE, is described in detail in Chapter 4. This includes design and construction details of the robot, as well as a description of the electrical and pneumatic components essential for operation. Chapter 5 describes the simulation strategy for depth control of ANNE, while Chapter 6 gives a description of the actual deep tank testing and the results. Concluding remarks and recommendations for future work are contained in Chapter 7.

Chapter 2

Background Review of Underwater Robotic Vehicles

The intent of this review is to give the reader information on the appearance of underwater vehicles and their uses. It does not focus on performance data interpretation. A detailed comparison of the performance of various underwater vehicles is beyond the scope of this work.

2.1 Remotely Operated Vehicles

The human diver has dominated the majority of underwater work in the past, as they tend to be the most effective for underwater work. ROVs have become increasingly popular in the last decade and since their introduction to the underwater world, they have gained the reputation of being effective for underwater inspection and surveying.

ROVs were traditionally designed for observation and emergency back up of human divers, while most recently they have been performing tasks that were only executed by human divers. These include such things as releasing hooks, cutting cables and placing explosive charges. The level of complexity has increased to specific assignments such as cleaning and inspecting drill rigs as well as burying pipelines through use of their robotic manipulators. ROVs are also reaching water depths beyond the capability of human divers.

ROVs are used for oceanographic research, development of offshore oil industries, hydrographic surveys, and exploration in the survey industry. There has been a growing trend towards their development for task-specific services as opposed to multiple uses. Specifically for the offshore oil industry, they are a kinesthetic means of examination.

Classification of ROVs is based on the type of work they perform, and they can be tethered or untethered vehicles. Tethered vehicles account for the majority of ROVs and they are dependent on a surface supply vessel through an umbilical or tether. Thus they can be suspended, towed mid-water, or cable-controlled. For work on the ocean floor, there are towed bottom and crawling vehicles. The tether is a design advantage as it can supply unlimited power to the vehicles. It is also the biggest disadvantage as it limits the diving range and speed that the vehicle can travel.

Suspended vehicles are an important class of tethered vehicles that are deployed and operated through cables. Suspended vertically under the support vessel by the cable, they are useful for local work tasks in construction related operations such as pipeline repair.

Crawling vehicles are intended for specific observation such as work tasks on the seabed or on an underwater structure. Power is transmitted through the tether or umbilical cable and propulsion is provided through wheels or tracks that are in contact with the surface bottom. They are primarily used for pipeline and cable burial.

Towed vehicles are the simplest to design and construct. It is a towed unit which can be launched from a supply vessel and towed at a certain depth and distance from the surface bottom. They are useful for pipeline inspections.

Untethered vehicles are making their way into the offshore sector as the drive from oil companies and the scientific community is to explore work in deeper waters. Untethered vehicles are useful for exploring drill rigs in ice-infested waters. They are self-propelled, self-powered, controlled from the surface and are tracked through the use of acoustic signals. They are used for the surveillance and inspection of drill rigs and are extremely effective in ice-infested waters, as they require no cables or umbilical cords.

As ROVs can operate in depths up to 8000 m, it is necessary to have a reliable tracking system, thus the need for greater use of acoustic navigation systems. Proper position display can give the operator a line of sight between the supply vessel and the ROV. By using additional beacons to mark subsea locations, the relocation time of the ROV is reduced. Using a tracking system with ROVs permits the operator to know its exact location at all times. The acoustic navigation system can be used to reduce the chance of damage incidents and collisions. During inspection and damage survey operations, the subsea tracking system is the critical link between the subsea operation and the real world. By integrating the ROV position data with the surface vessel or platform position, the global coordinates of the ROV position can be plotted. For example, if an inspection on a pipeline reveals damage then the exact position of this damage can be determined.

2.2 Autonomous Underwater Vehicles

In order to eliminate the presence of humans from conducting underwater tasks, a subsea robot must be designed to be preprogrammed and autonomous. Autonomous means that the vehicles are independent as they carry their own power supply and have no physical connection to the surface. For these vehicles, control is an area that requires intense work. There are six spatial degrees of freedom (heave, pitch, surge, roll, yaw and sway) that must be considered and not all of the physical control issues can be solved. As there are unpredictable influences from the underwater environments and ocean currents, AUVs are prone to severe nonlinear instabilities or unwanted motions. The propulsion requirements are costly, and are often slow and limited.

The desire to change to AUVs did not happen suddenly, as the technologies that existed had to be adapted. The underwater environment contains modeling uncertainties and nonlinearities, which gives the motivation for robust control. AUVs require an adaptive control approach meaning that the subsea robot learns as it goes, changing its control techniques and path planning during its mission.

AUVs permit a search of the ocean floor and waters for such things as minefield location and avoidance, beach access, hazardous materials and navigation. They provide for remote sensing in the military and scientific areas and oceanographical, biological and geological explorations are possible in regions where access is difficult. They can be used for the localization of pollutant sources and evaluation of hull damage in high sea states [3].

The physical environment in which AUVs operate is generally inaccessible, remote and unattended with communications being intermittent or nonexistent. Extreme pressure and temperature changes are often experienced. Sonar sensing is much slower and not as effective as visual sensing which results with the deployment, operation and recovery of the AUV being time-consuming and expensive. For these robots, reliability, stability and autonomy are paramount. The constraints are generally worst-case for any subsea robot and the underwater environment leaves many theoretical and engineering problems open for exploration.

2.3 Comparison of Remotely Operated Vehicles and Autonomous Underwater Vehicles

The increasing depth requirement for underwater work is the motivation for the use of underwater vehicles, ROVs and AUVs alike. The depth range for the human diver is near 450 m, while the depth range for underwater vehicles is between 1800 m and 6000 m, depending on the level of complexity of the vehicle [4]. Figure 2.1 from [4] illustrates the underwater depth range for various examples of ROVs and AUVs, as well human divers. This creates a disadvantage for the ROV when compared to the AUV as the maximum depth of the ROV is directly linked to the length of the tether.

The tether in the design of the ROV is essential as it transmits communication, power and control requirements. They can become entangled requiring large cranes and winches to be deployed into the water to release the ROV. The tether also increases the overall drag force. Tether problems have created the promotion of AUVs, as they do not require contact with the surface. They are programmed, through an on-board computer, and contain their own source of power.

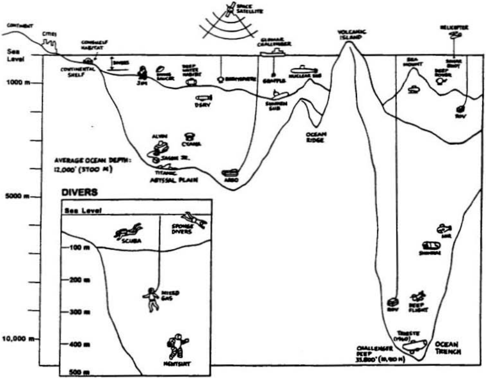

Figure 2.1 Depth range for ROVs and AUVs [4]

The underwater environment does not permit either ROVs or AUVs to have high performance characteristics due to problems with effective control strategies. Both types of vehicles are inefficient when considering propulsion, thrusting mechanisms, and the use of sensors. For example, ducted propellers mounted close to the main structure of the robot are often used for propulsion. This creates complex flow interactions with the main structure making characterization with these devices difficult.

When comparing the use of underwater vehicles to human divers, both ROVs and AUVs are less efficient for complex assignments. The human diver is more effective than teleoperated systems for complete visual inspection, as television systems hard-wired to ROVs fail to transmit generated visual cues. This problem is being overcome by the use of fiber optics and sonar. Underwater vehicles will perhaps not replace the human diver in depths of their competence unless human lives are at risk.

The uses for ROVs and AUVs are infinite and the further exploration of these vehicles is clearly a continuing objective of researchers and designers. This includes possible applications for unique remote technology in areas outside the offshore oil industry. With the advancement of technology and innovation, the progression of ROVs and AUVs will thrive with a consolidation of the leaders in the research area.

As the population of ROVs and AUVs increase and designers become more experienced, reliability factors will be established that will lead to improvement in current designs of

ROVs and AUVs. Interface capabilities of ROVs and AUVs will be required as deeper waters and harsher environments are explored. The overall size of ROVs and AUVs will likely remain the same as they are today, but they will be equipped with greater load capacity, providing for more flexibility. Design attention should be focussed on allowing the underwater vehicles to remain on site for longer durations.

Communication and power requirements for tethered vehicles are implemented through the use of cables that often have low bandwidth and significant time delay. This delay between the time the information and power is sent and received can be critical in the functioning of the vehicle in specialized applications. This major drawback of tethered vehicles encourages the design of autonomous underwater vehicles. However, future development of untethered vehicles will face problems, primarily centering on communications and power requirements.

2.4 Industrial Autonomous Underwater Vehicles

As the main focus of this thesis is on the design of an AUV, some of the more important AUVs used in industry are discussed herein.

2.4.1 Autonomous Benthic Explorer

The most important characteristic of the Autonomous Benthic Explorer (ABE) is that it can operate independently and remain on site for months at a time. It was designed by Bradley and Yoerger [5] with the need for long term monitoring of the ocean floor. The main structure consists of three horizontal tubes arranged in a triangular pattern as shown in Figure 2.2. Two bladders are used to fine tune buoyancy where one bladder contains a liquid heavier than water and the other contains a liquid lighter than water. Expelling the heavier liquid makes ABE rise while expelling the lighter liquid makes it sink.

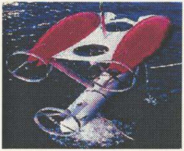

Figure 2.2 Autonomous Benthic Explorer

The mobility of the vehicle can significantly enhance data from moored and bottom mounted instruments. ABE can descend to a prepared site on the bottom of the ocean floor, dock to a suitable mooring and place itself in a very low power or sleep state. At pre-programmed intervals, ABE will undock, perform a grid survey with video cameras and other sensors, redock to the mooring and return to the sleep state, where the majority of the mission time is spent.

ABE is designed as a three body open frame vehicle in order to minimize cost. Glass balls are used for flotation. There are three glass balls in each of the two free-flooded upper pods. The open frame permits all of the batteries and electronics to be put in a single housing. The separation of buoyancy and payload creates a large righting moment that simplifies control and allows the propellers to be put in the protected space between the three body open frame. ABE has seven thrusters and can move in any direction.

ABE uses distributed control architecture designed for flexibility, testability, maintainability and survivability. There are two layers of capability, which are very low electrical power and modest computational efficiency, and modest electrical power with large and expandable computational resources. ABE is powered by rechargeable gelled lead-acid batteries to facilitate testing and reduce costs. These batteries permit ABE to travel well over 50 km in a straight line [5]. In a real mission, the energy required to maneuver and operate the sensors will limit the range to a fraction of the available battery power. For longer missions and future design improvements, alkaline or lithium batteries could be used for a twelve-fold improvement over the lead-acid batteries.

The top-level controller, called ABE, is in charge of mission planning and speaks to a group of officers. CON controls the seven thrusters that operate at ambient pressure in an oil environment. NAV is the navigator, AM is the altitude sensor, DP is the depth sensor and XPD is the safety communications. NAV can communicate with AM and DP. XPD will call for help and drop weights to anchor if it does not receive a message that everything is operating normally over set periods of time.

A typical mission consists of sleeping periods, vehicle movements and data recording sequences. Such missions are specified in the top-level mission controller. The flexible command interface that permits the mission must then be re-programmed. ABE's architecture allows for nodes to be removed by only severing the simple bus connection to the rest of the vehicle and replacing it with a new and modified brain.

ABE is designed to operate independently of an operator. It carries two transponders for vehicle location and communication purposes. The transponders are electrically independent which allows for relocation if the main battery dies and can also provide a back up if ABE suffers major electrical or software trauma.

The most prominent feature of ABE is the variable ballast system. Since ABE must not waste energy fighting possible buoyancy errors, and because it is difficult to pre-ballast with sufficient accuracy, the variable ballast system is used. A single pump system pumps either a heavy or light fluid overboard from ambient pressure bladders that are nestled around the buoyancy spheres in the fiberglass fairings. The light fluid is alcohol ($sg = 0.78$) and the heavy fluid is a calcium bromide solution ($sg = 1.8$).

For redundancy and balance, there are identical pump and bladder systems in the port and starboard upper fairings. The pumps are peristaltic and in ambient pressure oil filled housings. Slip clutches allow the motor to drive one pump when it turns forward and the other when it operates in reverse.

2.4.2 Autosub-1

Autosub-1 is able to carry a scientific payload that can be replaced for each mission. It is cost effective, durable and can gather environmental data from sensors that can assist with oceanographic research and industrial use [6]. Autosub-1 was designed by Millard and his colleagues [6] and can be used in both coastal and environmental management to monitor waste, natural hazards, environmental changes and bio-diversity. For oil exploration, it is equipped with housing sensors. Autosub-1 can also be used in the chemical industry for monitoring and detecting dissolved chemicals such as oxygen and nitrate ions.

Autosub-1 is able to collect multiple sets of data simultaneously including physical, biological, chemical and geophysical data with major implications for climate change studies. Another use includes routine sampling for underwater satellites, which will reduce the need for large research ships and crew.

Resembling a torpedo as pictured in Figure 2.3, Autosub-1 is 7 m long and has a diameter of 0.9 m. It has a mass of 1400 kg when it is dry and is positively buoyant by 15 kg. A pressure vessel holds the batteries and power management system. Foam cells provide buoyancy and ballast weight provides trim.

A radio modem is linked with the support vessel so that missions can be downloaded for the retrieval of data. Argos satellite beacons are used for locating Autosub-1 at the surface.

Figure 2.3 Autosub-1

2.4.3 Autonomous Lagrangian Circulation Explorer

The Autonomous Lagrangian Circulation Explorer (ALACE), designed by Davis and Webb [7] is a subsurface float that cycles vertically from a depth where it is neutrally buoyant to the surface. System Argos satellites, to which it can relay data, can locate ALACE. ALACE is intended to allow for exploration of low scale low frequency currents and to provide repeated vertical profiles of ocean variables. There are three major components or subsystems that compose ALACE. These include a hydraulic system to adjust buoyancy, a microprocessor to schedule and control various functions, and the Argo transmitters and antenna. These features are visible in Figure 2.4 where ALACE is pictured with one of the designers.

Figure 2.4 Autonomous Lagrangian Circulation Explorer

ALACE can periodically change its buoyancy by changing the volume of an external bladder. Pumping hydraulic fluid from an internal reservoir to an external bladder increases float volume and buoyancy. Buoyancy changes can also be produced by allowing fluid to flow from the external bladder back into the internal reservoir.

To ascend, hydraulic fluid flows from the internal reservoir through a filter to a small motor-driven hydraulic pump, which pumps high-pressure fluid through a one way check valve and into the external bladder. To descend, a latching valve opens to allow the oil to flow from the external bladder back to the internal reservoir which is maintained at the internal pressure of the float [7].

Positioning and data relay are accomplished by satellite but ALACE has links with acoustic tracking networks which makes them suitable for global deployments in arrays of any size. While providing only a sequence of displacements between surfacing intervals, they are efficient in gathering long term observations that are needed to map large-scale average flow.

2.4.4 NO MAD

NO MAD is an intelligent yet inexpensive subsea robot designed by Lu [2] and Hinchey [8] that has yet to undergo sea trials. It uses a simple air-water ballast tank for depth control, having only a precise trajectory vertically. To date, there is no lateral control which means it would drift with local ocean currents. It can be deployed into the ocean to record temperatures at preset depths or to explore the seabed. NO MAD remains inexpensive as it does not contain any complex propulsion mechanisms or sensors and there are no preset three-dimensional (3D) trajectories.

NO MAD is modular in construction having a cylindrical shape as shown in Figure 2.5. Measuring 1 m in height and having a mass of 30 kg, it would be used mainly in shallow water depths of 10 m. There are two main components, namely a divers bottle and a ballast tank. The divers bottle is located near the bottom of NO MAD where a payload would hang. The ballast tank is positioned at the top, having large holes at the top and bottom. When the top hole is closed, high-pressure compressed air is permitted to flow into the ballast tank to force water out of the bottom hole in order for NO MAD to rise. Similarly, with both holes open, high-pressure compressed air flows out of the ballast tank through the top hole and water flows in through the bottom hole causing NO MAD to sink.

Figure 2.5 NO MAD

When outside an error band surrounding the command depth, a Z-WORLD Rugged Giant C-Programmable Miniature Controller (controller) allows water in or forces water out to make NO MAD move towards the established error band surrounding the command depth at a specified speed. Once the set speed is reached, the holes at the top and bottom of the ballast tank are closed. Inside the error band, the controller sends signal to the pneumatic valves that control pneumatic pistons which permit water in or force water in order to make NO MAD neutrally buoyant. Once this is done, the top and bottom holes of the ballast tank are closed. The drag on the robot causes its speed to decay to zero. Faster speeds could have been achieved, but this demand requires high-pressure air consumption at an increased rate.

Pneumatic pistons are used to open or close the holes at the top and bottom of the ballast tank. The use of pistons and large holes allows for quick filling and purging of the ballast tank, creating a fast response. Pneumatic valves are used to control the flow of the high-pressure compressed air from the divers bottle to the pistons and the ballast tank. The divers bottle containing high-pressure compressed air is rated at 200 bar. A pressure regulator is used to reduce 200 bar to 12 bar and a second pressure regulator takes 12 bar down to 4 bar, which is the operating pressure of the pneumatic components. A manual flow control valve sets a limit on the flow of high-pressure compressed air from the divers bottle.

There are two pressure transducers utilized as sensors. One of these measures pressure inside the ballast tank while the other measures pressure outside the ballast tank, and acts as a depth sensor. The use of two sensors permits for a check on the stresses on the walls of the ballast tank. A relief valve vents pressure to the surroundings if the relative pressure across the walls of the ballast tank becomes too high. One way valves are utilized to keep the pneumatic components dry. Five simple float switches evenly spaced vertically are used to estimate the amount of water in the ballast tank. This could have been done with a continuous level sensor but was considered to be too expensive.

The controller is used on-board for pneumatic valve operation and sensor measurements. There are ten high voltage-current drivers to execute the pneumatic valves and seven analog to digital channels for intake signals such as pressure and water level sensors.

These can be seen in Figure 4.11 of Chapter 4. Three 24V DC Nickel-Cadmium batteries power the computer, which allows for twenty-four hour operation. The real time kernel feature in the software allows for various control tasks to be isolated and performed at set intervals of time.

The success or failure of the NO MAD concept depends on how long the high-pressure compressed air supply lasts, which determines the mission duration. This is highly dependent on the depth control strategy employed. The control strategy for NO MAD is at the drive level with a switching type of error-driven strategy. The depth error and rate of change of depth error are used to get a command water level in the ballast tank. The main control loop is given as a finite number of IF-THEN Rules. The inner feedback loop operates pneumatic valves and makes the actual water level, measured by the float switches, home in on the command level so that NO MAD moves to the command depth.

When computational simulations were executed, it suggested that the switching nature of the strategy and the use of the float switches would cause NO MAD to undergo a limit cycle near the command depth. It was thought that the use of hysteresis and phase lead compensation could perhaps suppress the limit cycle [8]. Actual tests of NO MAD in a tank 5 m deep were performed in which NO MAD was controlled manually from a computer keyboard. It was commanded to go from its initial depth of 1.25 m to 3 m, then to the water surface 0 m, and back to 1.25 m. At the final command, a limit cycle was produced as predicted by the simulation with an amplitude of 0.15 m and a period of 20 s.

2.5 Development of a Virtual World

When considering AUVs, it is noted that there are only a select few working today and each has limited functionality. However, there are thousands of indoor and outdoor land-based mobile subsea robots, hundreds of airborne and space-based autonomous robots and hundreds of underwater ROVs. The limited number of AUVs is a result of the complex design and manufacturing procedures involved and the lack of testing ability before commissioning in the real world.

Perhaps the construction of a virtual world for subsea robot development and evaluation of performance will become a pre-requisite for successful AUV development. Several researchers like Brutzman are attempting to design virtual worlds [3]. Testing subsea robots in the actual underwater environment contains an element of risk as the threat of losing the subsea robots exists, which can become costly. It is tremendously difficult to observe, communicate with and test AUVs, because they operate in remote and hazardous environments.

A virtual world would provide a way for engineers and designers, as well as the subsea robots themselves, to view and interact with distant and hazardous environments in a 3D sense. Thus the goal of the designer is to provide the complete functionality of the targeted environment in a laboratory setting. This would produce a simulation strategy that would allow interaction capability to reduce the design flaws associated with classical simulation approaches.

Simple simulation schemes are inadequate in predicting the reaction of subsea robots to underwater environments. The classical analytical simulation techniques are generally performed on very isolated problems and interactions between the models are rarely considered. As the real world imposes many physical and timing constraints that are often overlooked when defining a simulation scope, simple simulation is only a preliminary proof of the design concepts. There is no guarantee of how the subsea robot will react in real world applications.

The 3D virtual world must be developed with specific characteristics. These include an obvious recreation of the complete environment external to the subsea robot, the physical behaviour of the subsea robot, and sensor interactions. In order to prevent a bias, the subsea robot must not be able to recognize a difference between the virtual world and the actual environment. The successful implementation of the virtual world would be validated by the robot performance in the real world domain.

The incorporation of the above components would require a cross-disciplinary approach in the modeling efforts. An underwater virtual world would allow for simulation, operation, evaluation and modification of the subsea robots without incurring a huge expense or taking the risk of losing the subsea robot during testing.

Chapter 3

Control Strategies for Subsea Robots

The control strategy used by ANNE is quite simple, however, for completeness, an overview of strategies used by other researchers will be described. These control strategies are all suitable for subsea robot implementation with the ultimate selection depending on specified design criteria which include stability, accuracy, speed of response, disturbance rejection and robustness.

Stability would indicate the nature of ANNE during a disturbance from a rest state with the desire for transients to decay, as opposed to grow, with time. Accuracy would determine how close ANNE would settle near the command depth. The speed of response would indicate how fast, or slow, ANNE would approach the command depth. The control strategy must be able to reject disturbances, which becomes important when ANNE is subjected to sudden wave impulses, where it is essential that the controller can stabilize ANNE at the command depth. Robustness would determine how ANNE reacts to large changes in the system or the surroundings. This criteria is important due to the frequency of such occurrences, which are often either difficult to measure or unknown.

The underwater environment contains numerous simulation and modeling uncertainties that must be considered when designing a control system for subsea robots. This is a direct result of the underwater environment being without structure and uniformity.

Considering the underwater environment as a vertical profile, it can be broken down into three regions. These regions are the atmosphere above the water surface, the water column, and the sea floor [9]. The water column is the region which greatly influences subsea robotics as it includes surface and internal gravity waves, drag due to wave generation, as well as the temperature, salinity, pressure and density properties of seawater. These factors must be considered in the design and operation of ROVs and AUVs near the ocean surface.

Control strategies are divided into two categories, namely classical and supervisory. Classical control strategies generate drive signals with the majority based on state error. These are said to be error-driven, although some make use of the system governing equations. These strategies try to make the system home in on set points. Supervisory control strategies are designed to replicate a human operator, operating at higher levels than classical control strategies. Supervisory control strategies can decide when classical control will be successful and can set necessary points and gains. For example, they can feed information, such as set points and appropriate gains, down to the classical level.

Presently, control strategies for subsea robotics are derived from a combination of both classical and supervisory. When human operators are utilized, supervisory control will often take the form of rules-of-thumb or heuristics which include neural networks, fuzzy logic and subsumption [10]. A good overview of control strategies for subsea robots is detailed by Farbrother and Stacey [11].

3.1 Classical Control Strategies

Dynamically positioning a small subsea robot vertically is an excellent example to illustrate various classical control strategies. The system governing equation for dynamically positioning a small subsea robot with slow up and down motion is given by:

$$M\frac{d^2O}{dt^2}+C\frac{dO}{dt}\left|\frac{dO}{dt}\right|=F+D \tag{3.1}$$

where:

M = inherent and added water mass of small subsea robot
C = term which accounts for wake drag
F = force generated by the propulsion system
D = disturbance force from the surroundings
O = actual vertical position of small subsea robot
t = time

It is important to note that M, C and D are not exactly known.

3.1.1 Proportional Integral Derivative

This type of control contains a conventional feedback loop, which incorporates proportional, integral and derivative controllers [12]. In a digital control loop, a PID scheme for a small subsea robot allows F to be calculated by:

$$F = K_P E + K_I \sum E\Delta t + K_D \frac{\Delta E}{\Delta t} \tag{3.2}$$

where:

Δt = sampling or loop rate
$\Sigma E\Delta t$ = approximation of the integral of error with respect to time
$\Delta E/\Delta t$ = approximation of the derivative of error
K_P = proportional gain
K_I = integral gain
K_D = derivative gain

This form of control allows F to be a function of the depth error, E, which is the difference between the desired and the actual small subsea robot position. This is calculated by:

$$E = I - O \tag{3.3}$$

where:

I = command position of small subsea robot

For subsea robots, in order for the control loop to function properly it is required that Δt be at least ten times smaller than the dominant subsea robot period [9]. This period is determined by the natural frequency of the small subsea robot.

Proportional controllers permit good stability criterion but are not well suited for applications that involve system disturbances. Integral controllers are able to reject disturbances and they eliminate the steady-state system error, but they often overshoot the command input creating an oscillatory response leading to instabilities. As derivative controllers respond to the rate of change of the error, they can anticipate the error and produce corrective action before the error becomes too large, however, they do not respond to steady-state error itself. Thus, they must be used in combination with proportional controllers, integral controllers or both.

A combination of all three strategies, known as PID, allows the best characteristic of each strategy to be employed. Some advantages for PID control for subsea robots include high computational efficiency, stability and the ability for adaptation to computer control. The gains in a PID controller could be made directly dependent on the system and/or surroundings. This creates a potential for the existence of adaptive control.

3.1.2 Switching

Switching schemes are generally of good performance and easy to implement with hardware. An ideal relay scheme allows F for a small subsea robot to be calculated by:

$$F = K_R sign(E) \tag{3.4}$$

where:

K_R = relay gain
$sign(E) = +1$ for $E > 0$
$sign(E) = -1$ for $E < 0$

This simple control scheme often causes mechanical systems, such as small subsea robots, to undergo finite amplitude oscillations, or limit cycles, about the command position. Modifications can be made to avoid these complications by introducing hysteresis or by the use of deadbands.

3.1.3 Computed Load

Computed load control is a form of open loop control, which is based on the system equations of motion. The drive loads correspond to desired motions while the control signals are sent to the drives in an attempt to generate the appropriate loads.

Independently, this control strategy is not very precise as the parameters such as *M*, *C* and *D* are not exactly known. Even when *M*, *C* and *D* are known, the propulsion system for the subsea robot usually cannot generate the computed load for *F* exactly. For vertical positioning, the computed load for *F* is represented by:

$$F = M\frac{d^2I}{dt^2} + C\frac{dI}{dt}\left|\frac{dI}{dt}\right| - D \tag{3.5}$$

3.1.4 Sliding Mode

This control strategy combines a form of computed load control with a switching type of error-driven control compensation. It is a popular control strategy for subsea robots [13,14]. The switching counteracts the uncertainties that exist and allows the control to become more robust. When the uncertainties have known upper bounds, there is always some form of control, as the system can be directed back toward the command state.

Sometimes ideal relay compensation by itself generates a chattering or limit cycle about a sliding line. A boundary layer on either side of the sliding line can be used to counteract this. In this case, sliding mode tries to ensure movement towards the boundary layer so that once inside the layer, a linear control strategy can be used.

For the vertical positioning case of a small subsea robot, the sliding line is represented by:

$$S = \frac{dE}{dt} + \lambda E \tag{3.6}$$

where:

S = control signal
λ = bandwidth

The sliding equation is one order lower than the system order. If *S*, which ultimately drives *E*, can be made equal to zero, then *E* must decay. *S* is a filtered version of *E*, and acts as a buffer. Thus, in terms of *S*, a pseudo-energy, *V*, can be defined by:

$$V = \frac{M}{2} S^2 \tag{3.7}$$

where:

V = pseudo-energy

If *dV/dt* is negative, then all the trajectories must move toward *S* = 0. This implies that:

$$\frac{dV}{dt} = SM \frac{dS}{dt} \tag{3.8}$$

From Equation 3.3, an equation for *S* and *dS/dt* can be determined. Using Equation 3.1 and substituting the expression for d^2O/dt^2 into Equation 3.8 gives:

$$\frac{dS}{dt} = \frac{d^2I}{dt^2} - \frac{F}{M} - \frac{D}{M} + \frac{C}{M}\frac{dO}{dt}\left|\frac{dO}{dt}\right| + \lambda\frac{dI}{dt} - \lambda\frac{dO}{dt} \tag{3.9}$$

If ***M***, ***C*** and ***D*** are the best estimates of the uncertain parameters *M*, *C* and *D*, and the assumption is made that *dS/dt* = 0, then the computed load expression for ***F*** is given by:

$$\mathbf{F} = \mathbf{M}\frac{d^2 I}{dt^2} - \mathbf{D} + \mathbf{C}\frac{dO}{dt}\left|\frac{dO}{dt}\right| + \mathbf{M}\lambda\frac{dI}{dt} - \mathbf{M}\lambda\frac{dO}{dt} \tag{3.10}$$

Ideal relay compensation is used for the lowest level sliding mode scheme where *F* is computed by:

$$F = \mathbf{F} + K sign(S) \tag{3.11}$$

where:

K = relay strength
$sign(S) = +1$ for $S > 0$
$sign(S) = -1$ for $S < 0$

This expression of *F* will give a new expression for *dS/dt* in terms of both the best estimates, ***M***, ***C*** and ***D***, and the uncertain parameters, *M*, *C* and *D*.

If the parameters were certain, Equation 3.9 would reduce to that representing the switching scheme for an ideal relay. In this case, *S* would go to zero and cause *E* to dissipate. This implies that:

$$\frac{dS}{dt} = -\frac{\mathbf{K}}{\mathbf{M}} sign(S) \tag{3.12}$$

With uncertain parameters, sliding mode will try to adjust the relay gain K so that dV/dt is always more negative than $\gamma|S|$ where γ is some negative number. Using Equation 3.8 and substituting dS/dt from Equation 3.9 and Equation 3.12 gives:

$$\frac{dV}{dt}=\left[\left[(\Delta C)\frac{dO}{dt}\left|\frac{dO}{dt}\right|-(\Delta D)+(\Delta M)\frac{d^2I}{dt^2}+\lambda(\Delta M)\frac{dI}{dt}-\lambda(\Delta M)\frac{dO}{dt}\right]-Ksign(S)\right]S \tag{3.13}$$

where:

$\Delta C = C - \mathbf{C}$
$\Delta D = D - \mathbf{D}$
$\Delta M = M - \mathbf{M}$

This can be represented by:

$$\frac{dV}{dt}=\left[(\Delta L)-Ksign(S)\right]S \tag{3.14}$$

with:

$$\Delta L=(\Delta C)\frac{dO}{dt}\left|\frac{dO}{dt}\right|-(\Delta D)+(\Delta M)\frac{d^2I}{dt^2}+\lambda(\Delta M)\frac{dI}{dt}-\lambda(\Delta M)\frac{dO}{dt} \tag{3.14a}$$

where:

$\Delta L = L - \mathbf{L}$
L = constant involving C, D and M
$\mathbf{L}$ = best estimate of constant involving $\mathbf{C}$, $\mathbf{D}$ and $\mathbf{M}$

This gives:

$$K=|\Delta L|-\gamma \tag{3.15}$$

This sliding mode control technique focuses on directing the system towards the command state. The method is useful for controlling linear systems using discontinuous control action, and it has also been adapted for the control of nonlinear systems with continuous control action. It has been determined that sliding mode control used as an adaptive control algorithm requires a good estimate of the system and its surrounding parameters, which are often not always easy to obtain for small subsea robots. Thus, it is essential for a good estimate of $|\Delta L|$ in order for this scheme to work.

Consider the case where C and M are certain but D is uncertain. In this case, the theoretical equations that are of particular interest include:

$$\frac{dS}{dt}=\frac{d^2I}{dt^2}-\frac{d^2O}{dt^2}+\lambda\frac{dI}{dt}-\lambda\frac{dO}{dt} \tag{3.16}$$

and:

$$\frac{d^2O}{dt^2}=\frac{1}{M}\left(F+D-C\frac{dO}{dt}\left|\frac{dO}{dt}\right|\right) \tag{3.17}$$

The best estimate for the force of the propulsion system must also be uncertain as there is one uncertainty in the equation. Thus:

$$F=C\frac{dO}{dt}\left|\frac{dO}{dt}\right|-D-M\lambda\frac{dO}{dt} \tag{3.18}$$

Figure 3.1 gives a phase portrait for this case. The appropriate code and data file for this case are given in Appendix A. The parameters are $M = 5$, $C = 5$, $\gamma = -25$ and $\lambda = 5$. Initially the small subsea robot is at rest with $O = 0$ and is commanded to go to $O = 5$. The disturbance load is given by:

$$D = \boldsymbol{D} + \Delta D \sin\left[\frac{2\pi}{T}\right]t \tag{3.19}$$

D is the best estimate for D with ΔD accounting for the uncertainty. The parameters are such that $\boldsymbol{D} = 1$, $\Delta D = 1$ and $T = 1$. As can be seen in Figure 3.1, the small subsea robot does home in on the command depth but it is affected by the uncertain component of D.

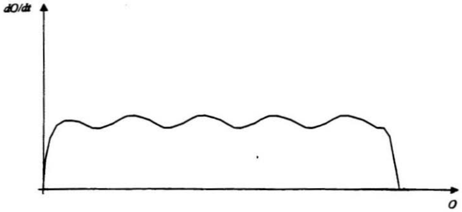

Figure 3.1 Phase portrait with uncertain parameters

Considering the case where all parameters are certain, there is no upper bound for the sliding mode mechanism to work with. Thus, there is no error associated with the $|\Delta D|$ term. Figure 3.2 shows a phase portrait for this case. The appropriate code and data file for this case are also given in Appendix A. It is illustrated that the small subsea robot now adapts continuously to changes in *D*.

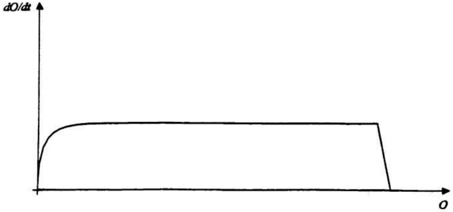

Figure 3.2 Phase portrait with no uncertain parameters

For the case of a small subsea robot, there is a sudden drop off. This can be explained by considering the following equations:

$$\frac{dS}{dt} = -\frac{dL}{dt} - \lambda L \tag{3.20}$$

with:

$$L = \frac{dO}{dt} \tag{3.21}$$

and:

$$\frac{dS}{dt} = -\frac{K}{M} sign(S) = \pm \frac{K}{M} \tag{3.22}$$

Generally *sign(S)* is +1 as *S* is greater than zero, thus:

$$\frac{dS}{dt} = -\frac{K}{M} \tag{3.23}$$

However, for the drop off case, it can be shown that *sign(S)* has a value of -1 as *S* is less than zero, thus:

$$\frac{dS}{dt} = +\frac{K}{M} \tag{3.24}$$

When the value of *S* becomes negative, the phase portrait flips and heads in the opposite direction. In addition, the apparent height of the phase portrait, as shown in Figure 3.2, is a representation of Equation 3.24 divided by λ. When the parameter values substituted into Equation 3.24 are K = 25, M = 5 and λ = 5, this results in an apparent height with a value of unity as presented below.

$$\frac{(dS/dt)}{\lambda}=\frac{K}{M\lambda}=\frac{25}{(5)(5)}=1 \tag{3.25}$$

3.1.5 Neural Networks

Neural networks can be used to construct fits to either supervisory or drive-level control strategies [10]. Drive level control is considered herein. A neural network mapping generally consists of three layers of neurons, namely an input layer, a middle or hidden layer and an output layer, as shown in Figure 3.3. Both the input and hidden layers contain one bias neuron that has an input of unity. A nonlinear squashing function, *f*, processes the summed inputs contained in the hidden layer of neurons. The sigmoidal or S-shape that is used to represent this process is given by:

$$f(a)=\frac{1}{1+e^{-a}} \tag{3.26}$$

This function is zero for large negative values of a and unity for large positive values of a. The information flows through the network from input to output.

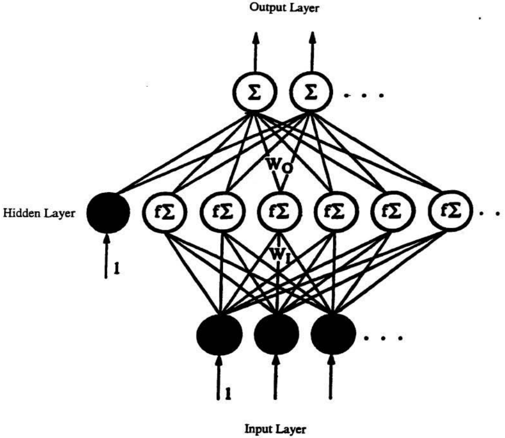

Figure 3.3 Neural network mapping

The mapping equation for a three layer network with only one hidden neuron is represented by:

$$O_N = W_{BO} + W_{XO} f(W_{XI} I_N + W_{XJ} J_N + W_{BX}) \tag{3.27}$$

This equation can be used to show that in an O_N versus $I_N J_N$ plot, weights can be used to shift both horizontally and vertically features generated by the squashing functions.

Inspection of Equation 3.27 shows that W_{BO} can be used to shift an O_N versus $I_N J_N$ plot vertically, while a positive W_{BO} will move the plot up and a negative W_{BO} will move the plot down. A weight which multiplies an *f* function determines its contribution to the O_N versus $I_N J_N$ plot. Again, these weights can be either positive or negative. If one of the weights has a value of zero, it will remove its *f* function entirely.

The weights inside the *f* function are more difficult to explain. Consider the first function in the Equation 3.27:

$$f(W_{XI} I_N + W_{XJ} J_N + W_{BX}) \tag{3.28}$$

This will create a feature in the plot where its arguments $W_{XI}\, I_N + W_{XJ}\, J_N + W_{BX}$ is zero. This is the point where the *f* function itself is one-half or midway between its two limits, which are zero and unity.

Consider the case where W_{BX} is a large negative number and J_N is zero. In this case, on the I_N axis, the feature is defined by:

$$W_{XI} I_N + W_{BX} = 0 \tag{3.29}$$

$$I_N = -\frac{W_{BX}}{W_{XI}} \tag{3.30}$$

If the W_{XI} is a small positive value then it will appear at a larger positive value of I_N, while a small negative value will appear at a large negative value of I_N.

If W_{XO} is positive, a positive value of W_{XI} will cause a feature to grow in the positive I_N direction, while a negative value of W_{XI} will cause a feature to grow in the negative I_N direction. Small values of W_{XI} spread the feature, while large values of W_{XI} steepen it. Similar statements can also be made about W_{XJ}.

Figure 3.4 shows a simple map generated by squashing functions. It is actually a relay with deadband, with an ideal relay in the I_N direction and proportional with saturation in the J_N direction. The appropriate code and data file for this are given in Appendix A.

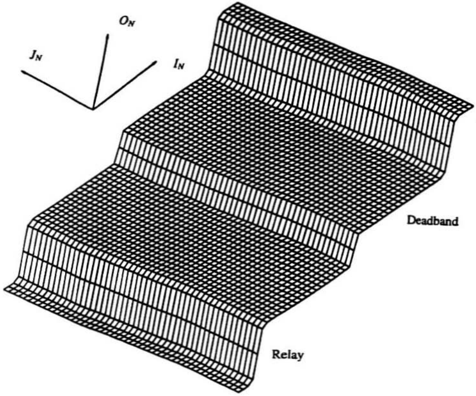

Figure 3.4 Simple neural network map

Figure 3.5 shows an extremely complex map generated by only three squashing functions with appropriate code and data file given in Appendix A. Many functions would allow construction of almost any map that could be imagined.

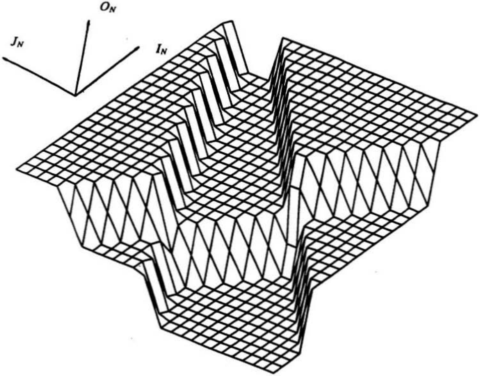

Figure 3.5 **Extremely complex neural network map**

To construct the map for a neural network controller, its weights could be adjusted by iteration until the output from the system matches the desired output. If the basic map shape is known, then the controller weights can be adjusted until its map matches the known shape. In conclusion, a neural network has the capability to represent extremely complicated control strategies.

3.1.6 Fuzzy Logic

Fuzzy logic can be used to construct fits to either supervisory or drive level control strategies [10]. Drive level control is considered herein.

The concept of fuzzy logic uses a fuzzy set where linguistic concepts are treated mathematically and human thought processes are replicated. The experience of a human operator is required and the procedure uses such linguistic terms as *large*, *medium* or *small* to assign values to the variables. The linguistic terms are treated mathematically in order to develop a set of IF-THEN Rules.

For example, consider the case for Proportional Derivative Control (PD) with given values of error, E, error rate, dE/dt, and the control signal, S, where membership functions need to be determined using standard fuzzy logic manipulations. The membership functions contain negative inputs (N), zero inputs (Z), and positive inputs (P).

Each fuzzy logic statement or rule would have a format such as:

"If E is negative (N) and dE/dt is negative (N),
then the control signal, S, should be double negative (NN)".

Membership functions can be used to quantify the degree to which a parameter belongs to a particular class. The interpolation or decision process can be eliminated when the intelligent experience of a human operator is used to generate the rules and membership functions. Membership function shapes can include triangles, trapezoids and smooth bell shapes, with neighboring membership functions permitted to overlap. Previous input information is used to develop the membership functions to help the operator generate the fuzzy logic rules and other membership functions. Numerical simulations can be used to study how the control strategy for the small subsea robot will proceed.

For a specific set of membership functions such as E and dE/dt, manipulation of each fuzzy logic rule produces a contribution to an overall fuzzy range of the control signal, S. For this particular manipulation, it is assumed that the rule is an IF-AND-THEN Rule structure, where the minimum membership value to the left of THEN will dominate. If there was an IF-OR-THEN Rule, the maximum membership value would dominate. Crisp depth is obtained from the overall range using a process known as defuzzification where determining the centroid of area is a commonly used defuzzification scheme.

In some cases, the first run of the fuzzy logic scheme does not agree with the direct predictions of the human operator. Thus, the human operator must assist in fine tuning the logic code by adjusting membership function breaking points and shapes. Tuning can be accomplished by specifying new rules, deleting old rules, or by changing the value of the scaling parameters which define the membership functions.

Fuzzy logic is a versatile control strategy. It is most simply described as a set of linguistic IF-THEN Rules, which can be compared to rules-of-thumb for human operations and thought processes. Unlike expert systems, fuzzy logic does not require that the outputs be determined for each and every input. The output can be determined through the membership function manipulations.

3.1.6.1 Linear Fuzzy Logic

Membership functions for a PD controller for *E* and *dE/dt* are given in Figure 3.6. Both *E* and *dE/dt* range from -5 to +5 while the control signal, *S*, ranges from -9 to +9. It is constructed to make four divisions with five points for both *E* and *dE/dt* such that the positioning of the values of *E* and *dE/dt* would be -5, -2.5, 0, +1, +2.5 and +5. The first combination would be *E* = -5 and *dE/dt* = -5, the second combination would be *E* = -5, *dE/dt* = -2.5, and so on, such that there would be 5*5 combinations for a total of twenty-five possible values of the control signal, *S*.

For clarity, to obtain the results as indicated in Figure 3.6, consider the case where $E = 0$ and $dE/dt = -2.5$. This is the second case in Figure 3.6 and indicated by the arrows. For this case with $E = 0$, then N = 0%, Z = 100% and P = 0%. For a value of $dE/dt = -2.5$, then N = 50%, Z = 50% and P = 0%. Thus, nine combinations must be considered.

Recall that membership functions take the minimum value as its final result. Thus for the cases NN, NZ and NP, there is no result as N = 0% when $E = 0$. Now, consider when Z = 100%, then ZN = 50%, ZZ = 50% and ZP = 0%, which results in two contributions. Finally, when P = 0%, there is no result for the remaining terms PN, PZ and PP. Performing defuzzification, the centroid of the area for the case in point, results with a value of –1 for the control signal, S.

This procedure is followed for all combinations for the linear case. For Figure 3.6, when $E = 0$, the results for the control signal, S, are –2, -1, 0, +1, +2. The case for –1 was detailed above. These values are inputs for the appropriate code given in Appendix A, corresponding to the case when $E = 0$, which is the third point of the four divisions.

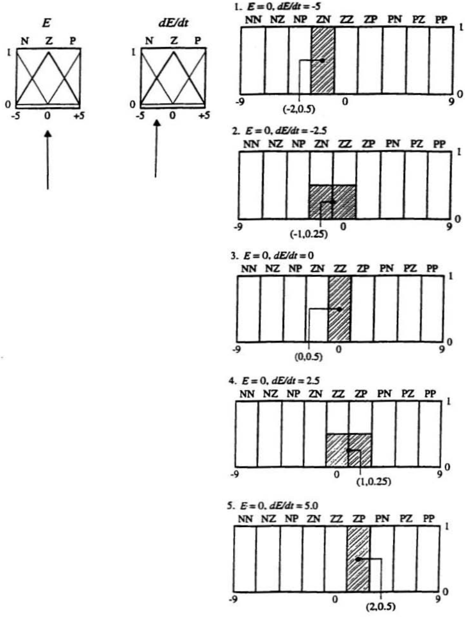

Figure 3.6 **Membership functions for linear map**

From Figure 3.7. it is visible that no nonlinear features occurred as the plot is flat in nature. This linear feature results from the fact that the membership functions for N and P for *E* and *dE/dt* contained only one flat portion and one sloping linear portion. The value of Z for both *E* and *dE/dt* contained two sloping linear portions from -5 to a peak at the top and then sloping back to +5. thus the value was never zero except at -5 and +5. The results show that for the majority of the cases, three membership functions inputs have some percentage of both *E* and *dE/dt*. The results vary for the percentages as they were not always 100% NN. The appropriate code and data file are given in Appendix A.

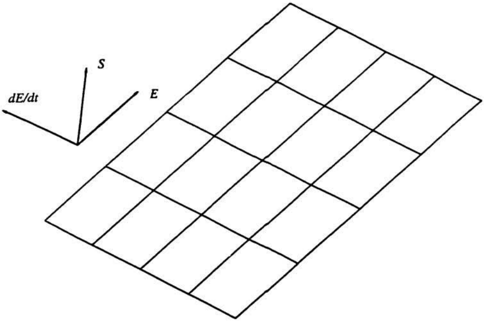

Figure 3.7 Linear fuzzy logic map

3.1.6.2 Nonlinear Fuzzy Logic

Membership functions for another PD controller for *E* and *dE/dt* are given in Figure 3.8. Both *E* and *dE/dt* range from -5 to +5 while the control signal, *S*, ranges from -9 to +9. It is constructed to make eight divisions with nine points for both *E* and *dE/dt* such that the positioning of the values of *E* and *dE/dt* would be -5, -3, -1, 0, +1, +3 and +5. The first combination would be $E = -5$ and $dE/dt = -5$, the second combination would be $E = -5$, $dE/dt = -3$, and so on such, that there would be 9*9 combinations for a total of eighty-one possible values of the control signal, *S*. The same procedure was followed as outlined in Section 3.1.6.1.

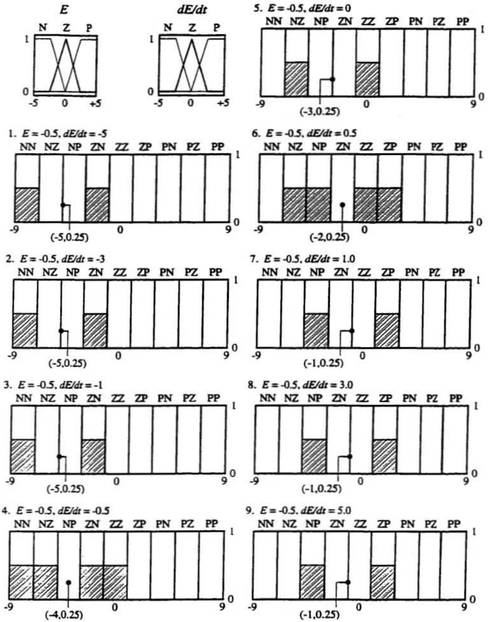

Figure 3.8 **Membership functions for nonlinear map**

From Figure 3.9. it is apparent these membership functions produced nonlinear features or steep jumps within the plot. This is due to the many locations where the control signal, *S*, was either 100% NN, 100% PN, 100% ZN, 100% ZZ. 100% ZP. 100% NP or 100% PP. This resulted from the two flat portions of the membership functions for N and P for both *E* and *dE/dt* with only one sloping linear portion. The value of Z for both *E* and *dE/dt* was mainly zero due to two flat portions with a value of zero with two linear sloping portions. The results show that for the majority of the cases, two of the inputs of the membership function were 0% with the other being 100% for both *E* and *dE/dt*. The nonlinear features result from local concentration of membership functions. The appropriate code and data file are given in Appendix A.

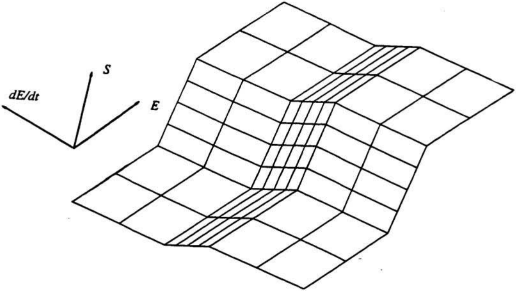

Figure 3.9 Nonlinear fuzzy logic

3.2 Supervisory Control Strategies

3.2.1 Neural Networks

Mechanically, neural network fits to supervisory strategies are no different than fits to drive level strategies. For example, consider a supervisory strategy that would pick a safe depth for a small subsea robot to drive during a storm. Inputs into the network would include the wave period and the wave steepness, with the output being the safe depth.

The supervisory experience of human operators and/or the simulation of the small subsea robot in waves could be used to generate data to train the network. Once trained, it will give a safe depth for any wave period and steepness within the range of training data.

3.2.2 Fuzzy Logic

Fuzzy logic fits to supervisory strategies are similar to the fits to drive level strategies. For the depth selector case, membership functions would have a format such as:

> "If wave period is large and wave steepness is large,
> then safe depth would be very large".

As with drive level control, a human operator would probably have to fine tune the logic before it could be used on the small subsea robot.

3.2.3 Subsumption

Subsumption is a control strategy that was developed by Rodney Brooks and his colleagues at the Massachusetts Institute of Technology [15]. Each layer in subsumption is a behaviour where layers or behaviours operate independently of each other. The top layers have higher priority and take over or subsume control from lower layers when conditions permit.

Brooks believes that human intelligence is far too complex to be understood, as the process of intelligence is broken down into sections with the interfaces between them impossible to duplicate. He suggests that the thought process be broken down into a number of levels, each of which has relatively simple intelligence, and then build these increments up step by step to the capability of an intelligent system like that of the human brain [15]. Each intelligent system is constructed of independent, parallel activity layers which all connect directly to the outside environment through perception and action.

Consider the example where subsumption would be used to keep a small subsea robot from colliding with a hill in the ocean floor. A lower layer would try to keep the robot a certain distance from the bottom of the ocean floor. However, the robot may approach an underwater hill which would permit the higher layers to subsume control from lower layers in order to get the robot above the hill without incurring any damage. Once the robot was clear of the obstacle, the higher layers would pass the control back to the appropriate lower layer so that the robot would continue on its original path.

This layered type of control strategy has been used in the application of mobile robots, which can operate independently in a closed environment. The subsumption architecture is broken into three layers, namely avoidance, wandering and exploration. Every layer is built on top of existing layers where lower layers never rely on the existence of the top layers. These subsea robots can operate autonomously in a complex changing environment mimicking insect-like intelligence.

In subsumption, the surroundings determine the nature of control as the higher layer behaviours are activated by the surroundings. The subsea robots using subsumption control are said to have insect-like intelligence, as they react to the surroundings much like that of insects. This control strategy provides robustness, as adding extra behaviours does not change existing behaviours. Subsumption is not computationally expensive and the coding for its use is modest.

3.3 Control Strategy Selection for ANNE

The strategy selected for use in ANNE is a two level switching error-driven control strategy which employs a depth error band. Outside the band, one level moves ANNE towards the band surrounding the command depth, creating a depth error-driven control strategy. This strategy is based on switching as discussed in Section 3.1.2.

The other level is used when ANNE is within the band. This attempts to bring ANNE to a stop within the band using a buoyancy error-driven control strategy. Within the band, readings are substituted into the depth equation of motion to estimate buoyancy. The use of a system governing equation as detailed in Section 5.1.5 makes the second level resemble a computed load strategy as discussed in Section 3.1.3.

This control strategy is selected because the simulation suggests that it demonstrates an excellent combination of error-driven and computed load control. In addition, it is a control strategy that is compatible with the switching hardware on ANNE, most of which is supplied by NO MAD as discussed in Section 4.4.1.

Chapter 4

Autonomous Pneumatic Nautical Explorer

The first NO MAD prototype has a number of areas which require improvement. Even though NO MAD is modular in construction, all of the electrical components are hard-wired into their positions, making it difficult to modify the setup. Similarly, the majority of components are bolted or screwed in place. As a result, assembly of NO MAD is time consuming.

NO MAD uses five float switches that are equally spaced in the vertical direction of the ballast tank. These switches are employed to sense the water level in the ballast tank, as required by the depth control strategy. Due to the discrete nature of the information, stable operation of NO MAD is impossible and limit cycles exist around the command depth. To overcome this, ANNE uses an accelerometer instead of the float switches [16].

One of the major goals of the present work was to redesign NO MAD such that all of the components would permit easy assembly. For ease of obtaining parts, the majority of the components of the first NO MAD prototype were utilized in ANNE but more efficiently. For simplification, ANNE is modular in construction and requires no tools for assembly. The detailed fabrication drawings are given in Appendix B. ANNE was designed for missions in shallow water to depths of 100 m. It has a mass of 50 kg and an overall height of 1.2 m. ANNE requires at least two people and an overhead crane for deployment and recovery. An overall illustration of ANNE is shown in Figure 4.1.

Figure 4.1 Autonomous Pneumatic Nautical Explorer

ANNE has holes at the top and bottom of its ballast tank. Pneumatic pistons mounted outside the ballast tank are used to open or close the holes. To make ANNE sink, water is allowed to enter the ballast tank as both holes are open. To make ANNE surface, high-pressure compressed air is used to purge water from the ballast tank with the top hole closed and the bottom hole open.

The main components consist of an air-water ballast tank, two divers bottles, of which only one is used during a mission, a Z-WORLD Rugged Giant C-Programmable Miniature Controller (controller) for control, batteries for power during missions, and pneumatic components for operation of the pistons for the ballast tank. The electrical and pneumatic schematics of ANNE are given in Appendix C. There is also ample space for a payload.

The two divers bottles are used as the source of high-pressure compressed air for the ballast tank and the pistons. Pneumatic valves are used to control the high-pressure compressed air flows. These pneumatic valves are solenoid activated and pilot pressure operated.

4.1 Structure and Shell

The structure and shell of ANNE consists of five cylindrical plastic tubes that are held together by an aluminum frame at the top. Figure 4.2 shows the center cylinder and the two aluminum frames. Figure 4.3 shows the top aluminum frame before it is attached to the center cylinder. Figure 4.4 depicts the bottom aluminum frame that is attached to the bottom of the center cylinder that is used to hold the instrumentation boxes. This center cylinder, which is the longest of the five tubes at 1.2 m, houses the ballast tank and acts as a support for the four remaining tubes as can be seen in Figure 4.2.

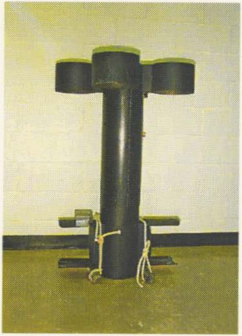

Figure 4.2 Center cylinder with both frames

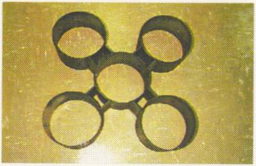

Figure 4.3 Top frame

Figure 4.4 Bottom frame

4.2 Ballast Tank

Figure 4.5 shows the ballast tank with the pneumatic pistons attached. The ballast tank, taken from NOMAD, was designed and sized from previous work by Lu [2]. Specific parameters of the ballast tank are given in Section 5.1.6, Table 5.1. Figure 4.6 shows the pneumatic pistons together with the ballast tank. They are double acting pistons meaning that high-pressure compressed air is used to move them back and forth. There is another type of pneumatic piston known as single acting that uses air pressure to extend the actuator rod with a spring to retract it. These were not used in ANNE.

Figure 4.5 Ballast tank

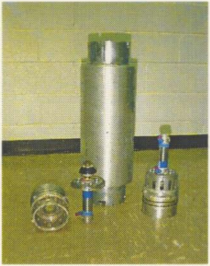

Figure 4.6 Ballast tank with pistons

4.3 Outside Tubes

The outside tubes consist of two intermediate length cylindrical plastic tubes at 76.5 cm and two shortest length cylindrical plastic tubes at 56 cm.

4.3.1 Intermediate Length Tubes

Two intermediate length cylindrical plastic tubes are used to hold the smaller size divers bottles that supply the high-pressure compressed air to the ballast tank. These tubes have been designed to be able to hold regular size divers bottles, however, they are not used due to the weight restrictions. The maximum pressure supplied by one of the divers bottle is 200 bar (3000 psi) with a capacity of 300 stpL. A first pressure regulator followed by a second pressure regulator are required to limit the operation pressure of ANNE to 4 bar.

The divers bottles are held in place within the cylinders by styrofoam rings. Figure 4.7 shows the intermediate length tubes and the small divers bottles before assembly. These tubes are also able to house payloads.

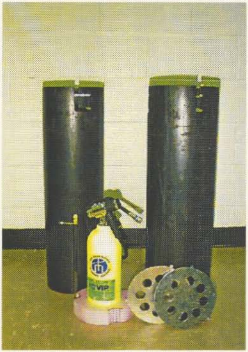

Figure 4.7 Intermediate length tubes

4.3.2 Shortest Length Tubes

The remaining two cylindrical plastic tubes of the shortest length contain styrofoam rings that are used for roughly tuning buoyancy as the ballast tank is used for fine tuning buoyancy. Figure 4.8 shows these tubes and the styrofoam rings before assembly.

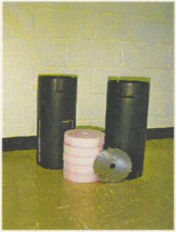

Figure 4.8 Shortest length tubes

4.4 Instrumentation Boxes

There are three instrumentation boxes and they can be seen in Figure 4.1 of the overall photograph of ANNE.

4.4.1 Controller Box

Figure 4.9 shows the largest of these boxes with an outside diameter of 27 cm and a height of 14.1 cm. This box houses a Z-WORLD Rugged Giant C-Programmable Miniature Controller, an *ICSensors* pressure transducer (Model 114) and an *ICSensors* accelerometer (Model 3145). Appendix D gives specification sheets from the manufacturer on these three devices together with the specifications sheets for *Subconn* connectors and the necessary components from FESTO.

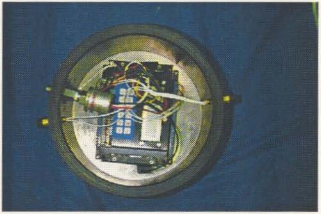

Figure 4.9 Controller box

The sensors were chosen to be compatible with the controller. Both require 24V DC to operate and the controller, powered by the batteries, can supply this. Since they draw low current, the devices should not drain the batteries. The current drawn in milliAmps (mA) from the batteries would be the sum of that needed by the controller and that needed by each of the sensors. The power drawn by the controller is far greater than that drawn by the sensors. The controller, which reads sensors in milliVolts (mV), requires a very small voltage from the sensors.

The 15 psi pressure transducer, from *ICSensors*, has a calibration factor of 2 mm per mV and is sufficient for the deep tank tests. A plot of the calibration factor for the pressure transducer is given with the specification sheet in Appendix D. This results in a depth accuracy of 2 mm, which is an acceptable level. The 100 psi pressure transducer, that would be used at sea, has a calibration factor of 7 cm per mV, which is also reasonable. The accelerometer, also from *ICSensors*, is rated at 1000 mV per gravity, *g*, gives low precision as the *g* levels are very low during the deep tank tests. However, this precision is adequate for the experimental purposes of the ANNE deep tank tests. The calibration results for the accelerometer are also given with the specification sheet in Appendix D.

A component layout of the controller, purchased from Z-WORLD, is shown in Figure 4.10. The controller has the capability to receive digital inputs from limit switches, but this was not needed for ANNE. It also has the capability for analog inputs from pressure transducers and accelerometers as utilized in ANNE. These are referred to as universal inputs in the schematic. Digital outputs for operating solenoid valves, are used to operate pneumatic valves for controlling flow into and out of the air-water ballast tank. The controller also has the capability to output one analog signal, and can operate two normally closed-normally open (NC - NO) relays, which are not used in this work. These digital inputs and outputs can be seen in Figure 4.11.

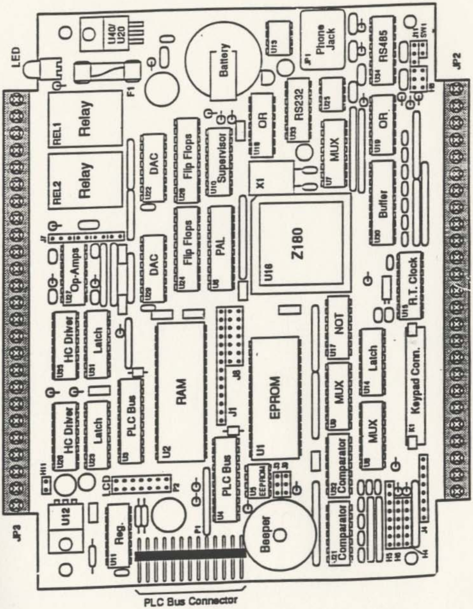

Figure 4.10 Component layout of controller

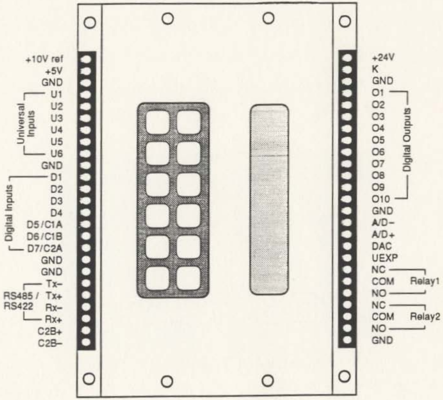

Figure 4.11 Component layout of controller illustrating inputs and outputs

4.4.2 Battery Box

The power to the controller is provided by three DC batteries (two 7.2V and one 8.4V) in series. Together, they have a voltage rating 22.8 V, which is sufficient to power the controller, and a current rating of 1800 mAh. The controller itself draws 220 mA. The calculation for the power requirements of the three batteries is given in Appendix E

(Sample Calculation 4.1). This illustrates that for a mission of ANNE the batteries should last for four hours. The batteries are housed in the smallest of the instrumentation boxes, shown in Figure 4.12. This box has an outside diameter of 27 cm and a height of 5.8 cm. A 3 Amp (A) fuse is inserted in series to protect the controller from a short circuit external from the battery box.

Figure 4.12 Battery box

4.4.3 Pneumatic Box

Figure 4.13 shows the third box, which has an outside diameter of 27 cm and a height of 8.9 cm. This box houses the two types of pneumatic valves that were used. Figure 4.14 shows a schematic of the valve used to control flow of high-pressure compressed air into the ballast tank when it is necessary to purge water from the ballast tank to make ANNE rise. The pneumatic valve, as shown in the schematic, would allow air to vent from the ballast tank. This is prevented by installing a check valve in the pneumatic line to the ballast tank. With the solenoid on the right of the schematic activated, the flow paths on the right move over allowing a flow path from the high-pressure compressed air to the ballast tank to be created which purges the ballast tank.

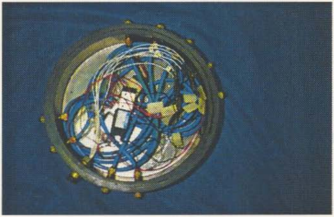

Figure 4.13 Pneumatic box

The second pneumatic valve that is used is shown schematically in Figure 4.15. As shown, the valve would create a flow path from the high-pressure compressed air to one end of a pneumatic piston and a vent from the other end. With the left solenoid deactivated and the right solenoid activated, the flow paths on the right would move to the right and create a reverse set of flow paths. With the right solenoid deactivated and the left solenoid activated, the original flow paths shown would reappear.

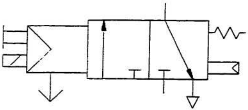

Figure 4.14 Schematic of pneumatic valve for air supply to ballast tank

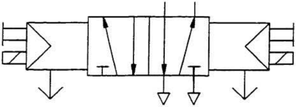

Figure 4.15 Schematic of pneumatic valve for piston operation

Pneumatic and electrical bulk-head connectors are used to connect the three instrumentation boxes to each other and to the pistons and the ballast tank. These can be seen in Figure 4.9, Figure 4.12 and Figure 4.13.

Aluminum covers are used to close the boxes and are designed so that screws are not used as they are held together by the principle of suction. Each box has a small hole in one cover allowing air to be removed through suction by using a vortex blower in reverse operation [17]. Duct tape is used to cover the appropriate hole after sufficient suction, or negative pressure, has developed within each instrumentation box. Two O-Rings are present in the aluminum covers (one in the top and one in the bottom) that assists in maintaining the seal, once proper lubrication grease is applied to the O-Rings.

The instrumentation boxes are the only structural components subjected to high-pressure which could create hoop stresses. This type of box has been pressurized to approximately 10 bar or 100 m [18] with no problems noted.

4.5 Simple Twist Lock Mechanism

To assist in the modular construction of ANNE, the elimination of bolts and screws is essential. This is done by the use of a simple twist lock mechanism where the component fits into place and secured by a simple twist. This appears in the majority of the components of ANNE.

Consider Figure 4.2 which illustrates the center cylindrical tube, and the top and bottom aluminum frames. Slots in the cylindrical tubes and lugs in the aluminum frames allow for a tight fit and a reliable means of support for both frames. A close inspection of Figure 4.3 will permit a view of some of these lugs.

This simple twist lock mechanism is also employed in the design of the ballast tank. This permits the connection of the pneumatic piston support to the ballast tank. This design can be seen in Figure 4.6. The slots are in the support for the pneumatic pistons, at the top and bottom of the ballast tank, and the lugs are placed in the housing of the pneumatic pistons.

The simple twist lock mechanism is also used to hold the divers bottles in place in the intermediate length tubes. In Figure 4.7, it can be seen that the slots exist in the cylindrical tubes and the lugs are present in the support that holds the divers bottle. A support is also placed on top of the divers bottle to prevent its loss during a mission. There are also slots for positioning these tubes on to the top aluminum frame.

For the smallest of the cylindrical tubes, the simple twist lock mechanism is used to hold the styrofoam in place, which can be seen in Figure 4.8. The slots are in the cylindrical tubes, while the lugs are in the support. There are also slots for positioning these tubes on the top aluminum frame.

4.6 Cost Estimate

A cost estimate of the overall development of ANNE is presented in Table 4.1.

Table 4.1 Cost Estimate of ANNE

Component	Company	Qty	Unit Cost ($)	Rounded Cost ($)
Accelerometer	*ICSensors*	1	375	375
Batteries (Ni-Ca)	Signal Hobbies	3	30	90
Controller	Z-WORLD	1	550	550
Divers Bottles	Sub Aqua	2	195	390
Electrical Bulkhead Connectors	*Subconn*	2	177	355
Flow Regulator	FESTO	1	30	30
Framework/Tubes and Shopwork	MUN Technical Services			1000
Pneumatic Connectors	TubeCraft	9	20	180
Pneumatic Piston	FESTO	2	100	200
Pressure Transducer	*ICSensors*	1	385	385
Pressure Regulators	FESTO	2	25	50
Pneumatic Valve	FESTO	2	150	300
Pneumatic Valve	FESTO	1	100	100
Reducer	Sub Aqua	1	520	520
Quick Disconnect Low Pressure Line	Sub Aqua	1	90	90
Miscellaneous Components and Shopwork		N/A	N/A	400
TOTAL				**$5015**

These values are rounded to the nearest dollar. The total cost is calculated to be approximately $5000, which is relatively inexpensive for this subsea robot design. If ANNE is to be made in mass production, this cost can be reduced. The potential cost of losing ANNE during an at sea mission can be seen as expensive.

Chapter 5

Simulation

The success or failure of ANNE depends on the length of time the high-pressure compressed air lasts as this determines the mission duration. Critically, this depends on the depth control strategy employed. Thus, it became essential to develop a simulation to test the depth control strategy employed by ANNE.

5.1 Parameter Determination

5.1.1 Volumetric Flow Rate

A simulation trial lasts about three minutes of real time. During this time, only a small amount of high-pressure compressed air is consumed. This implies that the pressure is fixed during a trial. The pressure in the divers bottle creates choked flow that causes the mass flow rate, *dM/dt*, from the high-pressure compressed air to be constant and insensitive to ballast tank conditions. For clarity, the volumetric flow rate of water flowing into the ballast tank is denoted as Q_W, which will be a positive quantity. When the ballast tank is being purged with high-pressure compressed air, Q_W will be a negative quantity. Thus, it is assumed that when a flow of high-pressure compressed air is released to force water out of the ballast tank through the bottom hole, the outward flow of water, Q_W, is negative with no storage permitted.

The volumetric flow rate of water, Q_W, from the ballast tank is calculated by:

$$Q_w = \frac{-\frac{dM_A}{dt}}{\rho} \tag{5.1}$$

where:

M_A = mass of high-pressure compressed air from divers bottle to the ballast tank
ρ = density of air in the ballast tank

The density of air in the ballast tank, ρ, is a function of the vertical submergence depth of the small subsea robot, *R*. For ANNE, *dM/dt* is set to a level that makes Q_W approximately equal to -1.0 L/s when flow is to standard atmosphere. With the cross-sectional area of the ballast tank fixed, this Q_W will permit purging of the ballast tank at a reasonable rate. Specific parameters of the ballast tank are presented in Section 5.1.6, Table 5.1.

The volumetric flow rate for air of 1.0 L/s can be obtained from ANNE when the divers bottles are fully charged. Gas dynamics could be used to estimate the pressure drop in the divers bottle as well as the volumetric flow rate. This is not done in the present stages of ANNE design.

5.1.2 Driving Pressure

With both top and bottom holes of the ballast tank open, the positive Q_W upward through the ballast tank is governed by the resistance created at the bottom. The given flow through the ballast tank creates a greater pressure drop at the bottom, as the density of the flowing fluid (water), σ, is greater than air. For steady flow, the orifice flow equation [19] is given by:

$$Q_W = C_o H \sqrt{\frac{2P}{\sigma}} \tag{5.2}$$

where:

Q_W = volume flow rate of water through the orifice
C_o = head loss coefficient
H = flow area
P = driving pressure
σ = density of the flowing fluid (water)

Manipulation of Equation 5.2 gives:

$$P = \frac{\sigma}{2}\left(\frac{Q_W}{C_o H}\right)^2 \tag{5.3}$$

The maximum overall pressure head is equal to the height of the ballast tank, which is 500 mm. The pressure driving free flow up through the ballast tank cannot be greater than the hydrostatic pressure corresponding to the height of the ballast tank.

From fundamental fluid mechanics [20], the pressure-elevation relationship is given by:

$$\Delta P = \sigma g(\Delta h) \tag{5.4}$$

where:

ΔP = change in pressure
g = acceleration due to gravity
Δh = change in elevation

With the water level measured positive downward from the center of the ballast tank and denoted by Y, then the neutrally buoyant point is taken as $Y = 0$. If both top and bottom holes of the ballast tank are open and Y is known, the change in driving pressure using Equation 5.4 can be calculated by:

$$\Delta P = \sigma g(T + Y) \tag{5.5}$$

where:

T = half height of the ballast tank
Y = water level measured positive downward from the center of the ballast tank

Substituting the applicable values given in Section 5.1.6, Table 5.1 into Equation 5.5, results in $\Delta P = 4905$ Pa (Sample Calculation 5.1, Appendix E). This causes the pressure of the high-pressure compressed air in the ballast tank to be approximately equal to the pressure in the water just outside the top of the ballast tank. This implies that the pressure driving the water flow through the bottom hole would be equal to the hydrostatic pressure corresponding to the height of the air cavity. With both hole sizes fixed, the average water flow Q_W into the ballast tank is approximately equal to +1.0 L/s. This results in equal filling and purging rates as the magnitudes are the same.

$$|Q_{fill}| = |Q_{purge}| = 1.0\ L/s \tag{5.6}$$

The equation for head loss, h_L is given by:

$$h_L = \frac{2T\rho}{\sigma} \tag{5.7}$$

Substituting the values given in Table 5.1 into Equation 5.7 gives $h_L = 0.5$ mm (Sample Calculation 5.2, Appendix E). Thus, it can be shown that, in shallow water, no more than 0.5 mm of pressure head could result from high-pressure compressed air flow through the top hole of the ballast tank.

The equation for the purge period, t_p, is given by:

$$t_p = \frac{AT}{Q_w} \tag{5.8}$$

where:

A = cross-sectional area of the ballast tank

Substituting the values that are listed in Section 5.1.6, Table 5.1 into Equation 5.8 results with $t_p = 6.25$ s (Sample Calculation 5.3, Appendix E).

The flow through the bottom hole is assumed to be steady. An inertance and resistance orifice flow model would give the bottom hole volume flow rate more accurately, but such a model is beyond the scope of this work. With very high-pressure compressed air used to create a strong air jet through the top hole, choked flow through the top hole would result accompanied by strong shock waves. This type of flow is difficult to model, and seldom used, thus it was not used in the present work.

5.1.3 Conservation of Mass

A conservation of mass equation for the high-pressure compressed air in the ballast tank can be used to take air compressibility into account [19]. This is given by:

$$\frac{d(\rho V_a)}{dt} = \rho Q_{in} - \rho Q_{out} \tag{5.9}$$

where:

V_a = volume of air in the tank
Q_{in} = flow rate of air into ballast tank from the divers bottles
Q_{out} = flow rate of air out of the ballast tank through the top hole

Manipulation of Equation 5.9 gives:

$$\frac{V_a}{K}\frac{dP}{dt} + \frac{dV_a}{dt} = Q_{in} - Q_{out} \tag{5.10}$$

A measure of air compressibility, K_a, is known to be calculated by:

$$K_a = \rho a^2 \tag{5.11}$$

with:

$$a = \sqrt{kRT} \tag{5.12}$$

For isothermal compression-expansion, K_a is equal to the ballast tank pressure as the value of $K_a = 1.0$. For isentropic compression-expansion, it becomes k times the ballast tank where $k = 1.4$ is the specific heat ratio. For ANNE, it is assumed that K_a is between these two limits.

Equation 5.10 shows that compressibility adds a period to the dynamics that are small relative to the ballast tank filling and purging periods. This would have little or no effect on performance and simulation runs with and without compressibility confirms this result.

5.1.4 Buoyancy

The rate of change of the water level Y in the tank is given by:

$$\frac{dY}{dt} = \frac{-Q_W}{A} \tag{5.13}$$

From Equation 5.2, Equation 5.6 and Equation 5.13, this allows for a calculation for Q_W and Y by integration.

From fundamental fluid mechanics [20], the weight force is given by:

$$W = \sigma g V_f \tag{5.14}$$

where:

W = weight force
V_f = volume of fluid

Substitution of the applicable parameters into Equation 5.14 gives the calculation for buoyancy force on the small subsea robot, **B**:

$$B = \sigma g (AY) \tag{5.15}$$

The maximum absolute value of **B/g** is denoted as **M_{max}**. This assumes that **Y** is given the maximum value of **T**. This is calculated by:

$$M_{max} = \frac{B}{g} = \frac{\sigma g A T}{g} = \sigma A T \tag{5.16}$$

This value is **M_{max} = 6.25 kg** when the parameters given in Section 5.1.6, Table 5.1 are substituted into Equation 5.16 (Sample Calculation 5.4, Appendix E).

ANNE has a basic mass of 50 kg when neutrally buoyant. The added mass is estimated to be 25 kg. An explanation for this value is detailed in Section 5.1.6. Both of these components are included in **M**, which is 75 kg. If **B** is increased, then **M** would decrease by **B/g**.

5.1.5 Governing Equation of Motion

With B known, the vertical submergence depth of the small subsea robot, R, can be computed from the equation of motion that is derived from Newton's Second Law and given by:

$$M\frac{d^2R}{dt^2} = -B - \frac{C_D A_f \sigma \frac{dR}{dt}\left|\frac{dR}{dt}\right|}{2} \tag{5.17}$$

where:

M = inherent and added mass of small subsea robot
R = vertical submergence depth of small robot depth
C_D = drag coefficient
A_f = frontal area exposed to flow

The maximum terminal speed of ANNE is calculated from setting the left hand side of Equation 5.17 to zero as there is no acceleration. The value of the buoyancy force is substituted from equation 5.15 and setting Y equal to T. This gives:

$$\frac{C_D A_f \sigma \left(\frac{dR}{dt}\right)^2}{2} = \sigma g A T \tag{5.18}$$

Solving Equation 5.18 for *dR/dt* gives:

$$\frac{dR}{dt} = \sqrt{\frac{2ATg}{C_D A_f}} = V_t \tag{5.19}$$

With the parameters substituted into Equation 5.19 as listed in Section 5.1.6, Table 5.1, this gives the maximum terminal velocity as $V_t = 0.313$ m/s (Sample Calculation 5.5, Appendix E).

5.1.6 Justification of Uncertain Parameters

Table 5.1 lists all of the known and calculated parameters involved in the simulation calculations for ANNE. The measurements are taken directly from ANNE where applicable.

Table 5.1 Parameter Definitions and Values

Symbol	Definition	Value
A	cross-sectional area of ballast tank	$0.025\ \text{m}^2$
T	half height of the ballast tank	0.250 m
g	acceleration due to gravity	$9.81\ \text{m/s}^2$
σ	density of the flowing fluid (water)	$1000\ \text{kg/m}^3$
M	inherent and added mass of small subsea robot	75 kg
C_D	drag coefficient	2.5
A_f	frontal area exposed to flow	$0.50\ \text{m}^2$
C_o	head loss coefficient	0.5
H	flow area	$0.0010\ \text{m}^2$
V_t	maximum terminal speed of small subsea robot	0.313 m/s
t_p	purge period	6.25 s
M_{max}	maximum mass of water that ballast tank can withstand	6.25 kg

The uncertain parameters in Table 5.1 include the hole loss factor, C_o, and the wake drag coefficient, C_D. In addition, the added mass of ANNE is taken as 50% of the basic robot mass (a typical value used by other researchers).

To determine these parameters precisely, experiments could have been performed. However, as the purpose of the simulation is to approximate the overall influence of these and other parameters, rough estimates are sufficient.

5.2 Depth Control Strategy

For most survey or exploration type missions of ANNE, depth control does not have to be extremely accurate. ANNE is required to get close to the command depth and hover or drift very slowly up and down. ANNE uses a two level switching error-driven control strategy to achieve this. One level of the control strategy moves it towards a band surrounding the command depth, creating a depth error-driven control strategy. The other level attempts to bring ANNE to a stop within the band and uses a buoyancy error-driven control strategy to achieve this.

Water is allowed to enter the ballast tank when ANNE is above a preset band surrounding the command depth and is either rising or not moving towards the band fast enough. Water is forced out of the ballast tank when ANNE is below the band and is either sinking or not moving up to the band fast enough. Within the band, water is allowed to enter the ballast tank when ANNE is moving upwards and buoyancy is positive. Water is forced out of the ballast tank when ANNE is moving downwards and buoyancy is negative. Within the band, the goal is to force the buoyancy to zero and stop ANNE near the command depth.

Figure 5.1 shows the block diagram for inside the error band. For this case, the response of the apparent depth of the subsea robot is fed back for comparison with the command depth. The controller then acts on the depth error and the rate of response, which is how fast the robot moves toward the band. On this basis, the control signal is sent to the pneumatic valves which then permit flow into or out of the ballast tank through the pneumatic pistons. This in turn causes a change in the buoyancy that is fed to the plant, the subsea robot, and results in motion of the subsea robot to the specified command depth.

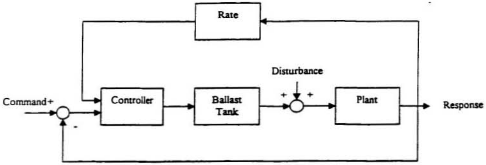

Figure 5.1 Block diagram inside the error band

Figure 5.2 shows the block diagram for outside the error band. For this case. the rate of response of the motion of the subsea robot, together with the acceleration. are used to calculate the buoyancy. The controller acts on both the estimate of the buoyancy and the rate of response. The response of the apparent depth of the subsea robot is also fed back to the controller for comparison with the command depth. Similarly to the case of Figure 5.1. the control signal is sent to the pneumatic valves which then permit flow into or out of the ballast tank through the pneumatic pistons. This in turn causes a change in the buoyancy that is fed to the plant, the subsea robot, and results in motion of the subsea robot to the specified command depth.

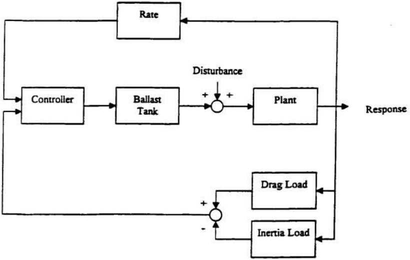

Figure 5.2 Block diagram outside the error band

The flow of water into the ballast tank is pulsed. Between the pulses, ANNE is permitted to drift. This is done because the natural filling rate turns out to be more than expected. The use of Equation 5.2 is questionable for this pulsed flow. A lumped inertance-resistance model for the flow would perhaps be more accurate but this has not been developed in the present work.

A simple one step scheme is used to integrate the entire set of ordinary differential equations given by Equation 5.10, Equation 5.13, and Equation 5.17. In the simulation, buoyancy is calculated from the ballast tank flow equations. For ANNE, this is not accurate, because there are numerous uncertain parameters in the equations. An estimate of buoyancy is made using Equation 5.17, however, this equation has uncertain parameters but fewer than those in the ballast tank flow equations.

Manipulation of Equation 5.17 gives:

$$B = -M\frac{d^2R}{dt^2} - \frac{C_D A_f \sigma \frac{dR}{dt}\left|\frac{dR}{dt}\right|}{2} \tag{5.20}$$

The accelerometer provides the value of d^2R/dt^2 and dR/dt is obtained through numerical differentiation of the depth sensor readings.

5.3 Simulation

Using the simulation code developed in Fortran, see Appendix F, the pattern shown in Figure 5.3. was produced. The applicable parameters were substituted into the simulation code as given in Section 5.1.6, Table 5.1. This pattern is actually a time trace generated by the simulation for the case of the actual hover test discussed in Chapter 6.

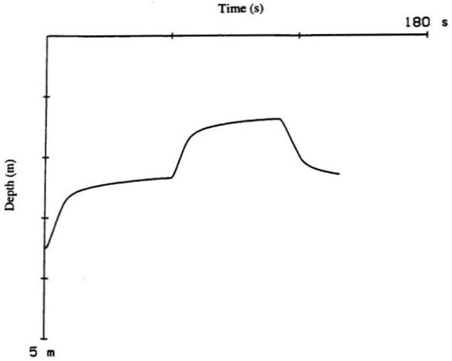

Figure 5.3 Simulation time trace

For this test, ANNE is initially at the bottom of a water tank 3.5 m deep. It is then commanded to rise 1 m up from the bottom, pause, and then commanded to rise to a level of 2 m, pause, and then return to the 1 m level. As can be seen in Figure 5.3, ANNE is able to approach the command depth and the motion is stable.

The simulation of ANNE permitted an exploration of the behaviour of the subsea robot in waves near the ocean surface. Due to the nonlinear nature of the controller, motions were found to be chaotic, which is expected near the water surface. As this is a very interesting problem, it deserves further study but was beyond the scope of the present work.

Chapter 6

Experimentation

6.1 Preliminary Trials

In order to confirm the operation of ANNE, several tests had to be performed. In the early stages of design, specific components had to be examined to ensure that they would maintain a water tight seal while in operation. This began with the three instrumentation boxes that house the controller, the batteries and the pneumatic components. Once the boxes achieved adequate suction, they were lowered into the towing tank at MUN at a depth of 2 m and left for various periods of time.

The first time period was twenty minutes. There were no problems with two of the boxes, but the controller box had leaked and water was found inside. This leak was caused by a poor pressure transducer connection and proper care was taken to reinstall the pressure transducer with teflon tape. This box was retested and no leaks were present for the twenty minute time period. All the boxes were placed in the towing tank and left for thirty minutes and no leaks were detected. They were then tested for sixty minutes and again, no leaks were detected. It was confirmed that the suction created in the instrumentation boxes using the vortex blower in reverse operation and the duct tape used to maintain the seal, was adequate to prevent leaks for a three hour test period.

Once the critical components were tested and no fear of water leaks existed, it was time to place ANNE in the towing tank. With a compressed air pressure of 4 bar and both holes of the ballast tank closed, a test was conducted to ensure that none of the FESTO tubing and connections had any possible leaks. Some minor air bubbles were present, and the appropriate fittings were adjusted to reduce the leakage.

This test demonstrated that ANNE was not quite neutrally buoyant, as ANNE did not float to the surface as predicted. It was then decided that additional styrofoam would be required, thus a modification was made to the design of ANNE. Two additional cylinders were added to hold the styrofoam, illustrated in Figure 4.8, which assisted in creating stability. Two lead weights were also added to the bottom of ANNE and two small lead weights were attached using duct tape to the side that holds the controller box, in order to balance with the other two boxes. This was done because the three batteries were creating a weight imbalance.

ANNE was then placed in the towing tank, at a depth of 2 m, with a compressed air pressure of 4 bar. ANNE sank to the bottom of the towing tank floor as both holes of the ballast tank were open, was left for thirty minutes and then retrieved using two ropes attached to the structure. This was a successful test as there were no leaks within the instrumentation boxes, no air bubbles were present as a result of the FESTO tubing and connections, and ANNE was stable on the towing tank floor.

6.2 Hovering Trials

The time came to run the Dynamic C Code for the controller outside of the towing tank. This was to ensure that all of the pistons were operating and the high-pressure compressed air from the divers bottle was entering the ballast tank at an acceptable flow rate. All systems were operating effectively so ANNE was prepared for testing in the deep tank at MUN at a maximum depth of 3.5 m.

The routine for a typical test consisted of many important steps. This list of instructions is given in Appendix G. Before deployment, it was ensured that the proper code was developed for the test. Next, the three batteries were recharged and connected properly with the 3 A fuse in place. Following this, the divers bottles were checked to ensure that sufficient high-pressure compressed air was present. All of the pneumatic valve electrical connections, as well as the pneumatic tubing connections were checked to ensure tight connections.

A vortex blower was used in reverse to permit suction of the battery box and then duct tape was applied to maintain suction before the box was placed on ANNE. Following this, the same procedure was followed for the suction of the pneumatic box and it was placed next to the battery box. These were then held into place on one side of the bottom frame using a screw handle as shown in Figure 4.1.

The code was loaded from the host computer to the controller and then the cable was disconnected from the controller. The code required the accelerometer to be oriented in a certain way so this had to be checked to ensure proper positioning. Once again, the vortex blower was used for suction of the controller box and duct tape was applied before it was placed on the other side of ANNE. Another screw handle was used to keep the controller box in place on the bottom aluminum frame. Once all the instrumentation boxes were placed on ANNE, the manual flow control valve on the divers bottle was opened so that the high-pressure compressed air was turned on and all pneumatic components were checked for leaks.

Due to the weight of ANNE, it had to be placed into the deep tank using an overhead crane as shown in Figure 6.1. Ropes were attached to a lifting lug so that ANNE could be hooked to the crane that was used to place ANNE in the deep tank.

When recovered, if another test was planned, suction was removed from the controller box only and the controller was reconnected to the host computer and an appropriate code was reloaded. If another test was not planned, all of the instrumentation boxes were removed from ANNE, suction was released and all of the instrumentation boxes were checked for leaks. The compressed air was turned off and ANNE was sent back to home base.

Figure 6.1 ANNE with testing apparatus

The first test of ANNE with the first code loaded was successful. ANNE sank to the bottom of the tank, at a depth of 3.5 m, as both holes of the ballast tank were open and at the specified time, ANNE rose to the surface. No hovering characteristics were attempted or observed at this time, as they were not entered into the code.

It was decided that the hovering commands would be employed by a new code. Several tests were required to obtain satisfactory hovering performances and remove any errors. After numerous manipulation of the code, the most typical mission was quite successful. The data for this test is presented in Table 6.1. ANNE began at rest at the bottom of the tank and then lifted and hovered to the specified depth, returned to the bottom of the tank, lifted again and hovered to the specified depth, rested on the bottom of the tank and finally returned to the surface of the water and floated.

Time (s)	Depth (m)
0	3.50
12	2.70
17	2.25
19	2.25
28	2.30
36	2.30
37	2.30
47	2.20
48	2.20
53	2.15
55	2.20
56	2.20
69	1.50
73	1.45
75	1.50
80	1.50
83	1.50
92	1.45
102	1.40
108	1.50
114	2.00
117	1.95
119	1.95
123	1.85
124	1.85
129	2.05
130	2.00
134	1.95

Table 6.1 Testing Data

The data in Table 6.1 was obtained from measuring the distance that a fixed point on ANNE moved. This was done through video taped footage of an actual test. A rope with increments of 0.25 m was placed in the deep tank. As ANNE passed by, the measurements were taken from the video screen through the use of calipers. The time was determined from a clock on the video screen.

Figure 6.2 shows both the simulation data and the actual test data for comparison. ANNE was initially at the bottom of the deep tank at a depth of 3.5 m. It was commanded to rise up from the bottom 1 m, hover there for approximately one minute, rise another 1 m, hover for another minute, move down 1 m, hover there for another minute, and finally come up to the surface and wait to be retrieved. The Dynamic C Code, which was successful for hovering, is given in Appendix H.

As can be seen in Figure 6.2, ANNE reaches the command depth and motion is stable. This can be compared with that produced in the simulation plot shown in Figure 5.3. The simulation code and data file are given in Appendix F.

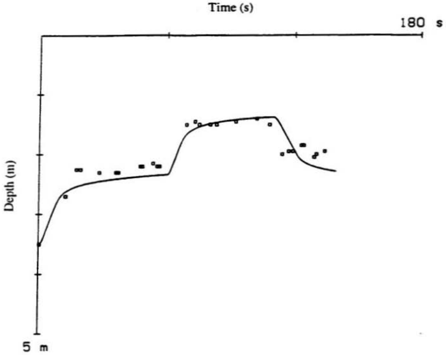

Figure 6.2 Comparison of simulation time trace and testing data

It is possible to estimate the amount of high-pressure compressed air consumed by recording both the number of times the pistons in the ballast tank were activated during a trial run and the total amount of time that high-pressure compressed air flowed into the ballast tank. This is accounted for in the simulation discussed in Chapter 5. The simulation suggests that during a three minute run, only 4 stpL are used. The two divers bottles contain 2000 stpL and they should last up to 3000 minutes or 50 hours. If the trial runs did not have such high demands, these requirements would be reduced. It is also possible that a better control strategy would also reduce the high-pressure compressed air requirements.

As stated at the beginning of Chapter 5, it was assumed that the success or failure of ANNE depended on how long the high-pressure air lasts as this determined the mission duration. From actual test operation of ANNE, it has been discovered that the mission duration is ultimately determined by the battery power. The actual time duration provided by the battery supply for ANNE has been calculated to be four hours (Sample Calculation 4.1, Appendix E). This has been confirmed through the actual deep tank tests.

Chapter 7

Conclusions and Recommendations

For educational purposes, the development of the subsea robot ANNE proved to be quite successful. The design, construction, simulation and testing phases in completing such a task illustrated the importance of ensuring that all components function properly and effectively to achieve the main task. From the work to date, ANNE has proved to have potential for industrial use.

An extensive review of previous robots that have been designed allowed for some research insight to the importance of their uses and their limitations. In reviewing the control strategies, it was concluded that the most effective subsea robot control for ANNE was the switching strategy with error-driven control. The goal was to develop a more robust version of the subsea robot NO MAD and this thesis illustrates that this goal was accomplished through the development of the subsea robot ANNE.

Compared to NOMAD, ANNE is easier to assemble and disassemble. This is due in part to the use of a simple twist lock mechanism to lock the components and parts together, and the use of suction to close the instrumentation boxes. NO MAD has unwanted up and down motions, known as limit cycles, near the command depth. ANNE uses a different control strategy that results in the motion settling down near the command depth.

For future work with respect to the design of ANNE, it would be in the best interest of future designers to turn the educational benefits gained into a subsea robot more suitable for industrial use which would allow for ocean missions. This would entail that many of the current features of ANNE be modified.

New design features should allow the mass of the subsea robot to be reduced substantially. Although ANNE allows for easy assemble, it is too heavy for one person to operate and requires the uses of an overhead crane for deployment. To simplify deployment and retrieval, the ocean going version should be much lighter than the subsea robots, NO MAD and ANNE, developed to date.

The pneumatic valves ANNE uses have pilot exhausts, which cannot be ported. This causes pressure to build up in the pneumatic valve box during a mission. For ANNE, two check valves are positioned in series to periodically vent this unwanted pressure to the external surroundings. Valves have now been designed such that fittings allow pilot exhausts to be ported. This type of pneumatic valve should be tested in any future subsea robots.

A new subsea robot must use the high-pressure compressed air and battery power consumption at maximum efficiency. The control strategy should be such that it requires less use of the high-pressure compressed air. For power consumption, higher capacity batteries should be utilized for extension of battery life.

A new ocean going subsea robot should be tested initially from a wharf, and finally from a supply vessel at sea. For such tests, the robot would need a fail-safe system onboard to bring it back to the ocean surface if it suffered a computer or power failure. Confidence to test at sea is perhaps the most important recommendation for subsea robot design.

The simulation employed by ANNE permitted an exploration of the behaviour of the subsea robot in waves near the ocean surface. Due to the nonlinear nature of the controller, motions were chaotic, which is expected near the water surface. As this is a very interesting problem, it also deserves further study.

References

[1] Blidberg, D., and Yoerger, D. (1990). *Guest Editional – Special Issue on Autonomous Underwater Vehicle Technology*, IEEE Journal of Ocean Engineering, Vol. 15, No. 3, pp. 141-143.

[2] Lu, Z. (1996). Development of the Subsea Robot NO MAD, Doctoral Thesis, Memorial University of Newfoundland: St. John's, Newfoundland.

[3] Brutzman, D. (1997). Autonomous Underwater Vehicle Technology, Ocean Engineering Professional Course: Halifax, Nova Scotia.

[4] Bohm, H., and Jensen, V. (1997). Build Your Own Underwater Robot and Other Wet Projects, Westcoast Woods: Vancouver, British Columbia, pp. 20-21.

[5] Bradley, A., and Yoerger, D. (1995). *Design and Testing of the Autonomous Benthic Explorer*, Department of Applied Ocean Physics and Engineering, Woods Hole Oceanographic Institution: Woods Hole, Massachusetts, p. 1.

[6] Millard, N., Griffiths, G., Finegan, G., McPhail, S., Meldrum, D., Pebody, M., Perrett, J., Stevenson, P., and Webb, A. (1998). *Versatile Autonomous Submersibles – the realising and testing of a practical vehicle*, Journal of the Society for Underwater Technology, Vol. 23, No. 1, pp. 7-17.

[7] Davis, R., Webb, D., Regier, L., and Dufour, J. (1992). *The Autonomous Lagrangian Circulation Explorer (ALACE)*, Journal of Atmospheric and Oceanic Technology, 1992 American Meteorological Society.

[8] Lu, Z., Hinchey, M., and Friss, D. (1996). *Development of the Pneumatic Subsea Robot NO MAD*, Oceanic Engineering International, Memorial University of Newfoundland: St. John's, Newfoundland, p. 11.

[9] Muggeridge, K. (1994). Investigation of Control Strategies and Development of a Hydraulic Actuator for Accurate Positioning of Subsea Robots, Masters Thesis, Memorial University of Newfoundland: St. John's, Newfoundland.

[10] Hinchey, M. (1996). *Supervisory Control Strategies for Autonomous Subsea Robots*, Memorial University of Newfoundland: St. John's, Newfoundland.

[11] Farbrother, H., and Stacey, B. (1993). *Aspects of Remotely Operated Vehicle Control – A Review*, Underwater Technology, Vol. 19, No. 1, pp. 24-36.

[12] Phillips, C., and Harbor, R. (1996). Feedback Control Systems (3rd ed.), Prentice-Hall, Inc.: Englewood Cliffs, New Jersey.

[13] Yoerger, D. (1990). *Precise Control of Underwater Robots: Why and How*. International Advanced Robotics Programme, First Workshop on Mobile Robots for Subsea Environments: Monterey, California, pp. 113-117.

[14] Yoerger, D., Cooke, J., and Slotine, J.J. (1990). *The Influence of Thruster Dynamics on Underwater Vehicle Behaviour and Their Incorporation Into Control System Design*, IEEE Journal of Oceanic Engineering, Vol. 15, No. 3, pp. 167-178.

[15] Brooks, R. (1989). *A Robot that Walks: Emergent Behaviours from a Carefully Evolved Network*, Massachusetts Institute of Technology: Massachusetts.

[16] Woolgar, R., Hinchey, M., and Hiscock. J. (1998). *Development of the Subsea Robot ANNE*, Proceedings of NECEC 1998, Memorial University of Newfoundland: St. John's, Newfoundland.

[17] Hinchey, M., and Woolgar, R. (1998). *Some Subsea Robot Concepts*, Institute of Marine Dynamics Underwater Vehicle Workshop, Memorial University of Newfoundland: St. John's, Newfoundland.

[18] Moores, G. (1995). Development of Instrumentation Boxes for Subsea Robots, Work Term Project, Memorial University of Newfoundland: St. John's, Newfoundland.

[19] White, F. (1986). Fluid Mechanics (2nd ed.), McGraw-Hill, Inc.: New York, New York.

[20] Mott, R. (1994). Applied Fluid Mechanics (4th ed.), Prentice-Hall, Inc.: Upper Saddle River, New Jersey.

Bibliography

Allmendinger, E. (1990). Submersible Vehicle Systems Design, The Society of Naval Architects and Marine Engineers: Jersey City, New Jersey.

Brutzman. D., Healey, T., Marco, D., and McGhee, B. (1997). *The Pheonix Autonomous Underwater Vehicle*, Center for AUV Research: Monterey, California.

Cox, E. (1992). *Fuzzy Fundamentals*, IEEE Spectrum, Vol. 29, No. 3, pp. 58-61.

Dean, R., and Dalrymple, R. (1984). Water Wave Mechanics for Engineers and Scientists, Prentice-Hall, Inc.: Englewood Cliffs, New Jersey.

Faltinsen, O. (1990). Sea Loads on Ships and Offshore Structures, Cambridge University Press: New York, New York.

Fossen, T. (1994). Guidance and Control of Ocean Vehicles, John Wiley and Sons, Inc.: West Sussex, England.

Goodfellow, R. (1977). Underwater Technology, Petroleum Publishing Company: Tulsa, Oklahoma.

Levine. W. (1996). The Control Handbook, CRC Press: Boca Raton, Florida.

Newman, J. (1980). Marine Hydrodynamics, The Massachusetts Institute of Technology Press: Cambridge, Massachusetts.

Meirovitch. L. (1970). Methods of Analytical Dynamics, McGraw-Hill, Inc.: New York, New York.

(1992). Proceedings of the Tenth Annual Intervention/ROV 1992 Conference and Exposition, sponsored by The ROV Committee and The San Diego Section of The Marine Technology Society, San Diego, California.

(1995). Proceedings of the Ninth International Symposium on Unmanned Untethered Submersible Technology, organized by the Autonomous Undersea Systems Institute and Marine Systems Engineering Laboratory Northeastern University, Lee, New Hampshire.

(1996). Proceedings of the 1996 IEEE Symposium on Autonomous Underwater Vehicle Technology, sponsored by The Oceanic Engineering Society of IEEE, Monterey, California.

(1997). Proceedings of the Tenth International Symposium on Unmanned Untethered Submersible Technology, organized by the Autonomous Undersea Systems Institute, Lee, New Hampshire.

(1997). Proceedings of Oceans 1997, sponsored by The Marine Technology Society and IEEE: Halifax, Nova Scotia.

Sarpkaya, T., and Isaacson, M. (1981). Mechanics of Wave Forces on Offshore Structures, Van Nostrand Reinhold Company: New York, New York.

Schilling, R. (1990). Fundamental of Robotics Analysis and Control, Prentice-Hall, Inc.: Englewood Cliffs, New Jersey.

Soloman, S. (1994). Sensors and Control Systems in Manufacturing, McGraw-Hill, Inc.: New York, New York.

Wang, P., and Chang, S. (1980). *Fuzzy Sets Theory and Applications to Policy Analysis and Information Systems*, Proceedings of the Symposium on Policy Analysis and Information Systems, Plenum Press: New York, New York.

Yeaple, F. (1996). Fluid Power Design Handbook (3rd ed.), Marcel Dekker, Inc.: New York, New York.

Appendix A

Control Strategy Codes (Fortran)

Sliding mode control code and data for
Figure 3.1 – Phase portrait with uncertain parameters

```
C
C
C     SLIDING MODE DEPTH CONTROL
C      OF A SMALL SUBSEA ROBOT
C
C     MASS = SUBSEA ROBOT MASS
C     DRAG = SUBSEA ROBOT DRAG
C
C
C     RNEW/ROLD = ACTUAL DEPTH
C     PNEW/POLD  = DEPTH RATE
C     COMMAND = COMMAND DEPTH
C
C
      IMPLICIT REAL*8(A-H,O-Z)
      REAL*4 XP,YP,XO,YO
      REAL*8 MASS,LOAD
      REAL*8 LAMBDA
      OPEN(5,file='gop.d',status='old')
      READ(5,*) LOAD,PERIOD
      READ(5,*) DELT,NIT,NIP
      READ(5,*) MASS,DRAG
      READ(5,*) ESTIMATE
      READ(5,*) COMMAND
      READ(5,*) LAMBDA
      READ(5,*) GAMMA
      READ(5,*) XO,YO
      READ(5,*) SX,SY
      READ(5,*) ROLD
      READ(5,*) POLD
      ZERO=0.D0
      PI=3.14159D0
      CALL PLOTS(53,0,-1)
      CALL PLOT(XO-0.07,YO,3)
      CALL PLOT(XO+0.07,YO,2)
      CALL PLOT(XO,YO-0.07,3)
      CALL PLOT(XO,YO+0.07,2)
      CALL SYMBOL(2.,2.,0.25,3HRCW,0.0,3)
      CALL PLOT(XO,YO,3)
      IP=NIP
      TIME=0.D0
      DO 11 IT=1,NIT
      SIGN=0.D0
      TIME=TIME+DELT
      WHAT=ESTIMATE+LOAD*DSIN(2.D0*
     * PI/PERIOD*TIME)
      S=LAMBDA*(COMMAND-ROLD)-POLD
      IF(S.NE.0.D0) SIGN=S/DABS(S)
      GAIN=-GAMMA
      CONTROL=DRAG*(POLD-ESTIMATE)*
     * DABS(POLD-ESTIMATE)-MASS*LAMBDA*POLD
C       CONTROL=DRAG*(POLD-WHAT)*
C     * DABS(POLD-WHAT)-MASS*LAMBDA*POLD
      CONTROL=CONTROL+GAIN*SIGN
```

```
      RATE=(CONTROL-DRAG*(POLD-WHAT)
     * *DABS(POLD-WHAT))/MASS
      RNEW=ROLD+DELT*POLD
      PNEW=POLD+DELT*RATE
      YP=PNEW*SY+YO
      XP=RNEW*SX+XO
      IF(IP.EQ.NIP)
     * CALL PLOT(XP,YP,2)
      IF(IP.EQ.NIP) IP=0
      ROLD=RNEW
      POLD=PNEW
      IP=IP+1
   11 CONTINUE
      CALL PLOT(0.0,0.0,999)
      CLOSE(5)
      STOP
      END
```

```
    1.D0    1.0D0             LOAD  PERIOD
0.001D0 100000 100            DELT  NIT  NIP
    5.D0    5.D0              SUB MASS  DRAG
    1.D0                      ESTIMATE
    5.D0                      COMMAND
    5.D0                      LAMBDA
   -25.D0                     GAMMA
    2.0  4.0                  PLOT ORIGIN
    1.0  1.0                  PLOT SCALE
    0.0                       OLD DEPTH
    0.0                       OLD RATE
```

Sliding mode control code and data for Figure 3.2 – Phase portrait with no uncertain parameters

```
C
C
C     SLIDING MODE DEPTH CONTROL
C      OF A SMALL SUBSEA ROBOT
C
C     MASS = SUBSEA ROBOT MASS
C     DRAG = SUBSEA ROBOT DRAG
C
C
C     RNEW/ROLD = ACTUAL DEPTH
C     PNEW/POLD  = DEPTH RATE
C     COMMAND = COMMAND DEPTH
C
C
      IMPLICIT REAL*8(A-H,O-Z)
      REAL*4 XP,YP,XO,YO
      REAL*8 MASS,LOAD
      REAL*8 LAMBDA
      OPEN(5,file='gop.d',status='old')
      READ(5,*) LOAD,PERIOD
      READ(5,*) DELT,NIT,NIP
      READ(5,*) MASS,DRAG
      READ(5,*) ESTIMATE
      READ(5,*) COMMAND
      READ(5,*) LAMBDA
      READ(5,*) GAMMA
      READ(5,*) XO,YO
      READ(5,*) SX,SY
      READ(5,*) ROLD
      READ(5,*) POLD
      ZERO=0.D0
      PI=3.14159D0
      CALL PLOTS(53,0,-1)
      CALL PLOT(XO-0.07,YO,3)
      CALL PLOT(XO+0.07,YO,2)
      CALL PLOT(XO,YO-0.07,3)
      CALL PLOT(XO,YO+0.07,2)
      CALL SYMBOL(2.,2.,0.25,3HRCW,0.0,3)
      CALL PLOT(XO,YO,3)
      IP=NIP
      TIME=0.D0
      DO 11 IT=1,NIT
      SIGN=0.D0
      TIME=TIME+DELT
      WHAT=ESTIMATE+LOAD*DSIN(2.D0*
     * PI/PERIOD*TIME)
      S=LAMBDA*(COMMAND-ROLD)-POLD
      IF(S.NE.0.D0) SIGN=S/DABS(S)
      GAIN=-GAMMA
C     CONTROL=DRAG*(POLD-ESTIMATE)*
C    * DABS(POLD-ESTIMATE)-MASS*LAMBDA*POLD
       CONTROL=DRAG*(POLD-WHAT)*
      * DABS(POLD-WHAT)-MASS*LAMBDA*POLD
      CONTROL=CONTROL+GAIN*SIGN
```

```
      RATE=(CONTROL-DRAG*(POLD-WHAT)
     * *DABS(POLD-WHAT))/MASS
      RNEW=ROLD+DELT*POLD
      PNEW=POLD+DELT*RATE
      YP=PNEW*SY+YO
      XP=RNEW*SX+XO
      IF(IP.EQ.NIP)
     * CALL PLOT(XP,YP,2)
      IF(IP.EQ.NIP) IP=0
      ROLD=RNEW
      POLD=PNEW
      IP=IP+1
 11   CONTINUE
      CALL PLOT(0.0,0.0,999)
      CLOSE(5)
      STOP
      END
```

```
    1.D0   1.0D0           LOAD  PERIOD
0.001D0 100000 100         DELT  NIT  NIP
    5.D0    5.D0           SUB MASS  DRAG
    1.D0                   ESTIMATE
    5.D0                   COMMAND
    5.D0                   LAMBDA
   -25.D0                  GAMMA
    2.0  4.0               PLOT ORIGIN
    1.0  1.0               PLOT SCALE
    0.0                    OLD DEPTH
    0.0                    OLD RATE
```

Neural network control code and data for
Figure 3.4 – Simple neural network map

```
C
C     3D IMAGE OF A THREE NEURON NEURAL NETWORK
C     WITH TWO INPUTS AND ONE OUTPUT
C
C
C
C     DATA
      OPEN(5,file='net.d',status='old')
      READ(5,*) WBO,WBX,WBY,WBZ
      READ(5,*) WXO,WYO,WZO
      READ(5,*) WIX,WIY,WIZ
      READ(5,*) WJX,WJY,WJZ
      READ(5,*) ALPHA,BETA
      READ(5,*) RANGE,DR,DI
      READ(5,*) SX,SY,SZ
      READ(5,*) NR,NI
      READ(5,*) XO,YO
      PI=3.14159
      ALPHA=ALPHA/180.0*PI
      BETA=BETA/180.0*PI
      CALL PLOTS(53,0,-1)
      CALL NUMBER(1.,9.5,0.07,WBO,0.0,2)
      CALL NUMBER(2.,9.5,0.07,WBX,0.0,2)
      CALL NUMBER(3.,9.5,0.07,WBY,0.0,2)
      CALL NUMBER(4.,9.5,0.07,WBZ,0.0,2)
      CALL NUMBER(2.,9.0,0.07,WXO,0.0,2)
      CALL NUMBER(3.,9.0,0.07,WYO,0.0,2)
      CALL NUMBER(4.,9.0,0.07,WZO,0.0,2)
      CALL NUMBER(2.,8.5,0.07,WIX,0.0,2)
      CALL NUMBER(3.,8.5,0.07,WIY,0.0,2)
      CALL NUMBER(4.,8.5,0.07,WIZ,0.0,2)
      CALL NUMBER(2.,8.0,0.07,WJX,0.0,2)
      CALL NUMBER(3.,8.0,0.07,WJY,0.0,2)
      CALL NUMBER(4.,8.0,0.07,WJZ,0.0,2)
      CALL SYMBOL(1.,6.0,0.25,3HRCW,0.0,3)
      CALL SYMBOL(1.,7.0,0.25,3HNET,0.0,3)
C      YP=-RANGE*SX*SIN(ALPHA)+YO
C      XP=+RANGE*SX*COS(ALPHA)+XO
C      CALL PLOT(XP,YP,3)
C      YP=+RANGE*SX*SIN(ALPHA)+YO
C      XP=-RANGE*SX*COS(ALPHA)+XO
C      CALL PLOT(XP,YP,2)
C      YP=-RANGE*SY*SIN(BETA)+YO
C      XP=-RANGE*SY*COS(BETA)+XO
C      CALL PLOT(XP,YP,3)
C      YP=+RANGE*SY*SIN(BETA)+YO
C      XP=+RANGE*SY*COS(BETA)+XO
C      CALL PLOT(XP,YP,2)
C      YP=+RANGE+YO
C      XP=XO
C      CALL PLOT(XP,YP,3)
C      YP=-RANGE+YO
C      XP=XO
C      CALL PLOT(XP,YP,2)
```

```
      SR=RANGE
      DO 22 NIT=1,NR
      SI=RANGE
      DO 11 MIT=1,NI
      CS=WBO+WXO*SQUASH(WIX*SR+WJX*SI+WBX)
     *    +WYO*SQUASH(WIY*SR+WJY*SI+WBY)
     *    +WZO*SQUASH(WIZ*SR+WJZ*SI+WBZ)
      YP=CS*SZ-SR*SX*SIN(ALPHA)+SI*SY*SIN(BETA)+YO
      XP=SR*SX*COS(ALPHA)+SI*SY*COS(BETA)+XO
      IF(MIT.EQ.1) CALL PLOT(XP,YP,3)
      CALL PLOT(XP,YP,2)
      SI=SI-DI
   11 CONTINUE
      SR=SR-DR
   22 CONTINUE
      SI=RANGE
      DO 44 NIT=1,NI
      SR=RANGE
      DO 33 MIT=1,NR
      CS=WBO+WXO*SQUASH(WIX*SR+WJX*SI+WBX)
     *    +WYO*SQUASH(WIY*SR+WJY*SI+WBY)
     *    +WZO*SQUASH(WIZ*SR+WJZ*SI+WBZ)
      YP=CS*SZ-SR*SX*SIN(ALPHA)+SI*SY*SIN(BETA)+YO
      XP=SR*SX*COS(ALPHA)+SI*SY*COS(BETA)+XO
      IF(MIT.EQ.1) CALL PLOT(XP,YP,3)
      CALL PLOT(XP,YP,2)
      SR=SR-DR
   33 CONTINUE
      SI=SI-DI
   44 CONTINUE
      CALL PLOT(0.0,0.0,999)
      CLOSE(5)
      STOP
      END
      FUNCTION SQUASH(X)
      IF(X.GT.+33.0) SQUASH=1.0
      IF(X.LT.-33.0) SQUASH=0.0
      IF(ABS(X).LE.+33.0)
     * SQUASH=1.0/(1.0+EXP(-X))
      RETURN
      END
```

```
-1.5 -25. +25. +50.      WBO WBX WBY WBZ
+1.0  +1.0  -1.0         WXO WYO WZO
+25.  +25.  +25.         WIX WIY WIZ
+25.  -25.  +50.         WJX WJY WJZ
-30.0    -30.0           ALPHA  BETA
2.5  0.2  0.2            RANGE  DR  DI
1.0  1.0  1.0            SX     SY  SZ
25     25                NR     NI
4.     5.                XO     YO
```

Neural network control code and data for
Figure 3.5 – Extremely complex neural network map

```
C
C        3D IMAGE OF A SIX NEURON NEURAL NETWORK
C        WITH TWO INPUTS AND ONE OUTPUT
C
C
C
C        DATA
         OPEN(5,file='not.d',status='old')
         READ(5,*) WBO
         READ(5,*) WBX,WBY,WBZ
         READ(5,*) WXO,WYO,WZO
         READ(5,*) WIX,WIY,WIZ
         READ(5,*) WJX,WJY,WJZ
         READ(5,*) WBU,WBV,WBW
         READ(5,*) WUO,WVO,WWO
         READ(5,*) WIU,WIV,WIW
         READ(5,*) WJU,WJV,WJW
         READ(5,*) ALPHA,BETA
         READ(5,*) RANGE,DR,DI
         READ(5,*) SX,SY,SZ
         READ(5,*) NR,NI
         READ(5,*) XO,YO
         PI=3.14159
         ALPHA=ALPHA/180.0*PI
         BETA=BETA/180.0*PI
         CALL PLOTS(53,0,-1)
         CALL NUMBER(1.0,9.5,0.07,WBO,0.0,1)
         CALL NUMBER(1.0,9.0,0.07,WBX,0.0,1)
         CALL NUMBER(2.0,9.0,0.07,WBY,0.0,1)
         CALL NUMBER(3.0,9.0,0.07,WBZ,0.0,1)
         CALL NUMBER(4.0,9.0,0.07,WBU,0.0,1)
         CALL NUMBER(5.0,9.0,0.07,WBV,0.0,1)
         CALL NUMBER(6.0,9.0,0.07,WBW,0.0,1)
         CALL NUMBER(1.0,8.5,0.07,WXO,0.0,1)
         CALL NUMBER(2.0,8.5,0.07,WYO,0.0,1)
         CALL NUMBER(3.0,8.5,0.07,WZO,0.0,1)
         CALL NUMBER(4.0,8.5,0.07,WUO,0.0,1)
         CALL NUMBER(5.0,8.5,0.07,WVO,0.0,1)
         CALL NUMBER(6.0,8.5,0.07,WWO,0.0,1)
         CALL NUMBER(1.0,8.0,0.07,WIX,0.0,1)
         CALL NUMBER(2.0,8.0,0.07,WIY,0.0,1)
         CALL NUMBER(3.0,8.0,0.07,WIZ,0.0,1)
         CALL NUMBER(4.0,8.0,0.07,WIU,0.0,1)
         CALL NUMBER(5.0,8.0,0.07,WIV,0.0,1)
         CALL NUMBER(6.0,8.0,0.07,WIW,0.0,1)
         CALL NUMBER(1.0,7.5,0.07,WJX,0.0,1)
         CALL NUMBER(2.0,7.5,0.07,WJY,0.0,1)
         CALL NUMBER(3.0,7.5,0.07,WJZ,0.0,1)
         CALL NUMBER(4.0,7.5,0.07,WJU,0.0,1)
         CALL NUMBER(5.0,7.5,0.07,WJV,0.0,1)
         CALL NUMBER(6.0,7.5,0.07,WJW,0.0,1)
C         YP=-RANGE*SX*SIN(ALPHA)+YO
C         XP=+RANGE*SX*COS(ALPHA)+XO
C         CALL PLOT(XP,YP,3)
```

```
C        YP=+RANGE*SX*SIN(ALPHA)+YO
C        XP=-RANGE*SX*COS(ALPHA)+XO
C        CALL PLOT(XP,YP,2)
C        YP=-RANGE*SY*SIN(BETA)+YO
C        XP=-RANGE*SY*COS(BETA)+XO
C        CALL PLOT(XP,YP,3)
C        YP=+RANGE*SY*SIN(BETA)+YO
C        XP=+RANGE*SY*COS(BETA)+XO
C        CALL PLOT(XP,YP,2)
C        YP=+RANGE+YO
C        XP=XO
C        CALL PLOT(XP,YP,3)
C        YP=-RANGE+YO
C        XP=XO
C        CALL PLOT(XP,YP,2)
      SR=RANGE
      DO 22 NIT=1,NR
      SI=RANGE
      DO 11 MIT=1,NI
      CS=WBO+WXO*SQUASH(WIX*SR+WJX*SI+WBX)
     *    +WYO*SQUASH(WIY*SR+WJY*SI+WBY)
     *    +WZO*SQUASH(WIZ*SR+WJZ*SI+WBZ)
     *    +WUO*SQUASH(WIU*SR+WJU*SI+WBU)
     *    +WVO*SQUASH(WIV*SR+WJV*SI+WBV)
     *    +WWO*SQUASH(WIW*SR+WJW*SI+WBW)
      YP=CS*SZ-SR*SX*SIN(ALPHA)+SI*SY*SIN(BETA)+YO
      XP=SR*SX*COS(ALPHA)+SI*SY*COS(BETA)+XO
      IF(MIT.EQ.1) CALL PLOT(XP,YP,3)
      CALL PLOT(XP,YP,2)
      SI=SI-DI
 11   CONTINUE
      SR=SR-DR
 22   CONTINUE
      SI=RANGE
      DO 44 NIT=1,NI
      SR=RANGE
      DO 33 MIT=1,NR
      CS=WBO+WXO*SQUASH(WIX*SR+WJX*SI+WBX)
     *    +WYO*SQUASH(WIY*SR+WJY*SI+WBY)
     *    +WZO*SQUASH(WIZ*SR+WJZ*SI+WBZ)
     *    +WUO*SQUASH(WIU*SR+WJU*SI+WBU)
     *    +WVO*SQUASH(WIV*SR+WJV*SI+WBV)
     *    +WWO*SQUASH(WIW*SR+WJW*SI+WBW)
      YP=CS*SZ-SR*SX*SIN(ALPHA)+SI*SY*SIN(BETA)+YO
      XP=SR*SX*COS(ALPHA)+SI*SY*COS(BETA)+XO
      IF(MIT.EQ.1) CALL PLOT(XP,YP,3)
      CALL PLOT(XP,YP,2)
      SR=SR-DR
 33   CONTINUE
      SI=SI-DI
 44   CONTINUE
      CALL PLOT(0.0,0.0,999)
      CLOSE(5)
      STOP
```

```
 END
 FUNCTION SQUASH(X)
 IF(X.GT.+33.0) SQUASH=1.0
 IF(X.LT.-33.0) SQUASH=0.0
 IF(ABS(X).LE.+33.0)
* SQUASH=1.0/(1.0+EXP(-X))
 RETURN
 END
```

```
    -0.5                              WBO
 0.    0.    0.                       WBX WBY WBZ
+0.5   +0.5   +0.5                    WXO WYO WZO
+100.  +1.0    0.0                    WIX WIY WIZ
0.0     0.0   +1.0                    WJX WJY WJZ
+50.   +50.    0.0                    WBU WBV WBW
-1.0   +1.0    0.0                    WUO WVO WWO
-25.  +25.    0.0                     WIU WIV WIW
0.0     0.0    0.0                    WJU WJV WJW
-30.0       -30.0                     ALPHA  BETA
2.5     0.1    0.1                    RANGE  DR  DI
1.0     1.0    1.0                    SX     SY  SZ
50      50                            NR     NI
4.      3.                            XO     YO
```

Fuzzy logic control code and data for Figure 3.7 –Linear fuzzy logic map

```
C
C     3D IMAGE OF A LINEAR FUZZY LOGIC CONTROLLER
C
C     DATA
      DIMENSION X(5),Y(5),S(5,5)
      OPEN(5,file='log.d',status='old')
C
      READ(5,*)  (X(I),I=1,5)
      READ(5,*)  (Y(I),I=1,5)
      READ(5,*)  (S(1,J),J=1,5)
      READ(5,*)  (S(2,J),J=1,5)
      READ(5,*)  (S(3,J),J=1,5)
      READ(5,*)  (S(4,J),J=1,5)
      READ(5,*)  (S(5,J),J=1,5)
      READ(5,*) ALPHA,BETA
      READ(5,*) SX,SY,SZ
      READ(5,*) XO,YO
      READ(5,*) NOP
      PI=3.14159
      ALPHA=ALPHA/180.0*PI
      BETA=BETA/180.0*PI
      CALL PLOTS(53,0,-1)
      DO 22 NIT=1,NOP
      SR=X(NIT)
      DO 11 MIT=1,NOP
      SI=Y(MIT)
      CS=S(NIT,MIT)
      YP=CS*SZ-SR*SX*SIN(ALPHA)+SI*SY*SIN(BETA)+YO
      XP=SR*SX*COS(ALPHA)+SI*SY*COS(BETA)+XO
      IF(MIT.EQ.1) CALL PLOT(XP,YP,3)
      CALL PLOT(XP,YP,2)
  11  CONTINUE
  22  CONTINUE
      DO 44 NIT=1,NOP
      SI=Y(NIT)
      DO 33 MIT=1,NOP
      SR=X(MIT)
      CS=S(MIT,NIT)
      YP=CS*SZ-SR*SX*SIN(ALPHA)+SI*SY*SIN(BETA)+YO
      XP=SR*SX*COS(ALPHA)+SI*SY*COS(BETA)+XO
      IF(MIT.EQ.1) CALL PLOT(XP,YP,3)
      CALL PLOT(XP,YP,2)
  33  CONTINUE
  44  CONTINUE
      CALL PLOT(0.0,0.0,999)
      CLOSE(5)
      STOP
      END
```

```
 -5.  -2.5  0  +2.5  +5.
 -5.  -2.5  0  +2.5  +5.
 -8.  -7.  -6.  -5.  -4.
 -5.  -4.  -3.  -2.  -1.
 -2.  -1.   0   +1.  +2.
 +1.  +2.  +3.  +4.  +5.
 +4.  +5.  +6.  +7.  +8.
-30.0      -30.0           ALPHA     BETA
 0.4  0.4  0.2             SX    SY   SZ
 4.     4.                 XO    YO
 5                         NOP
```

Fuzzy logic control code and data for Figure 3.9 – Nonlinear fuzzy logic map

```
C
C     3D IMAGE OF A NONLINEAR FUZZY LOGIC CONTROLLER
C
C     DATA
      DIMENSION X(9),Y(9),S(9,9)
      OPEN(5,file='log.d',status='old')
C
      READ(5,*)  (X(I),I=1,9)
      READ(5,*)  (Y(I),I=1,9)
      READ(5,*)  (S(1,J),J=1,9)
      READ(5,*)  (S(2,J),J=1,9)
      READ(5,*)  (S(3,J),J=1,9)
      READ(5,*)  (S(4,J),J=1,9)
      READ(5,*)  (S(5,J),J=1,9)
      READ(5,*)  (S(6,J),J=1,9)
      READ(5,*)  (S(7,J),J=1,9)
      READ(5,*)  (S(8,J),J=1,9)
      READ(5,*)  (S(9,J),J=1,9)
      READ(5,*) ALPHA,BETA
      READ(5,*) SX,SY,SZ
      READ(5,*) XO,YO
      READ(5,*) NOP
      PI=3.14159
      ALPHA=ALPHA/180.0*PI
      BETA=BETA/180.0*PI
      CALL PLOTS(53,0,-1)
      DO 22 NIT=1,NOP
      SR=X(NIT)
      DO 11 MIT=1,NOP
      SI=Y(MIT)
      CS=S(NIT,MIT)
      YP=CS*SZ-SR*SX*SIN(ALPHA)+SI*SY*SIN(BETA)+YO
      XP=SR*SX*COS(ALPHA)+SI*SY*COS(BETA)+XO
      IF(MIT.EQ.1) CALL PLOT(XP,YP,3)
      CALL PLOT(XP,YP,2)
   11 CONTINUE
   22 CONTINUE
      DO 44 NIT=1,NOP
      SI=Y(NIT)
      DO 33 MIT=1,NOP
      SR=X(MIT)
      CS=S(MIT,NIT)
      YP=CS*SZ-SR*SX*SIN(ALPHA)+SI*SY*SIN(BETA)+YO
      XP=SR*SX*COS(ALPHA)+SI*SY*COS(BETA)+XO
      IF(MIT.EQ.1) CALL PLOT(XP,YP,3)
      CALL PLOT(XP,YP,2)
   33 CONTINUE
   44 CONTINUE
      CALL PLOT(0.0,0.0,999)
      CLOSE(5)
      STOP
      END
```

```
-5. -3. -1. -0.5 0.0 +0.5 +1. +3. +5
-5. -3. -1. -0.5 0.0 +0.5 +1. +3. +5
-8. -8. -8. -7. -6.  -5. -4. -4. -4.
-8. -8. -8. -7. -6.  -5. -4. -4. -4.
-8. -8. -8. -7. -6.  -5. -4. -4. -4.
-5. -5. -5. -4. -3.  -2. -1. -1. -1.
-2. -2. -2. -1.  0.  +1. +2. +2. +2.
+1. +1. +1. +2. +3.  +4. +5. +5. +5.
+4. +4. +4. +5. +6.  +7. +8. +8. +8.
+4. +4. +4. +5. +6.  +7. +8. +8. +8.
+4. +4. +4. +5. +6.  +7. +8. +8. +8.
-30.0        -30.0                                  ALPHA        BETA
0.5    0.5   0.1                                    SX     SY    SZ
4.     4.                                           XO     YO
9                                                   NOP
```

Appendix B

Detailed Fabrication Drawings

Autonomous Pneumatic Nautical Explorer
Fabrication Drawings

Structure and Shell

Drawing A	Center Cylinder
Drawing B	Top Frame
Drawing C	Bottom Frame

Ballast Tank

Drawing D	Ballast Tank
Drawing E	Pneumatic Piston Support
Drawing F	Pneumatic Piston Support Component #1
Drawing G	Pneumatic Piston Support Component #2
Drawing H	Support for Ballast Tank

Intermediate Length Tubes

Drawing I	Intermediate Length Tubes
Drawing J	Covers and Supports for Intermediate Length Tubes
Drawing K	Styrofoam Rest for Divers Bottles

Shortest Length Tubes

Drawing L	Shortest Length Tubes
Drawing M	Covers for Shortest Length Tubes
Drawing N	Styrofoam

Controller Box

Drawing O	Controller Box
Drawing P	Beveled Edged Cover (with hole)
Drawing T	Cover (without hole)

Battery Box

Drawing Q	Battery Box
Drawing R	Beveled Edged Cover (without hole)
Drawing U	Cover (with hole)

Pneumatic Box

Drawing S	Pneumatic Box
Drawing U	Cover (with hole)
Drawing T	Cover (without hole)

Additional

Drawing V	Support for Screw Handle

Drawing A Center Cylinder

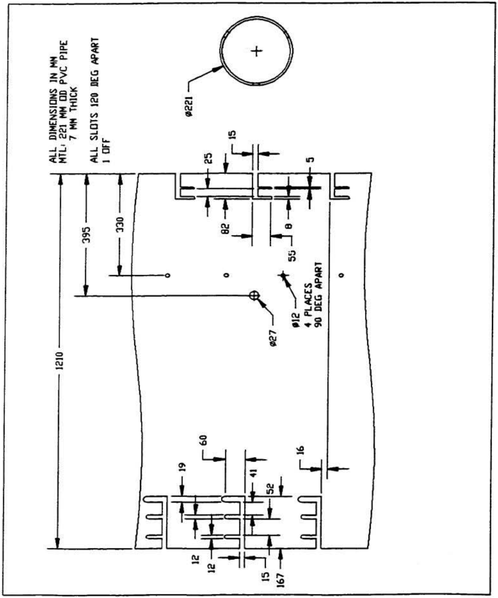

Drawing B Top Frame

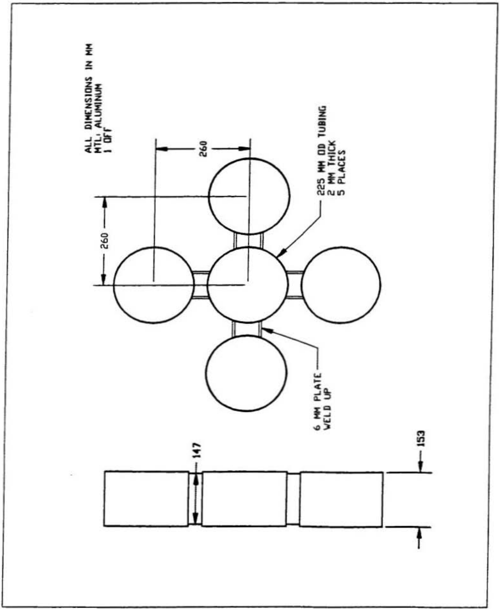

Drawing C **Bottom Frame**

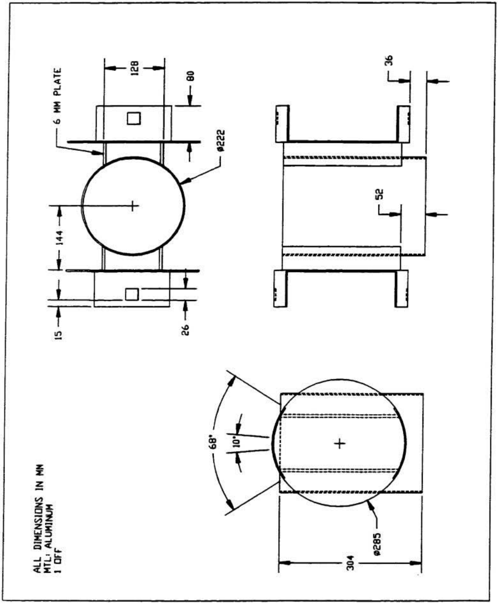

Drawing D **Ballast Tank**

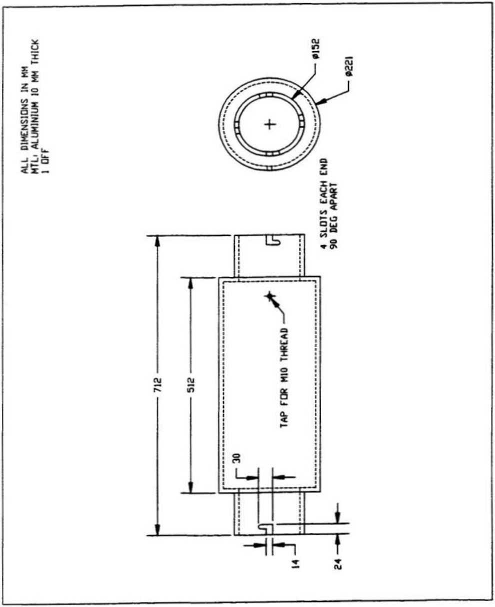

Drawing E **Pneumatic Piston Support**

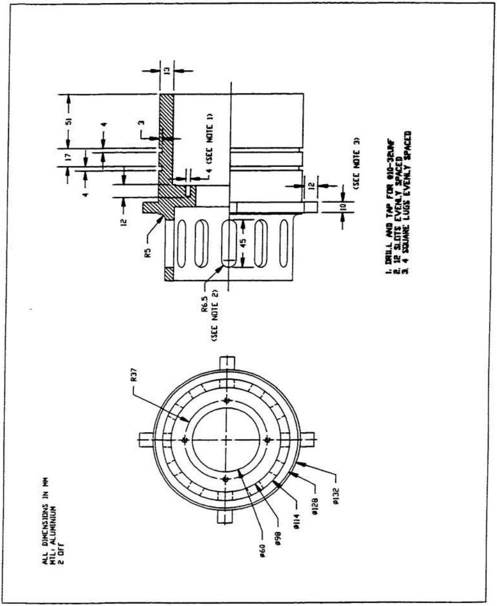

Drawing F Pneumatic Piston Support Component #1

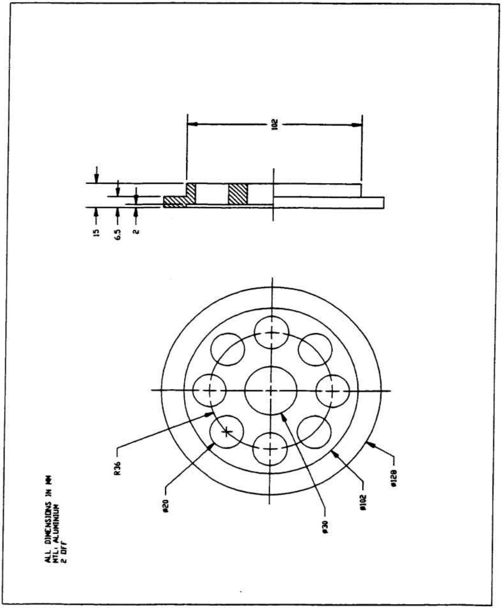

ALL DIMENSIONS IN MM
MTL: ALUMINIUM
2 OFF

Drawing G Pneumatic Piston Support Component #2

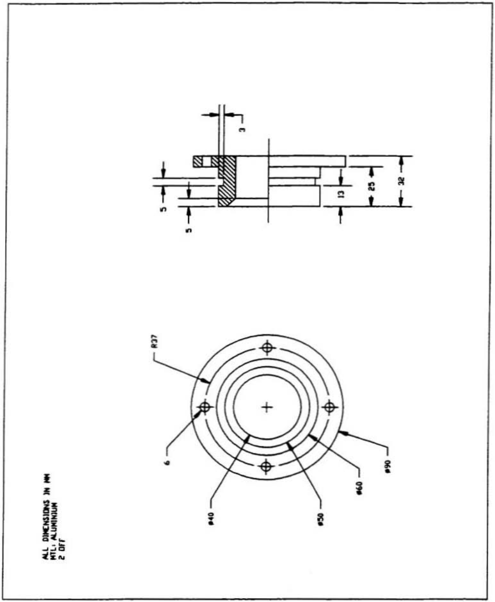

ALL DIMENSIONS IN MM
MTL: ALUMINIUM
2 OFF

Drawing H Support for Ballast Tank

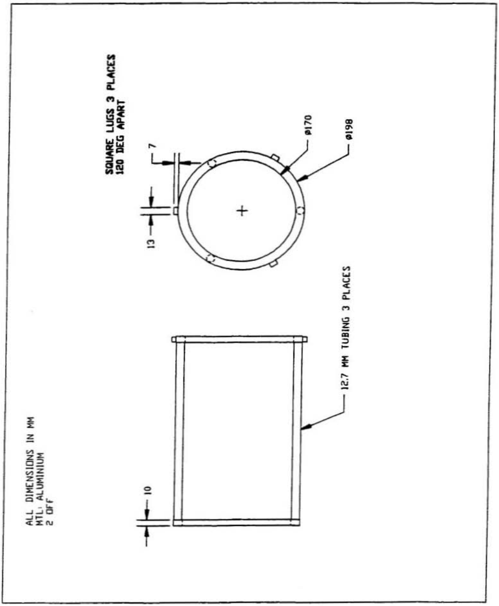

Drawing I Intermediate Length Tubes

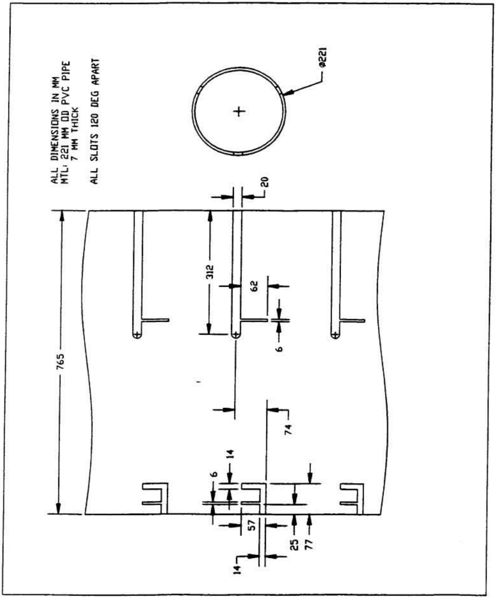

Drawing J Covers and Supports for Intermediate Length Tubes

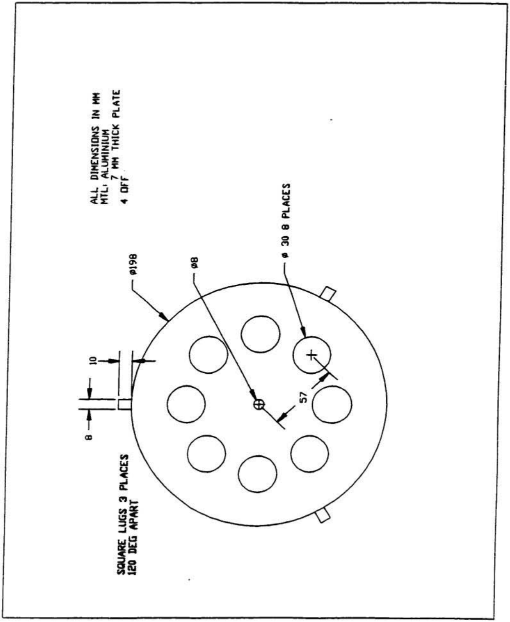

Drawing K **Styrofoam Rest for Divers Bottles**

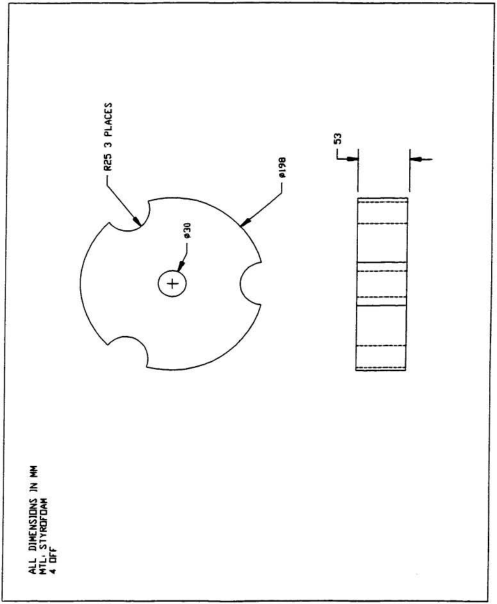

Drawing L Shortest Length Tubes

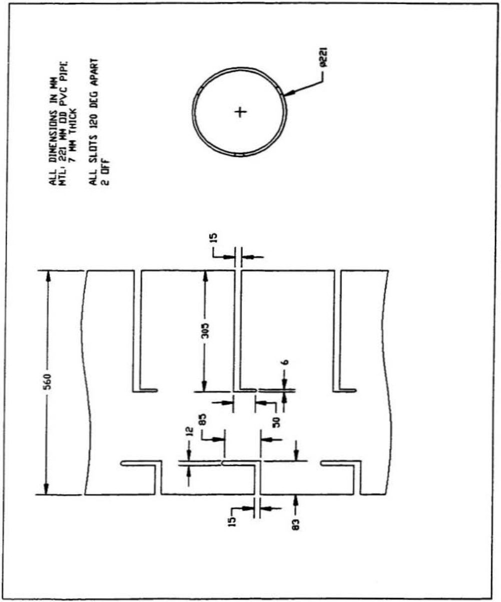

Drawing M Covers for Shortest Length Tubes

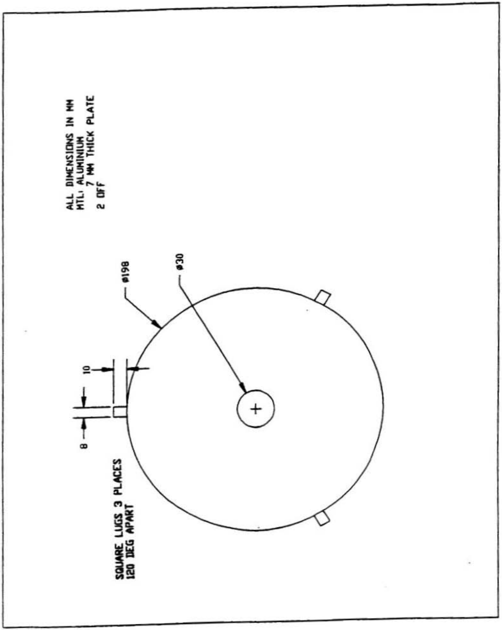

Drawing N Styrofoam

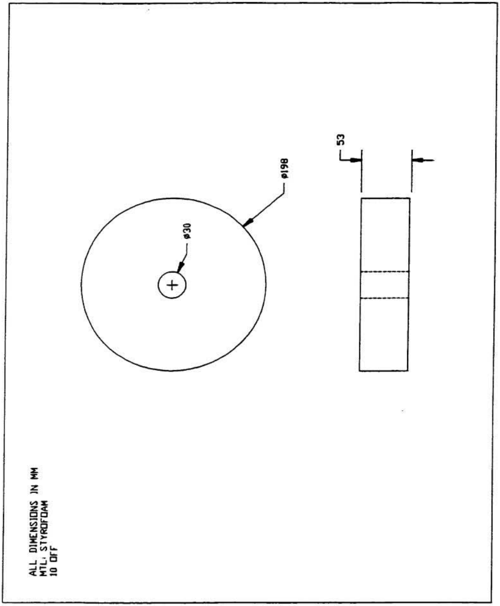

Drawing O Controller Box

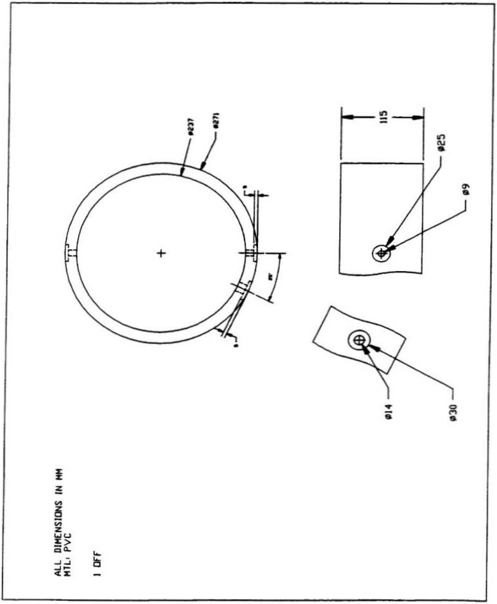

Drawing P Beveled Edged Cover (with hole)

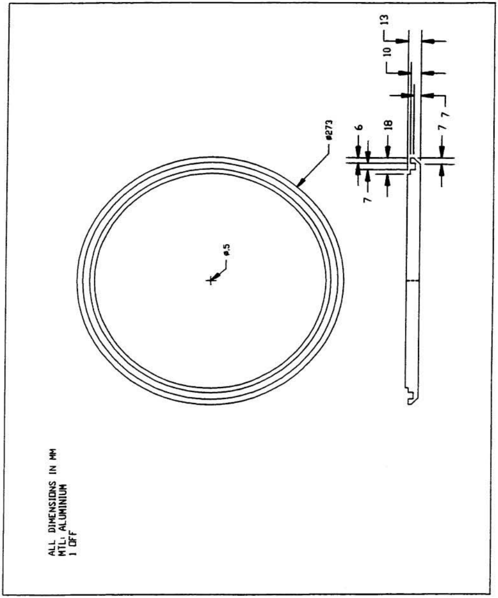

Drawing Q Battery Box

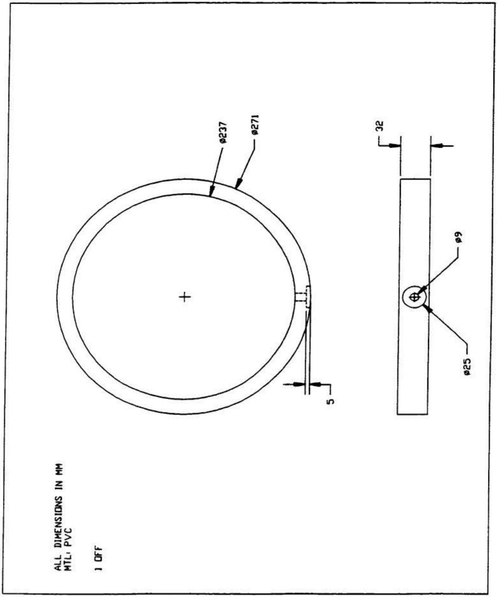

Drawing R **Beveled Edged Cover (without hole)**

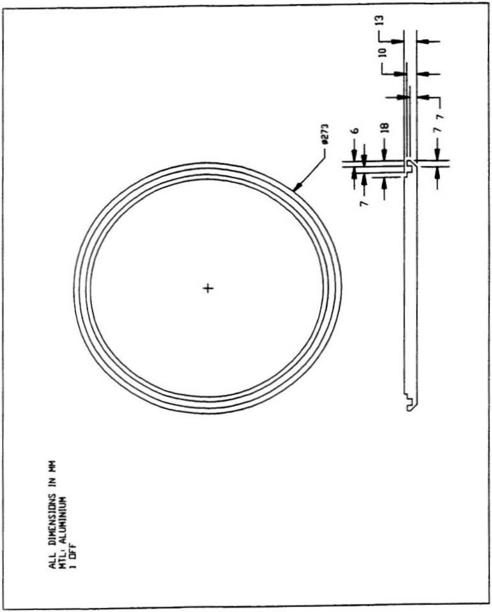

Drawing S Pneumatic Box

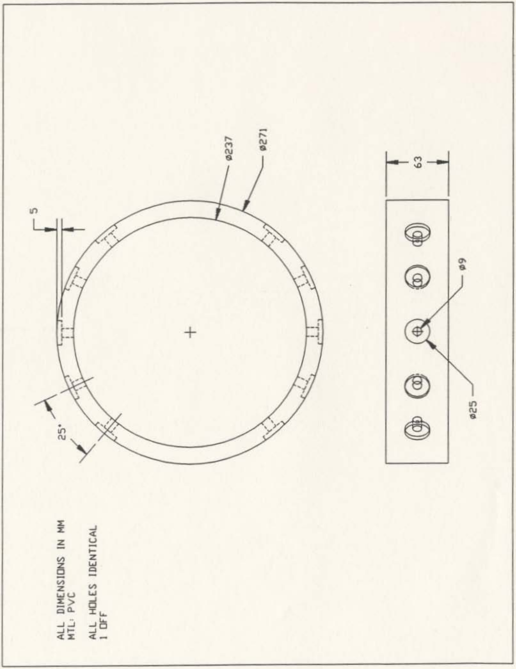

Drawing T Cover (without hole)

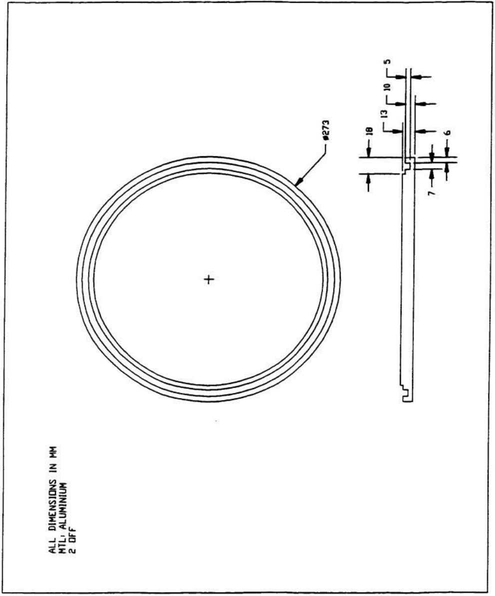

Drawing U Cover (with hole)

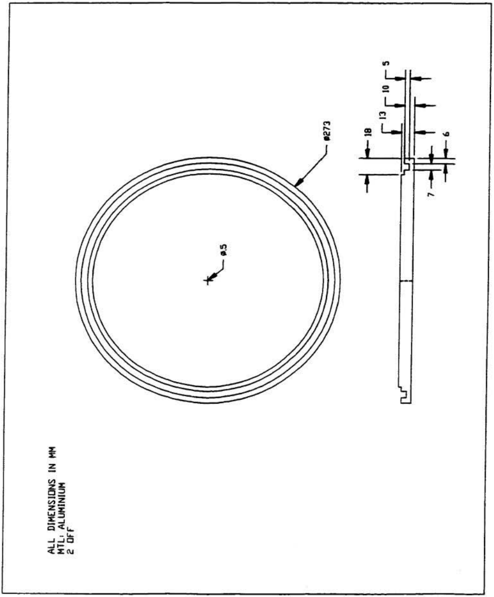

ALL DIMENSIONS IN MM
MTL: ALUMINIUM
2 OFF

Drawing V Support for Screw Handle

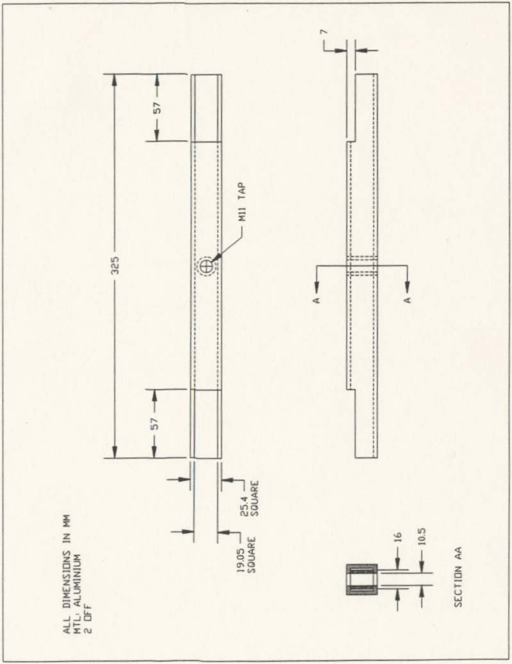

Appendix C

Electrical and Pneumatic Schematics

Electrical Schematic

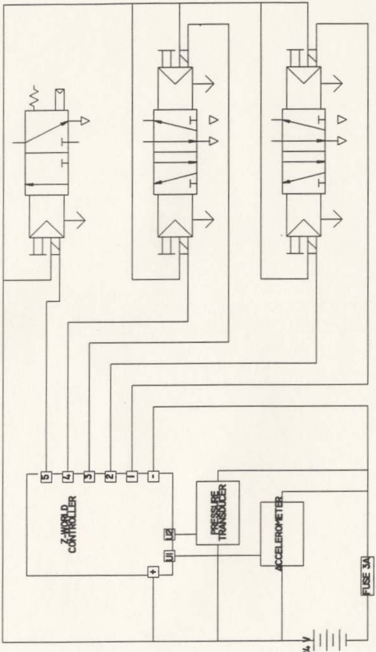
Z-WORLD CONTROLLER
5
4
3
2
1
-
+
U1
U2
PRESSURE TRANSDUCER
ACCELEROMETER
FUSE 3A
+24 V

Pneumatic Schematic

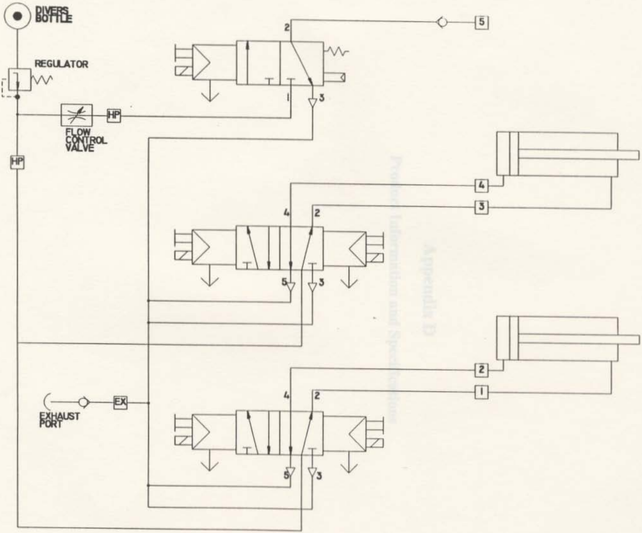
DIVERS BOTTLE
REGULATOR
FLOW CONTROL VALVE
HP
HP
EXHAUST PORT
EX
1
2
3
4
5
2
3
4
5
2
3
4
5
1
2
3

Appendix D

Product Information and Specifications

Z-WORLD Rugged Giant C-Programmable Miniature Controller Specifications Sheets

Rugged Giant™

C-Programmable Miniature Controller

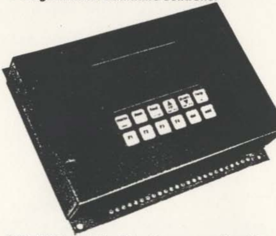

Z-World's Rugged Giant™ is a C-programmable miniature controller with extensive input and output interfaces. A modern solution for controlling all types of equipment, the Rugged Giant differs from other logic controllers because everything you need for most projects is already built in.

- *Six 10-bit universal* inputs*
- *One 10-bit analog output*
- *One high-gain, differential analog input*
- *Seven digital inputs*
- *Two counter inputs*
- *Ten high-current digital outputs*
- *Two relay-contact outputs*
- *PLCBus™ expansion port*
- *Rugged enclosure with 2×20 LCD and 2×6 keypad standard equipment*
- *One RS232 serial port*
- *One RS422/RS485/RS232 port*
- *Extensive software support*

In addition, the Rugged Giant's I/O channels have been designed to connect directly to many low-cost sensors without expensive intermediate signal conditioning.

***Universal Inputs...**

Universal inputs accept analog signals and report either the analog voltage level or a digital "1" or "0." Software interprets the analog level by comparing it either to a fixed threshold or to two program-selectable thresholds. When the analog level is below a low threshold, the software reports logic 0. When the level is above a high threshold, the software reports logic 1. Otherwise, the logic value remains unchanged. This is essentially software "hysteresis."

SPECIFICATIONS

Board Size: 5.5 × 6.9 × 1.5 inches (140 × 175 × 38 mm).

Enclosure Size: 5.5 × 7 × 1.6 inches (140 × 178 × 41 mm).

Temperature: 0°C to 50°C, with LCD. –40°C to 70°C, without LCD.

Power: Accepts unregulated DC voltage in the range of 18–35V and consumes approximately 220 mA. External PLCBus options or external use of the +10V reference will, of course, increase current requirements. A version of the Rugged Giant that takes 12-volt input is available.

Universal Inputs

Six 10-bit universal* inputs. Each can be used as a 0–10 volt analog input, or as a digital input with thresholds adjustable between 0 and 10 volts. One of the inputs can accept 0–20 mA current loop without an external load resistor. The circuitry is protected against overloads.

All universal inputs have internal pull-up and pull-down resistors that can be connected to the input with jumpers. The pull-ups are connected to the board's precision 10V reference. The following diagram shows a typical thermistor temperature sensor using a universal input channel.

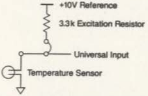

The exact voltage of the reference (usually about 10.3V) is stored in EEPROM at the factory. Other parameters relating to measurement are also stored in EEPROM.

Digital Inputs

Seven digital inputs accept voltages in the range –48 to +48 volts, with the logic threshold at 2.5 volts. Built-in pull-up resistors allow direct connection to contacts or to transistor outputs on external devices.

Counter Inputs

The Rugged Giant has two counter inputs. Counter 1 shares its inputs with two digital input lines. Counter 2 shares one digital input line and uses an RS485 receiver to provide a true differential signal for the other input. Both can count at speeds of 200 kHz and more.

Precision Analog Input

This differential input ranges from 0 to 1 volt with 10-bit accuracy. The common-mode voltage can range from 0 to 10 volts. It is suitable for resistance temperature devices (RTDs) or other devices requiring high input sensitivity. Its gain can be adjusted by changing on-board resistors and operational amplifiers. Higher voltages can also be measured on its positive input in the 0–10 volt range, also with 10-bit accuracy.

Relay Contact Outputs

Two relays, with three terminals for each relay: normally open, normally closed, and common. The relays are capable of handling 3 amperes at 48 volts.

High Current / High Voltage Port

Ten digital output lines, each capable of controlling inductive loads (up to 500 mA at 48 volts) such as relays, stepping motors, and solenoids. The total load on all outputs at the same time is subject to package heat dissipation limits.

Analog Output

The primary analog output can be configured as 0–10V (max 20 mA) voltage output, or as 0–20 mA current loop output. It has 10 bit resolution. A second analog output (0–10V, 10 bits) is available if the universal inputs are configured as fixed-threshold digital inputs.

Voltage Reference

One 10-volt reference, supplying up to 100 mA. This is suitable for powering external bridges or other devices.

Operator Interface

The Rugged Giant has a 2×20 liquid crystal display (LCD), a 12-button keypad, and a very audible beeper with high and low volume control. A backlit version of the LCD is available by special order.

The Rugged Giant's operator interface is driven by Z-World's FiveKey system (a Dynamic C library). The operator may scan multiple menus and submenus and change system parameters with only five keys, plus one additional key as a help key. You can easily customize the keypad legend with common desktop software. The six other keys are available for your application.

Bus Expansion

An expansion header allows connection to Z-World's PLCBus I/O expansion boards. It also provides an easy way to connect your own custom-designed expansion boards.

Serial Communication

The RS232 port provides full-duplex communication, with handshake lines and baud rates to 38,400 bits per second. The connector is an RJ12 "phone jack."

The RS422 / RS485 port provides full- or half-duplex asynchronous communications at up to 38,400 bits per second. It allows communications over twisted-pair wires up to three kilometers. You may also configure this port as RS232.

Other Standard Features

The Rugged Giant incorporates a Z180 processor with a 6.144 MHz clock (9.216 MHz optional), programmable timers, serial ports, EPROM, lithium battery, SRAM, EEPROM, real-time clock with time/date functions, watchdog timer, and power failure detection. See page 3 for more detail.

Developing Software for the Rugged Giant

Because of the size of the Rugged Giant libraries, it is important to order the 128K or 512K memory option for software development. (Finished programs, running from ROM, often do not require this option.)

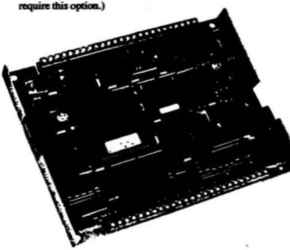

PRICE LIST

All versions include manual, schematic and wall transformer (24V standard or 12V optional).

Rugged Giant Controller: C-PLC-STD Standard Rugged Giant (pictured on facing page) complete with metal case, 2×20 LCD, and keypad.	**$399**
Rugged Giant Controller: C-PLC Board-only version (pictured above).	**$299**
Options	
12-Volt Option: C-PLC-12V Allows you to power the Rugged Giant with 12V DC.	**$35**
9.216 MHz System Clock: C-PLC-HS Increases the Rugged Giant clock speed to 9.216 MHz.	**$75**
128K byte SRAM: SDC-M128	**$50**
512K byte SRAM: SDC-M512	**$150**

ICSensors Pressure Transducer– Model 114
Specifications Sheets and Calibration Data

OEM Pressure Transducer Gage, Sealed Gage and Absolute 1 to 6 Vdc Output Span Stainless Steel Diaphragm

Features

- Solid State Reliability
- Iso-Pressure Structure
- Fully Calibrated
- Temperature Compensated
- ± 0.5% Accuracy
- Interchangeable
- Rugged Construction
- Internal Voltage Regulation
- Reverse Voltage Protection
- Cost Effective

Typical Applications

- Hydraulic Controls
- Robotics
- Water Management
- Air Conditioning
- Refrigeration
- Process Control
- Machine Tools
- Environmental Control
- Agricultural Sprayers
- Compressors

Standard Ranges

0 to 5 psig		
3 to 15 psig		
0 to 15 psig	0 to 15 psis	0 to 15 psia
0 to 30 psig	0 to 30 psis	0 to 30 psia
0 to 50 psig	0 to 50 psis	0 to 50 psia
0 to 100 psig	0 to 100 psis	0 to 100 psia
0 to 300 psig	0 to 300 psis	0 to 300 psia
	0 to 500 psis	0 to 500 psia
	0 to 1000 psis	0 to 1000 psia
	0 to 3000 psis	0 to 3000 psia
	0 to 5000 psis	0 to 5000 psia

Description

The Model 114 is a media compatible, Iso-Pressure, signal conditioned pressure transducer that is intended for a wide range of pressure sensing applications.

The Iso-Pressure sensor assembly utilizes an oil column to couple a diffused, piezoresistive sensor to a convoluted, flush 316 stainless steel diaphragm that can be interfaced with most harsh media. No O-ring is exposed to the media.

The sensor assembly and associated solid state electronics are enclosed in a cylindrical casing with a 1/4-18 NPT stainless steel pressure fitting.

Full calibration and temperature compensation is provided over 0-50° C, along with unit-to-unit interchangeability. A three-wire connector is included with color-coded, 18 gauge wire.

One performance grade is available in gage pressure ranges from 0-5 psi to 0-300 psi and in both sealed gage and absolute pressure from 0-15 psi to 0-5000 psi. In addition to the 1-6Vdc output span, other span ranges and pressure connections are available on special request. Each transducer is individually serialized.

Connections/Dimensions

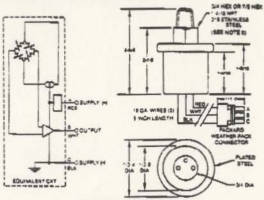

ALL DIMENSIONS ARE IN INCHES

Model 114

Performance Specifications

Supply Voltage = 12Vdc & Ambient Temperature =25°C (Unless otherwise specified)

PARAMETER	MIN	TYP	MAX	UNITS	NOTES
Full-Scale Output Span	4.95	5.00	5.05	V	
Full-Scale Output		5.00		V	
Zero Pressure Output	.95	1.00	1.05	V	2
Static Accuracy			.5	±%Span	3
Temperature Coefficient-Span			1.0	±%Span	1
Temperature Coefficient-Zero			1.0	±%Scan	1
Supply Voltage	10	12	30	V	
Supply Current		2.5		mA	4
Line Regulation		.005		%/V	
Output Resistance		100		mΩ	
Response Time		1		mS	
Output Noise		.5		mVP-P	
Output Load Resistance	2			KΩ	
Insulation Resistance (50V)	50			MΩ	
Pressure Overload			3X	Rated	5
Operating Temperature	-20°C to +85°C				
Storage Temperature	-40°C to +125°C				
Media	Compatible with 316 Stainless Steel				
Weight	6 oz. with connector				6

Notes

1. Temperature Range: 0-50°C in reference to 25°C.
2. Measured at vacuum for absolute (A) and one standard atmosphere for sealed gage (S).
3. Includes repeatability, pressure hysteresis and linearity (best fit straight line).
4. With no load at the output.
5. 3X or 7500 psi maximum whichever is less.
6. Mating connector, for use with 18-20 gauge wire, is available.
7. 7/8" HEX, 1/4-10 NPT (with 0.107" diam. port hole) is standard for full scale pressure ranges of 300 psi or lower. 3/4" HEX, 1/4-18NPT (with 0.1" diam. port hole) is standard for full scale pressure ranges of 500 psi or greater.

Ordering Information

114- 3000 -S

Type (S=Sealed Gage, A=Absolute, G=Gage)

psi Range

Model

Represented By

ICSENSORS

Pressure Transducer Calibration

Depth (m)	Voltage (V)
0	1.753
1	1.803

slope = 0.072 V/m

Current	5.30mA
Voltage	23.1V
Power	0.122W

used water for depth calibration

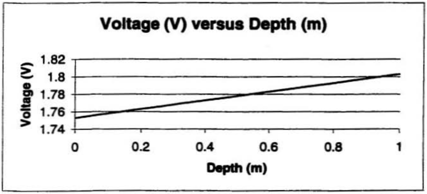

ICSensors Accelerometer– Model 3145
Specification Sheets and Calibration Data

Signal Conditioned Temperature Compensated 0.5 to 4.5 Vdc Output Low Cost

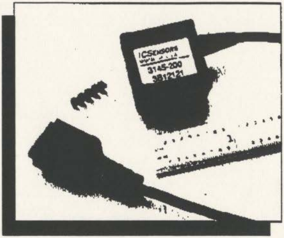

Features

- Full Calibration Data Supplied
- DC Response
- Internal Voltage Regulation
- High Sensitivity
- Built-in Overrange Stops
- Built-in Critical Damping
- Piezoresistive

Typical Applications

- Structural Analysis
- Modal Analysis
- Flight Dynamics Measurements
- Transportation Shock Monitoring
- Machine Tool Monitoring
- Industrial Vibration Monitoring
- Crash Testing
- Geophysical Monitoring
- Motion Control

Standard Ranges

± 2 g
± 5 g
± 10 g
± 20 g
± 50 g
± 100 g
± 200 g

Connections/Dimensions

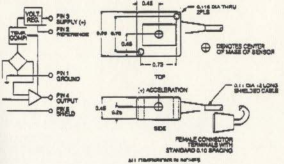

Description

The Model 3145 is a precision accelerometer intended for instrumentation applications where the high performance level of the Model 3140 is not required. This fully signal conditioned accelerometer provides the performance of traditional instrumentation accelerometers yet at a fraction of the cost.

The module consists of a silicon micromachined accelerometer, amplification, signal conditioning, and temperature compensation from -20 to +85° C. A single supply is required and full scale output is ±2 volts about a 2.5 volt offset.

The Model 3145 is designed with built-in damping, thereby allowing a wide useable bandwidth. In addition, the accelerometer element is protected from shock by overrange stops in the silicon microstructure. The lightweight Valox™ housing provides easy attachment to the measurement surface.

A detailed calibration sheet that provides the measured test and calibration data for the sensor is included with each unit. A sample of this calibration sheet is shown in Figure 1.

The accelerometer is available in standard ranges from ±2g to ±100g. Custom ranges are also available. Device performance characteristics and output range can be tailored to meet the requirements of specific applications.

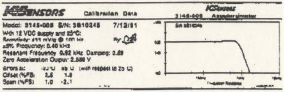

ICSENSORS Calibration Data

Model: 3145-005 S/N: 3B10245 7/12/91
With 12 VDC supply and 25°C:
Sensitivity: 411 mV/g @ 100 Hz
±5% Frequency: 0.40 kHz
Resonant Frequency 0.92 kHz Damping: 0.69
Zero Acceleration Output: 2.580 V

Errors at:	-20°C	85°C (with respect to 25°C)
Offset (%FS)	2.5	1.8
Span (%FS)	1.0	-2.1

Figure 1. Calibration Data Sheet
A calibration data sheet similar to the sample shown above is included with each unit. The calibration sheet provides the measured test and calibration data for the sensor.

Model 3145

Performance Specifications

Supply Voltage = 12 Vdc and Ambient Temperature = 25° C (Unless otherwise specified)

PARAMETER	RANGE						
	±2g	±5g	±10g	±20g	±50g	±100g	±200g
Frequency Response (TYP) (See Notes 8 & 9)	0-250 Hz	0-500 Hz	0-700 Hz	0-1000 Hz	0-1000 Hz	0-2300 Hz	0-2600 Hz
Mounted Resonant Frequency (TYP) (See Note 9)	450 Hz	850 Hz	1200 Hz	1800 Hz	2750 Hz	3900 Hz	5000 Hz
Sensitivity (Nominal)	1 V/g	400 mV/g	200 mV/g	100 mV/g	40 mV/g	20 mV/g	10 mV/g

PARAMETER	ALL RANGES				
	MIN	TYP	MAX	UNITS	NOTES
Full Scale Output Span	3.8	4.00	4.2	Volts	1,9
Zero Acceleration Output	2.40	2.50	2.60	Volts	1,9
Damping Ratio	0.4	0.7	0.9		2,9
Accuracy		0.2	1.0	±%Span	3
Transverse Sensitivity		1.0	3.0	±%Span	
Temperature Coefficient - Span (-20 to + 85°C)		2.0	4.0	±%Span	4,9
Temperature Coefficient - Zero (-20 to + 85°C)		2.0	4.0	±%Span	4,9
Supply Voltage	8.0	12.0	30.0	Volts	
Supply Current		5.0		mA	
Reference Voltage		2.5		Volts	6
Output Resistance		0.1		Ω	
Output Noise		0.5		mV p-p	5
Output Load Resistance	2			kΩ	
Acceleration Limits		20X		Rated	
Operating Temperature	−20		+85	°C	
Storage Temperature	−40		+125	°C	
Weight (Including Cable)		13		Grams	

Notes

1. The output voltage increases from the Zero Acceleration Output for positive acceleration and decreases for negative acceleration. The sensitivity is then 2V/Range. For example, the ±5g range has a sensitivity of 2V/5g or 400mV/g.
2. The 0.7 damping ratio represents critical damping. The damping ratio is controlled to within ±10% over the entire operating temperature range. Alternate damping ratios are available on a special order basis.
3. Includes repeatability, hysteresis and linearity (best fit straight line).
4. Compensated temperature range: -20 to +85°C in reference to 25°C.
5. 10 Hz to 1 kHz.
6. Pin 2 provides an optional 2.5V reference which may be used, if desired, to provide a stable zero-g reference. Thus, the full scale differential output between Pin 2 and Pin 4 would be ±2 VDC. If a single-ended output signal is preferred (0.5-4.5 VDC), make no connection to Pin 2. To avoid damage to the internal voltage regulator, do not connect Pin 2 to Pin 1 (gnd). Minimum load resistance connected to Pin 2 without affecting output is 100 kΩ
7. The case material is a carbon-filled Ultem™ plastic that forms a noise shield. Pin 5 allows the case shield and cable shield to be connected to ground to reduce noise susceptibility.
8. The useful frequency range is defined as the range of frequencies over which the device sensitivity is within ±5% of the DC value.
9. Actual test data for this parameter is included on the calibration sheet included with each sensor. A sample of this calibration sheet is shown in Figure 1.
10. To use an alternate electrical connector, refer to the following color code for proper electrical connections: Pin 1-Green; Pin 2-White; Pin 3-Red; Pin 4-Blue; Pin 5-Black. For cable extensions longer than 10 ft., please contact factory.

Ordering Information

3145 - 002

Acceleration Range
Model

Represented By

ICSENSORS

Accelerometer Calibration

Current	6.92mA
Voltage	23.1V
Power	0.160W

3.5V	top position
2.5V	center position
1.5V	bottom position

Subconn Connectors Schematics and Data

STANDARD 2 CONTACT CIRCULAR

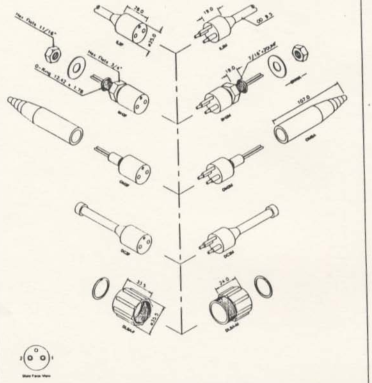

Standard Inline Cable Colour Code

1 Black
2 White

(Bulkhead Leads Number Tagged)

Connector Specification

Contact Rating	600 V @ 15 Amp
Contact Rating 2-4 pins	600 V @ 15 Amp
Contact Rating 5-10 pins	600 V @ 8 Amp
Contact Rating 12-16 pins	600 V @ 5 Amp
Insulation Resistance	>200 megaohm
Contact Resistance	<0.01 ohm
Wet Matings	>500
Temp. Rating	-4 to +60 degr. C
Depth Rating	1 400 bar - 20 000 psi

Standard Material Specification

Connector Body	Neoprene
Bulkhead Body	Naval Brass
Contacts	Naval Brass
Location pin	30353
'O' Rings	Nitrile
Locking Sleeve	Delrin
Snap Ring	30155
Inline Cables (60 cm)	18 AWG 1.34 mm² neopr. (2-8 pin) 18 AWG 1.0 mm² neopr. (10-16 pin)
Bh Leads (30 cm)	18 AWG 1.0 mm² teflon
Options	See ordering information (page 5)

Dimensions in mm
Threads in inches
1 inch = 25.4 mm

Drawing No.
BE 300-[illegible]

Rev.

STANDARD 8 CONTACT CIRCULAR

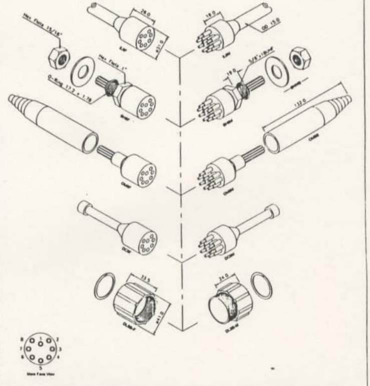

Standard Inline Cable Colour Code

1 Black
2 White
3 Red
4 Green
5 Orange
6 Blue
7 White/Black
8 Red/Black

(Bulkhead Leads Number Tagged)

Connector Specification

Contact Rating	600 V @ 15 Amp
Contact Rating 2-4 pins	600 V @ 15 Amp
Contact Rating 5-10 pins	600 V @ 8 Amp
Contact Rating 12-16 pins	600 V @ 5 Amp
Insulation Resistance	>200 megaohm
Contact Resistance	<0.01 ohm
Wet Matings	>500
Temp. Rating	-4 to +60 degr. C
Depth Rating	1 400 bar - 20 000 psi

Standard Material Specification

Connector Body	Neoprene
Bulkhead Body	Naval Brass
Contacts	Naval Brass
Location pin	30151
'O' Rings	Nitrile
Locking Sleeve	Delrin
Snap Ring	30753
Inline Cables (60 cm)	18 AWG 1.34 mm² neopr. (2-8 pin) 18 AWG 1.0 mm² neopr. (10-16 pin)
Bh Leads (30 cm)	18 AWG 1.0 mm² teflon
Options	See ordering information (page 5)

Dimensions in mm
Threads in inches
1 inch = 25.4 mm

Drawing No.
BE 301-1

Rev.

FESTO Components' Specification Sheets

Double acting cylinder
Type DSW-32-50-P-A

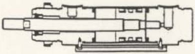

Order code (see sheet 1.245.1)	Part No. + DSW + piston dia. + stroke length + end position cushioning + proximity sensing *Example: piston dia. 63 mm , stroke length 80 mm = 6982 DSW-63-80-P-A*
Medium	Compressed air, filtered (lubricated or unlubricated)
Design	Piston cylinder
Max. permissible operating pressure	10 bar
Temperature range	−20 to +80 °C (check range of application of proximity switches)
Materials	Bearing cap and cover cap: naturally anodized aluminium; cylinder barrel: X 5 Cr Ni 18 9; piston rod: X 20 Cr 13, rolled thread; DUO rail: aluminium; seals: perbunan
Weights	See overleaf

Piston dia. mm	Standard stroke lengths mm	Stroke length min. – max. mm	Thrust at 6 bar N	(≈ kp)	Return force at 6 bar N	(≈ kp)	Connection	Cushioning length mm
32	25 40 50 80 100 160 200 300	10 to 500	450	(45)	360	(36)	G $^1/_8$	19
40			720	(72)	630	(63)	G $^1/_4$	22
50			1050	(105)	910	(91)	G $^1/_4$	27
63			1800	(180)	1650	(165)	G $^3/_8$	27

Non-return valve
Type H-M5

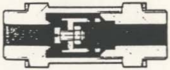

Order code Part No./Type	3671 H-M 5	3324 H-$^1/_8$ a/i	11689 H-$^1/_4$-B	11690 H-$^3/_8$-B	11691 H-$^1/_2$-B	11692 H-$^3/_4$-B
Medium	Compressed air, filtered (lubricated or unlubricated)					
Design	Non-return valve					
Mounting	Line fitting (screw-in thread)					
Connection	M 5	G $^1/_8$	G $^1/_4$	G $^3/_8$	G $^1/_2$	G $^3/_4$
Nominal bore	2.2 mm	4 mm	6 mm	8 mm	13 mm	16 mm
Standard nominal flow rate	115 l/min	280 l/min	1020 l/min	2300 l/min	5800 l/min	6650 l/min
Pressure range	0.4 to 8 bar		0.4 to 12 bar			
Temperature range	−10 to +60 °C					
Materials	Housing: brass; seals: perbunan					
Weight	0.015 kg	0.025 kg	0.070 kg	0.075 kg	0.150 kg	0.425 kg

Solenoid valve
Type MYH-3-M5-L-LED

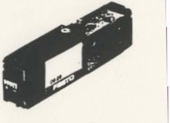

Function:

Type MZH

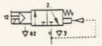

MOZH

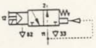

1.11 (P) = supply ports
2 (A) = working or outout line
3.33 (R) = exhaust
82 = pilot exhaust

Order code Part. No./Type	34 307 MYH-3-M5-L-LED	34 308 MOYH-3-M5-L-LED	34 301 MYH-3-2.3-L-LED	34 302 MOYH-3-2.3-L-LED
Medium	Compressed air, 5 µm filtered, unlubricated			
Design	Spool valve, indirectly actuated			
Mounting	Through-holes in housing			
Connection	M5 thread		optional with sub-base	
Nominal bore	2.3 mm			
Standard nominal flow rate (1 → 2)	190 l/min.		170 l/min.	
Pressure range	2 to 8 bar			
Response time at 6 bar	On: 11 ms; off: 30 ms			
Ambient temperature	+5 to 50 °C			
Medium temperature	+5 to 50 °C			
Materials	Housing: Al; seals: perbunan			
Weight	0.065 kg			
Operating voltage	$24\ V_{=}\ ^{+10\%}_{-15\%}$			
Power consumption	1.8 W			
Duty cycle	100%			
Degree of protection				

Double solenoid valve
Type JMYH-5/2-M5-L-LED

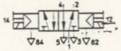

1 (P) = supply port
4.2 (A, B) = working or output line
5.3 (R, S) = exhaust
82, 84 = pilot exhaust

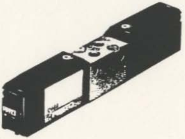

Order code Part. No./Type	34 310 JMYH-5/2-M5-L-LED	34 304 JMYH-5/2-2.3-L-LED
Medium	Compressed air, 5 µm filtered, unlubricated	
Design	Spool valve, indirectly actuated	
Mounting	Through-holes in housing	
Connection	M5 thread	optional with sub-base
Nominal bore	2.3 mm	
Standard nominal flow rate (1 → 2, 1 → 4)	190 l/min.	180 l/min.
Pressure range	2 to 8 bar	
Response time at 6 bar	10 ms	
Ambient temperature	+5 to 50 °C	
Medium temperature	+5 to 50 °C	
Materials	Housing: Al, seals: perbunan	
Weight	0.095 kg	
Operating voltage	$24\ V_{=}\ ^{+10\%}_{-15\%}$	
Power consumption	1.8 W	
Duty cycle	100%	
Degree of protection		

Flow control valve, adjustable
Type GRO-M5

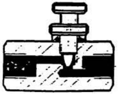

Order code	Part No./Type	4804 GRO-M 5	6500 GRO-1/8	2109 GRO-1/4
Medium		Compressed air, filtered (lubricated or unlubricated)		
Design		Flow control valve		
Mounting		2 through-holes in housing, or front-panel mounting		Line fitting
Connection		M 5	G 1/8	G 1/4
Nominal size		2 mm	2 mm	4.5 mm
Flow rate		0 to 45 l/min	0 to 100 l/min	0 to 350 l/min
Pressure range*		0 to 10 bar		
Temperature range		−10 to +60° C		
Materials		Housing: aluminium, brass; seals: perbunan		Housing: aluminium, steel; seals: perbunan
Weight		0.020 kg	0.030 kg	0.080 kg

Regulator
Type LR-1/8-F-7

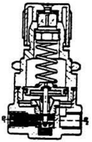

Order code	Regulator	7879 LR-1/8-F	7880 LR-1/8-F-7
Part no./type	Mounting bracket	3754 FV-32	
Medium		Compressed air, filtered	
Design		Piston type relieving regulator	
Mounting		Panel mounting, installation dia. 30.5 mm	
Installation position		Any	
Connection		G 1/8	
Standard nominal flow rate*		420 l/min	690 l/min
Max. upstream pressure		20 bar	
Max. working pressure		12 bar	7 bar
Temperature range		−10 to +60 °C	
Materials		Housing: brass, plastic; seals: perbunan	
Weight		0.280 kg	

Quick push-pull connector
Type CS-M5-PK-4

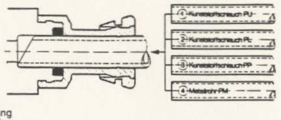

① Plastic tubing
② PL plastic tubing
③ PP plastic tubing
④ PM alloy tube

Order code		For tubing/ tube inside dia.	Connection	Nominal size	Material	Weight	Dimensions				
Part No.	Type		D	mm		kg	B	D_1	D_2	L	SW
With metal connector and sealing ring											
5787	CS-M 5-PK-3	3	M 5	2.4	Steel/ plastic	0.004	3.5	–	10.5	31	8
5788	CS-M 5-PK-4	4/4	M 5	2.4		0.005	3.5	–	11.5	31	10
10 100	CS-$^1/_8$-PK-3-B	3	G $^1/_8$	3	Aluminium/ plastic −0.95 to +10 bar* −10 to +60 °C	0.006	5	–	12.5	33	13
10 101	CS-$^1/_8$-PK-4-B	4/4	G $^1/_8$	4		0.006	5	–	14	33	13
12 620	CK-$^1/_8$-PK-6	6/5.2	G $^1/_8$	5.3		0.007	6.5	–	17	34.5	13
10 102	CS-$^1/_4$-PK-4-B	4/4	G $^1/_4$	4		0.009	6.5	–	14	35	17
10 103	CS-$^1/_4$-PK-6	6/5.2	G $^1/_4$	6		0.010	6.5	–	17	35	17
12 962	CS-$^1/_4$-PK-8	8	G $^1/_4$	8		0.150	6.5	–	21	47	17
10 104	CS-$^3/_8$-PK-6	6/5.2	G $^3/_8$	6		0.140	8.5	–	17	37	19
12963	CS-$^3/_8$-PK-8	8	G $^3/_8$	8		0.020	8.5	–	21	50	19
Plastic design											
5789	CS-$^1/_8$-PK-3-KU	3	G $^1/_8$	3	Plastic with moulded-on sealing rim −0.95 to +10 bar* −10 to +60 °C	0.004	6.5	14.2	12.5	32.4	13
5790	CS-$^1/_8$-PK-4-KU	4/4	G $^1/_8$	4		0.004	6.5	14.2	14	32.4	13
5792	CS-$^1/_4$-PK-4-KU	4/4	G $^1/_4$	4		0.005	8.5	14.2	14	34.5	17
6699	CS-$^1/_4$-PK-6-KU	6/5.2	G $^1/_4$	6		0.005	8.5	16	17	35	17
6700	CS-$^3/_8$-PK-6-KU	6/5.2	G $^3/_8$	6		0.007	10.5	16	17	37	19

Quick push-pull elbow
Type LCS-M5-PK-4

Order code		For tubing/ tube inside dia.	Connection	Nominal size	Material	Weight	Dimensions					
Part No.	Type		D	mm		kg	B	D_1	D_2	H	L	SW
With metal connector and sealing ring												
12 952	LCS-M5-PK-3	3	M5	3	Steel plastic	0.01	3.5	–	12.5	21.8	26.4	10
13 688	LCS-M5-PK-4	4/4	M5	4		0.01	3.5	–	14	21.8	26.4	10
10 105	LCS-$^1/_8$-PK-3	3	G $^1/_8$	3	Aluminium/ plastic 0.95 to +10 bar* −10 to +60 °C	0.008	5	–	12.5	20	26.5	13
10 106	LCS-$^1/_8$-PK-4	4/4	G $^1/_8$	4		0.008	5	–	14	20	26.5	13
12 621	LCS-$^1/_8$-PK-6	6/5.2	G $^1/_8$	5.3		0.008	5	–	17	23.1	27.9	13
10 107	LCS-$^1/_4$-PK-4	4/4	G $^1/_4$	4		0.012	6.5	–	14	21	26.5	17
10 108	LCS-$^1/_4$-PK-6	6/5.2	G $^1/_4$	6		0.014	6.5	–	17	22.5	28	17
12 964	LCS-$^1/_4$-PK-8	8	G $^1/_4$	8		0.025	6.5	–	21	31.2	40	17
10 109	LCS-$^3/_8$-PK-6	6/5.2	G $^3/_8$	6		0.017	8.5	–	17	22.5	28	19
12 965	LCS-$^3/_8$-PK-8	8	G $^3/_8$	8		0.028	8.5	–	21	32	40	19
Plastic design												
9618	LCS-$^1/_8$-PK-3-KU	3	G $^1/_8$	3	Plastic with moulded-on sealing rim −0.95 to +10 bar* −10 to +60 °C	0.005	6.5	14.2	12.5	18.5	26.3	13
6833	LCS-$^1/_8$-PK-4-KU	4/4	G $^1/_8$	4		0.005	6.5	14.2	14	18.5	26.3	13
6835	LCS-$^1/_4$-PK-4-KU	4/4	G $^1/_4$	4		0.007	8.5	14.2	14	18.7	26.3	17
6836	LCS-$^1/_4$-PK-6-KU	6/5.2	G $^1/_4$	6		0.008	8.5	16	17	20.2	27.8	17
9619	LCS-$^3/_8$-PK-6-KU	6/5.2	G $^3/_8$	6		0.010	10.5	16	17	20.3	27.8	19

Barbed tubing connectors
Type T-PK-4
Type Y-PK-4

Order code		Design	For tubing I.D.	Nominal bore mm	Material	Weight kg	D_1 dia.	H_1	L_1	L_2
Part No.	Type									
19539	L-PK-2	L-connector	2	1.5	Brass, Plastic	0.001	4	10.2	–	6
7473	L-PK-3		3	2.5		0.001	6.5	13.7	–	8.5
9584	L-PK-4		4	3.5		0.002	7.8	16.9	–	10.5
30919	T-PK-2	T-connector	2	1.5		0.001	4	20.4	12.2	6
7267	T-PK-3		3	2.5		0.002	6.5	26.5	17.2	8.5
9585	T-PK-4		4	3.5		0.003	7.8	32	20.8	10.5
30918	V-PK-2	V-connector	2	1.5		0.001	4	11	–	6
7268	V-PK-3		3	2.5		0.001	6.5	15.5	–	8.5
30920	V-PK-4		4	3.5		0.002	7.8	19.6	–	11.7
19540	Y-PK-2	Y-connector	2	1.5		0.001	4	18	–	6
7269	Y-PK-3		3	2.5		0.002	6.5	25.5	–	8.5
9586	Y-PK-4		4	3.5		0.003	7.8	31	–	10.5

Plastic tubing
Type PU-4

Pressure range*		−0.95 to +7 bar (PU-9, PU-13 max. 10 bar)					
Temperature range		−35 to +60 °C					
Order code		Inside dia. mm	Outside dia. mm	Material	Min. bending radius mm	Weight kg/m	Colour of tubing
Part No.	Type						
13365	PU-2	2.2	3.2	Polyurethane	13	0.005	Blue
13366	PU-2						Black
5732	PU-3	2.9	4.3		14	0.009	Blue
5731	PU-3						Black
6204	PU-4	3.9	6.1		20	0.021	Blue
5733	PU-4						Black
9159	PU-6	5.9	8.3		36	0.033	Blue
6731	PU-6						Black
8976	PU-8	8	11		84	0.055	Blue
11255	PU-8						Black
12134	PU-9	9	11.6	Polyurethane with fabric	76	0.051	Black
12133	PU-13	13	17.6		83	0.14	Black

Sample Calculations

4.1 Battery Life

Currents:	
Accelerometer	5.0 mA
Pressure Transducer	2.5 mA
Controller	220 mA
Pneumatic Valves	3 @ 75 mA = 225 mA
Total Current	452.5 mA
Voltage Supplied	22.8 V DC – 3 batteries in series (taken as 24 V DC)

Power = Voltage x Total Current
= 24 V DC x 0.4525 A
= 10.86 W

Time = Current Power Available/ Total Current Required
= 1800 mAh/452.5 mA
= 3.977 h
≅ 4 hours

These calculations assume the worst case scenario where

- all components are operating all the time
- not considering the voltage drop as the batteries are discharging

Thus, the battery set-up should last for four hours before recharging is required.

5.1 Pressure Drop in Ballast Tank, ΔP

$$\begin{aligned}\Delta P &= \sigma g(T + Y)\\ &= (1000\ \text{kg/m}^3)(9.81\ \text{m/s}^2)(0.250\ \text{m} + 0.250\ \text{m})\\ &= 4905\ \text{Pa}\end{aligned}$$

5.2 Head Loss, h_L

$$
\begin{aligned}
h_L &= (2T\rho)/\sigma \\
&= (2 \text{ x } 0.250 \text{ m x } 1 \text{ kg/m}^3)/1000 \text{ kg/m}^3 \\
&= 0.0005 \text{ m} \\
&= 0.5 \text{ mm}
\end{aligned}
$$

5.3 Purge Period, t_p

$$
\begin{aligned}
t_p &= AT/Q_W \\
&= (0.025 \text{ m}^2 \text{ x } 0.250 \text{ m})/0.001 \text{ m}^3\text{/s} \\
&= 6.25 \text{ s}
\end{aligned}
$$

5.4 Maximum mass of water that the ballast tank can withstand, M_{max}

$$
\begin{aligned}
M_{max} &= B/g = \sigma AT \\
&= 1000 \text{ kg/m}^3 \text{ x } 0.025 \text{ m}^2 \text{ x } 0.250 \text{ m} \\
&= 6.25 \text{ kg}
\end{aligned}
$$

5.5 Maximum terminal speed, V_t

$$
\begin{aligned}
V_t &= ((2ATg)/(C_D A_f))^{1/2} \\
&= ((2 \text{ x } 0.025 \text{ m}^2 \text{ x } 0.250 \text{ m x } 9.81 \text{ m/s}^2)/(2.5 \text{ x } 0.5 \text{ m}^2))^{1/2} \\
&= 0.313 \text{ m/s}
\end{aligned}
$$

Appendix F

Simulation Codes (Fortran)

Simulation code and data for
Figure 5.3 – Simulation time trace

```
C
C      PNEUMATIC SUBSEA ROBOT
C
C      D = SUBSEA ROBOT DEPTH
C      U = SUBSEA ROBOT VELOCITY
C      NIT = STEPS IN TIME
C      AREA = FRONTAL AREA
C      TANK = TANK HALF HEIGHT
C      BASE = TANK SECTIONAL AREA
C      HOLE = TANK HOLE AREA
C      CD = HOLE LOSS FACTOR
C      WAKE = DRAG LOSS FACTOR
C      BUOY = TANK BUOYANCY
C      SIZE = BUOYANCY BAND
C      SPEED = WATER IN FLOW
C      GAS = WATER OUT FLOW
C      SKG = SUBSEA ROBOT MASS
C      DELT = STEP IN TIME
C      BAND = DEPTH BAND
C      RATE = SPEED BAND
C      FAST = FAST SPEED
C      SLOW = SLOW SPEED
C      OLD = STEP START
C      NEW = STEP END
C      COM = COMMAND
C
       IMPLICIT REAL*8(A-H,O-Z)
       REAL*4 XP,YP,XO,YO,TOTAL
       OPEN(5,file='sod.d',status='old')
       READ(5,*) DOLD,DCOM
       READ(5,*) NIT,NIP
       READ(5,*) NIA,NIB
       READ(5,*) MIA,MIB
       READ(5,*) AREA,WAKE
       READ(5,*) SKG,DELT
       READ(5,*) BASE,TANK
       READ(5,*) HOLE,CD
       READ(5,*) ONE,TWO
       READ(5,*) SX,SY
       READ(5,*) XO,YO
       READ(5,*) BAND
       READ(5,*) RATE
       READ(5,*) FAST
       READ(5,*) SLOW
       READ(5,*) SIZE
       READ(5,*) GAS
       G=9.81D0
       DENSITY=1000.D0
       YP=YO-DOLD*SY
       CALL PLOTS(53,0,-1)
       CALL PLOT(XO,YO,3)
       CALL PLOT(XO+6.0,YO,2)
       CALL PLOT(XO,YO,3)
       CALL PLOT(XO,YO-4.0,2)
```

```
      CALL PLOT(XO+0.05,YO-4.0,3)
      CALL PLOT(XO-0.05,YO-4.0,2)
      CALL PLOT(XO+2.0,YO+0.05,3)
      CALL PLOT(XO+2.0,YO-0.05,2)
      CALL PLOT(XO+4.0,YO+0.05,3)
      CALL PLOT(XO+4.0,YO-0.05,2)
      CALL PLOT(XO+6.0,YO+0.05,3)
      CALL PLOT(XO+6.0,YO-0.05,2)
      CALL PLOT(XO,YP,3)
      IP=0
      ID=0
      TOTAL=0.0
      TIME=0.D0
      BUOY=0.D0
      UOLD=0.D0
      YOLD=0.D0
      UDOT=0.D0
      DO 22 IT=1,NIT
      IG=0
      IW=0
      AIR=GAS
      ERROR=DCOM-DOLD
      HIGH=(TANK+YOLD)*G
      IF(HIGH.GT.0.D0) SPEED=CD*HOLE*DSQRT(2.D0*HIGH)
      IF(ID.GT.NIA.AND.ERROR.GT.+BAND.AND.UOLD.LT.+SLOW) IW=1
      IF(ID.GT.NIA.AND.DABS(ERROR).LE.BAND.AND.UOLD.LE.-RATE
    *   .AND.BUOY.GE.0.D0) IW=1
      IF(ERROR.LT.-BAND.AND.UOLD.GT.-FAST) IG=1
      IF(DABS(ERROR).LE.BAND.AND.UOLD.GE.+RATE
    *   .AND.BUOY.LE.0.D0) IG=1
      IF(IT.EQ.MIA) DCOM=ONE
      IF(IT.EQ.MIB) DCOM=TWO
      IF(IG.EQ.0) AIR=0.D0
      IF(IW.EQ.0) SPEED=0.D0
      FLOW=AIR-SPEED
      WATER=FLOW*DENSITY*G
      BUOY=BUOY+WATER*DELT
      HIT=DENSITY*UOLD*DABS(UOLD)/2.D0
      DRAG=WAKE*AREA*HIT
      IF(IG.EQ.1) TOTAL=TOTAL+DELT*GAS
      YNEW=YOLD+DELT*FLOW/BASE
      SOG=SKG-YOLD*BASE*DENSITY
      UDOT=-BUOY/SOG-DRAG/SOG
      DNEW=DOLD+DELT*UOLD
      UNEW=UOLD+DELT*UDOT
      TIME=TIME+DELT
      XP=SX*TIME+XO
      YP=YO-DNEW*SY
      IP=IP+1
      ID=ID+1
      IF(IP.EQ.NIP) CALL PLOT(XP,YP,2)
      IF(IP.EQ.NIP) IP=0
      IF(ID.EQ.NIB) ID=0
      DOLD=DNEW
```

```
      UOLD=UNEW
      YOLD=YNEW
22    CONTINUE
      READ(5,*) NO
      DO 33 IO=1,NO
      READ(5,*) TIME,DEPTH
      DEPTH=3.5-DEPTH
      XP=SX*TIME+XO
      YP=YO-DEPTH*SY
      CALL SYMBOL(XP-0.05,YP-0.025,0.25,1H.,0.0,1)
33    CONTINUE
      TOTAL=TOTAL*1000.
      CALL SYMBOL(XO+5.65,YO+0.14,0.14,5H180 s,0.0,5)
      CALL SYMBOL(XO-0.21,YO-4.28,0.14,3H5 m,0.0,3)
      CALL SYMBOL(XO+0.5,YO-6.0,0.14,3HRCW,0.0,3)
      CALL NUMBER(XO+0.5,YO-7.0,0.14,TOTAL,0.0,2)
      CALL PLOT(0.0,0.0,999)
      CLOSE(5)
      STOP
      END
```

```
3.5d0     2.5d0             dold   dcom
140000       600            nit    nip
 1000  1500                 nia    nib
 50000 100000               mia    mib
0.15d0        5.0d0         area   wake
75.d0       0.001d0         skg    delt
0.025d0      0.25d0         base   tank
0.001d0     1.0d0           hole   cd
  1.5d0   2.5d0             one    two
   0.03333 0.8              sx     sy
   1.0   8.0                xo     yo
    0.5d0                   band
    0.00d0                  rate
    0.005d0                 fast
    0.0025d0                slow
    0.01d0                  size
    0.0025d0                gas
        28
```

Plotting code and data for
Figure 6.2 – Comparison of simulation time trace and testing data

```
C
C     "ANNE" DEEP TANK DEPTH DATA
C
      OPEN(5,file='sos.d',status='old')
      READ(5,*) SX,SY
      READ(5,*) XO,YO
      READ(5,*) ND
      YP=YO-3.5*SY
      CALL PLOTS(53,0,-1)
      CALL PLOT(XO,YO,3)
      CALL PLOT(XO+6.0,YO,2)
      CALL PLOT(XO,YO,3)
      CALL PLOT(XO,YO-4.0,2)
      CALL PLOT(XO+0.05,YP,3)
      CALL PLOT(XO-0.05,YP,2)
      CALL PLOT(XO+0.05,YO-4.0,3)
      CALL PLOT(XO-0.05,YO-4.0,2)
      CALL PLOT(XO+2.0,YO+0.05,3)
      CALL PLOT(XO+2.0,YO-0.05,2)
      CALL PLOT(XO+4.0,YO+0.05,3)
      CALL PLOT(XO+4.0,YO-0.05,2)
      CALL PLOT(XO+6.0,YO+0.05,3)
      CALL PLOT(XO+6.0,YO-0.05,2)
      CALL PLOT(XO,YP,3)
      DO 22 ID=1,ND
      READ(5,*) TIME,DEPTH
      DEPTH=3.5-DEPTH
      XP=SX*TIME+XO
      YP=YO-DEPTH*SY
      CALL SYMBOL(XP-0.05,YP-0.025,0.25,1H.,0.0,1)
 22   CONTINUE
      CALL SYMBOL(XO+5.65,YO+0.14,0.14,5H180 s,0.0,5)
      CALL SYMBOL(XO-0.21,YO-4.28,0.14,3H5 m,0.0,3)
      CALL SYMBOL(XO+0.5,YO-6.0,0.14,3HRCW,0.0,3)
      CALL PLOT(0.0,0.0,999)
      CLOSE(5)
      STOP
      END
```

```
0.03333 0.8                   sx    sy
1.0    8.0                    xo    yo
  28
 0.     0.00
 12.    0.80
 17.    1.25
 19.    1.25
 28.    1.20
 36.    1.20
 37.    1.20
 47.    1.30
 48.    1.30
 53.    1.35
 55.    1.30
 56.    1.30
 69.    2.00
 73.    2.05
 75.    2.00
 80.    2.00
 83.    2.00
 92.    2.05
 102.   2.10
 108.   2.00
 114.   1.50
 117.   1.55
 119.   1.55
 123.   1.65
 124.   1.65
 129.   1.45
 130.   1.50
 134.   1.55
```

Appendix G

Testing Instructions

Testing Instructions

Deployment of ANNE

- Ensure batteries are recharged and connected properly
- Ensure sufficient high-pressure compressed air is present in divers bottle being used
- Check all pneumatic valve electrical connections
- Check all FESTO tubing to ensure connected
- Use vortex blower for suction of battery box, apply duct tape and place box in position on ANNE
- Use vortex blower for suction of pneumatic box, apply duct tape and place box next to battery box
- Use screw handle to keep both boxes in place
- Turn on the air pressure
- Load code from computer to the Z-World
- Disconnect cable from Z-World
- Check location of accelerometer
- Use vortex blower for suction of controller box, apply duct tape and place box on other side of ANNE opposite of the battery and pneumatic boxes
- Use screw handle to keep controller box in place
- Make sure lead weights are placed on top of controller box (held by duct tape)
- Attach ropes for lifting lugs
- Use lifting lug to attach ropes and hook to crane
- Use crane to place ANNE in deep water tank

Recovery of ANNE (and preparation for next test)

- Use two ropes to ease ANNE out of the tank
- Use lifting lug to attach ropes and hook to crane
- Remove from tank and place on moving cart
- Use screw handle to release controller box
- Attach cable to Z-World
- Reload code
- Disconnect cable from Z-World
- Repeat as above in deployment

Recovery of ANNE (and end of testing)

- Use two ropes to ease ANNE out of the tank
- Use lifting lug to attach ropes and hook to crane
- Remove from tank and place on moving cart
- Turn off the air pressure
- Use screw handles to release controller, pneumatic valve and battery boxes
- Remove duct tape and release suction
- Take boxes apart and ensure there are no leaks
- Return ANNE and components to resting place

Appendix H

Testing Code (Dynamic C)

```
/*              ********************            */
/*                                              */
/*              ANNE HOVER TEST                 */
/*                                              */
/*              ********************            */


/*      declare variables                       */

        int n, m, a, b, p, i, j, k, h, iw, ig;
        int depth, gs, command, error;
        int slow, fast, rate, skg, water;
        int drag, area, band, count;
        long fax;

/*      start main program                      */
        root main ( )
{

/*      initialize hardware                     */
        uplc_init ( ) ;

/*      data                                    */
        ig=0; iw=0; count=0; h=10;
        i=2000; j=2400; k=2500; n=2200;m=2300;
        depth=0; slow=5; fast=10; water=1000;
        command=1000; band=250; drag=1;
        area=15; skg=75;

/*      sample depth                            */
        b=up_adcal (2) ;

/*      set pneumatic valves                    */
/*      1 - closes top hole                     */
/*      2 - opens top hole                      */
/*      3 - closes bottom hole                  */
/*      4 - opens bottom hole                   */
/*      5 - air flow to ballast tank            */

        up_setout (3,0) ; up_setout (4,1) ;
        up_setout (1,0) ; up_setout (2,1) ;
        up_setout (5,0) ;

/*      save power                              */
        p=1; while (p<10000)  {p++;}
        up_setout (4,0) ; up_setout (2,0) ;

/*      control loop                            */
        while (1)
{
        count++;
```

```
/*      sample sensors                                   */
        if (count==i)  {a=up_adcal (1) ;}
        if (count==i)  {depth=up_adcal (2) –b;}

/*      rest                                             */
        p=1; while (p,10000)  {p++;}

        if (count>i && count<j)  {gs=up_adcal (1) –a;}
        if (count>i && count<j)  {rate=up_adcal (2)-b-depth;}
        if (count>i && count<j)  (depth=up_adcal (2)-b;}

/*      hover tests                                      */
        if (count>i && count<j)
{
        if (count==n)  {command=500;}
        if (count==m)  {command=1000;}

        ig=0; iw=0;

/*      calculate ig and iw                              */
        error=command-depth;
        fax=skg*500*500*gs-drag*area*water*rate*abs(rate) ;
        if (error>+band && rate<+slow)  {iw=1;}
        if (error>+band && rate>+2*slow)  {ig=1;}
        if (error<-band && rate>-fast)  {ig=1;}
        if (error<-band && rate<-2*fast)  {iw=1;}
        if (abs(error)<band && rate>0 && fax<0)  {ig=1;}
        if (abs(error)<band && rate<0 && fax>0)  {iw=1;}
        if (abs(error)<band && rate>+slow)  {ig=1;}
        if (abs(error)<band && rate<-fast)  {iw=1;}
        if (ig==1)  {iw=0;}
        if (iw==1)  {ig=0;}

/*      operate pneumatic valves                         */
        if (iw==1 && ig==0)  {up_setout (2,0) ;
                 up_setout (1,1) ; up_setout (5,0) ;
                 up_setout (4,0) ; up_setout (3,1) ;}
        if (iw==1)          {up_setout (3,0) ;}
        if (iw==1)          {up_setout (4,1) ;}
        if (iw==1)          {up_setout (1,0) ;}
        if (iw==1)          {up_setout (2,1) ;}
        if (ig==1)          {up_setout (3,0) ;}
        if (ig==1)          {up_setout (4,1) ;}
        if (ig==1)          {up_setout (2,0) ;}
        if (ig==1)          {up_setout (1,1) ;}
        if (ig==1)          {up_setout (5,1) ;}
        if (ig==0)          {up_setout (5,0) ;}

/*      close holes of ballast tank and drift            */
        if (iw==1)  {p=1; while (p<2500)  {p++;}
        {up_setout (2,0) ; up_setout (1,1) ;
        up_setout (4,0) ; up_setout (3,1) ;}
}
```

```
/*      rise to water surface                          */
        if (count>j && count<k)
        {up_setout (2,0) ; up_setout (1,1) ;
        up_setout (3,0) ; up_setout (4,1);
        up_setout (5,1) ;}

/*      float at water surface                         */
        if (count==k)  {up_setout (5,0);
        up_setout (2,0) ; up_setout (1,1);
        up_setout (3,0) ; up_setout (4,1) ;}
}
}
```